CHEMICAL STUDIES OF MUONIC ISOTOPE EFFECTS

Submitted to the University of Glasgow in partial fulfilment of the requirements for the degree of Doctor of Philosophy in the Faculty of Science.

by

David Buttar

Chemistry Department

October 1991

ProQuest LLC.
789 East Eisenhower Parkway
P.O. Box 1346
Ann Arbor, MI 48106 – 1346

ACKNOWLEDGEMENTS

I should like to thank my supervisor Dr. Brian Webster for all his help, guidance and encouragement over the past three years.

For making available to me, the experimental facilities at the Paul Scherrer Institute and the University of Zürich I am indebted to Professor Hans Fischer. I would like also to thank Dr. Emil Roduner for his invaluable assistance and advice during my work at PSI, and for their help in performing experimental runs I would like to thank Drs. Ivan Reid, Toshiyuki Azuma and Christopher Rhodes.

I am grateful to Dr. Roderick Macrae for his advice and assistance during the course of my studies at the University of Glasgow.

For my early introduction to the experimental side of μSR and his help over the past three years I would like to thank Dr. Stephen Cox.

I extend my thanks to Professor Laurence Barron for the kind use of the laser printer on which this thesis has been printed.

To my family, I extend my greatest thanks for encouraging and supporting me throughout my studies and bearing with me through all my moods.

I would like also to thank all my friends and colleaques for keeping me linear.

Finally, I thank the Science and Engineering Research council for a research studentship and the travel grants which enabled me to undertake work at PSI.

CONTENTS

Page

Preface 1

Chapter 1 Aspects of Muonium Substituted Free Radical Chemistry 4

1.1 Introduction 4

1.2 Muon Production and Spectroscopy 6

1.3 Chemical States of μ^+ 8

1.3.1 Muonium 8

1.3.2 Muonic Diamagnetic States 10

1.3.3 Muonium Substituted Radicals 10

1.4 Transverse Field Muon Spin Rotation (TF-μSR) Spectroscopy 11

1.4.1 Experimental Aspects 11

1.4.2 Theoretical Background to TF-μSR 18

1.4.3 Evolution of Muon Spin Polarization under a Transverse Magnetic Field 20

1.4.4 Selection Rules for μSR Transitions 25

1.5 High Transverse Fields: Muonium and Muonium Substituted Radicals 27

1.5.1 Muonium 27

1.5.2 Muonium Substituted Radicals 29

1.6 Conformational and Internal Rotation Studies of Muonium Substituted Radicals 33

1.6.1 Analysis of μSR Spectra 33

Page

1.6.2 Temperature Dependence of the β-Hyperfine Coupling Constant..... 35

1.6.3 Theory of Rotational Averaging..... 36

Chapter 2 Experimental Studies Of Muonium Substituted Free Radicals..... 43

2.1 Solvent Effects on the Muon-Electron Hyperfine Coupling Constant and Barrier to Internal Rotation of the 2-Muoxyprop-2-yl radical..... 43

2.1.1 Introduction..... 43

2.1.2 TF-μSR Measurements..... 46

2.1.3 Internal Rotation Studies..... 58

2.2 Competitive Muonium Addition to 3-Methyl-2-Butenal..... 69

2.2.1 TF-μSR Studies of αβ-Unsaturated Carbonyl Compounds..... 69

2.2.2 Results and Discussion..... 71

Chapter 3 Molecular Orbital Methods for the Calculation of Selected Molecular Properties..... 76

3.1 Prelude..... 76

3.2 *Ab Initio* Molecular Orbital Theory..... 78

3.2.1 Theoretical Background..... 78

3.2.2 The Hartree-Fock Approximation..... 80

3.2.3 Orbitals and Basis Functions..... 86

3.3 *Ab Initio* One-Electron Properties..... 88

3.3.1 Hyperfine Coupling Constants..... 88

3.3.2 Nuclear Quadrupole Coupling..... 90

Page

3.4 Vibrational Corrections to *Ab Initio* Molecular Properties 92

3.4.1 Introduction 92

3.4.2 Theoretical Description 93

Chapter 4 Vibrational Corrections to Molecular Properties of the Water Molecule and Selected Isotopomers 100

4.1 Introduction 100

4.2 The Water Molecule 101

4.2.1 Computational Details 101

4.2.2 Vibrational Analysis 103

4.2.3 Comparisons with Experiment 124

Chapter 5 Vibrationally Averaged β-Hyperfine Coupling Constants for the Muonium Substituted Ethyl Radical 127

5.1 Prelude 127

5.2 Computational Procedure 128

5.3 Results and Discussion 134

5.4 The Residual Isotope Effect 151

Chapter 6 Summary and Suggestions for Further Work 153

References 160

Publications 169

PREFACE

The positive muon (μ^+) is an elementary particle formed in nature from the interaction of cosmic rays with the upper atmosphere. On implantation in matter the electronic and magnetic interactions experienced by the muon can be investigated by monitoring the evolution of the muon spin polarization using muon spin rotation (μSR) spectroscopy. Comparison between the positive muon and the proton in similar chemical states enables the study of isotope effects on molecular properties. This thesis presents theoretical and experimental investigations of the isotope effects resulting from substitution of hydrogen by muonium. Muonium is the bound state of a positive muon and an electron; and can be considered to be a light, short lived, isotope of hydrogen. These studies consider the isotope effects on, the molecular properties, the regioselectivity of muonium addition and the conformation, of selected muonium substituted species. The theoretical investigation of selected isotope effects is based upon *ab initio* molecular orbital theory and has been applied to both a diamagnetic and paramagnetic muonic species. This study should aid in the elucidation of the large isotope effect observed in selected molecular properties on substitution of hydrogen by muonium. To complement these theoretical studies, this thesis reports experimental studies on the temperature and solvent dependence of the muon-electron β-hyperfine coupling constant of the 2-muoxyprop-2-yl radical and the regioselectivity of muonium addition to the $\alpha\beta$-unsaturated ketone, 3-methyl-2-butenal.

Chapter one introduces the fundamental properties of the positive muon and describes the different chemical states that can be formed on

muon implantation in matter. A brief outline follows of the different types of μSR spectroscopy that can be used to study muonic species. In later sections, the experimental and theoretical aspects of transverse field μSR (TF-μSR) spectroscopy are described in more detail, with particular reference to muonium substituted radicals. The theoretical treatment of the TF-μSR technique shows how it is possible to derive the magnitude of the muon-electron hyperfine coupling constant from the experimental μSR spectra. The final sections of this chapter are concerned with the analysis of μSR spectra and the methods that can be used to relate the experimental data to the radical's conformation and internal dynamics. In particular a theory of rotational averaging is outlined, which enables the temperature dependent muon-electron hyperfine coupling constant of the radical to be related to the barrier hindering internal rotation.

The second chapter reports the experimental results obtained from a TF-μSR study of the 2-muoxyprop-2-yl radical formed in propan-2-one:water mixtures and a propan-2-one:n-hexane mixture. These experiments investigate the solvent and temperature dependence of the muon-electron β-hyperfine coupling constant of the radical formed. Through application of the rotational averaging technique described in chapter one the solvent effects on the barrier to internal rotation of the 2-muoxyprop-2-yl radical have also been studied. This chapter also reports the first clear observation of competitive muonium addition to an αβ-unsaturated ketone. These results were obtained from a TF-μSR study of 3-methyl-2-butenal. From the resultant μSR spectra the muon-electron hyperfine coupling constants, of the radicals formed on muonium addition to this substrate, have been determined. A study of the temperature dependence of these couplings has enabled assignments of the radical

structures to be made. Further, the fractional rate constants for the formation of the different muonium substituted radicals have been determined from the experimental fractional radical polarizations.

Chapter three describes the principal aspects of *ab initio* molecular orbital theory that are used in the theoretical treatment of muonic isotope effects presented in this thesis. This treatment employs a variation-perturbation approach to the computation of vibrational corrections to *ab initio* molecular properties. The computed vibrational corrections enable a study of the effects of isotopic substitution on molecular properties to be performed. Chapters four and five report the results that are obtained from application of this technique to isotopic variants of the water molecule and the ethyl radical, respectively. The muonic isotopic variants of these species are extensively studied and where possible the theoretically computed results have been compared with experimental data obtained from μSR experiments. This investigation provides an insight into the origin of the large isotope effect that occurs on muonium substitution of hydrogen by muonium.

A brief summary of the results reported in this thesis and suggestions for further work are presented in chapter six.

CHAPTER 1

1 Aspects of Muonium Substituted Free Radical Chemistry

1.1 Introduction

Neddermeyer and Anderson first discovered the positive muon (μ^+) in 1937 from photographic studies of a cloud chamber exposed to cosmic rays [1]. The muon is a decay product of the lightest meson, the pion (π). In nature pions are formed when cosmic rays interact with the upper atmosphere. The positive pions formed in this interaction decay with a mean lifetime of 26 ns to create a positive muon, as observed by Neddermeyer and Anderson, and a muon-neutrino (ν_μ).

$$\pi^+ \longrightarrow \mu^+ + \nu_\mu \qquad (1.1)$$

The products of this decay process are members of the family of fundamental particles known as leptons. The elementary particles of the lepton family include the positive and negative muon (μ^+, μ^+); the positron and the electron (e^+, e^-); the neutrinos of these particles (ν_μ, $\overline{\nu}_\mu$, ν_e, $\overline{\nu}_e$) and the heavier tau-particles (τ^+, τ^-). The muon-neutrino (ν_μ) created in decay process (1.1) has negative helicity [2], that is, the spin of the μ^+-neutrino is parallel to its momentum but directed in the opposite sense. Therefore in order to conserve angular momentum the muon must also have negative helicity. Consequently positive muons produced through decay process (1.1) are spin polarized. The muon itself is a short-lived particle having a mean lifetime of 2.2 μs before decaying

through the three-body decay mechanism,

$$\mu^+ \longrightarrow e^+ + \nu_e + \bar{\nu}_\mu \qquad (1.2)$$

to form a positron (e^+), an electron-neutrino (ν_e) and a muon-antineutrino ($\bar{\nu}_\mu$). Selected physical properties of μ^+ are listed in Table 1.1, also presented are the corresponding properties of the positron and the proton (p^+) to allow comparison.

Table 1.1 Selected physical properties of the muon, positron and proton

Physical property [a]	μ^+	e^+	p^+
Spin / $\hbar$	1/2	1/2	1/2
Charge	+1	+1	+1
Mass / m_e	206.76865	1	1836.1527
Magnetic moment (μ) / J T^{-1}	4.490474×10^{-26}	9.284832×10^{-24}	1.410617×10^{-26}
g-factor	2.002331848	5.585690	2.0023192
Gyromagnetic ratio ($\gamma/2\pi$) / MHz T^{-1}	135.5374	28024.71	42.5771
Lifetime (τ) / s	2.19714×10^{-6}	—	—

[a] Ref. [3].

The positron formed in decay process (1.2) is emitted preferentially along the muon spin direction. This is a consequence of the conservation of energy, momentum and angular momentum. The asymmetry in the muon decay process enables several spectroscopic methods to be applied to the study of the local environment of muons implanted in matter. The

experimental techniques used to study the different chemical states of the muon in condensed matter are described collectively as muon spin rotation (μSR) spectroscopy. These techniques can be used to identify and study the three possible chemical states that are formed on muon implantation in condensed matter.

In this thesis the experimental studies performed have been concerned with the identification and measurement of the muon-electron β-hyperfine coupling constant (A_μ) of muonium substituted free radicals. Such radicals are produced from the implantation of positive muons in selected unsaturated organic substrates. Therefore in this chapter the experimental method used to study these species and the approaches used to analyse the experimental data are outlined.

1.2 Muon Production and Spectroscopy

The production of positive pions by the interaction of cosmic rays with the atmosphere can be simulated by directing high energy protons on a production target of carbon or beryllium. The threshold energy of the nuclear processes that produce the pions is about 180 MeV. Through mechanism (1.2) the positive pions decay either at rest, near the surface of the production target or in flight over a distance of several metres to produce a diffuse muon beam. Momentum selection of pions produced at the surface of the target enables a low momentum, completely spin polarized muon beam to be produced. This type of beam is known as a μ^+-surface beam or, for historical reasons, an Arizona beam. Alternatively the pions decay in flight, in a decay channel consisting of a long superconducting solenoid. Using a bending magnet the momenta of the muon beam produced can be selected. The μ^+-beam is then directed onto

the sample of interest using a series of quadrupole magnets.

In practice the momentum selection usually selects forward (P_μ parallel to P_π) or backward emitted (P_μ antiparallel to P_π) muons, where P_μ and P_π are the muon and pion momentum respectively. The forward and backward muons are chosen since they produce μ^+-beams with the largest possible spin polarization. The polarization of the beams is reduced by the limited resolution of the muon momentum by the beam optics. Consequently the polarization of the beam is further reduced by the spread in the angle ϑ, the angle between P_π and P_μ. Muon beams produced from pions decaying in flight typically reduce the spin polarization to 60-80 %.

The muon beam is further characterized according to the method used to produce the protons that collide with the production target. If the particle accelerator produces pulsed beams of protons, the resulting muon beam will be delivered in short bursts separated by a small time interval and is known as a pulsed muon beam. The second form of beam is produced from a continuous source of protons and is therefore termed a continuous muon beam. Both forms of μ^+-beam can be used to study the implantation of positive muons in matter using the different techniques of muon spin rotation spectroscopy. The current main centres of μSR spectroscopy are the Paul Scherrer Institute, (PSI, Switzerland), the Tri-Universities Meson Facility, (TRIUMF, Canada), Boom-KEK (Japan), the Los Alamos Meson Physics Facility, (LAMPF, USA), the Rutherford Appleton Laboratory, (RAL, UK) and the Russian facility at Dubna.

There are four principal forms of μSR spectroscopy, muon spin rotation, muon spin relaxation, muon spin resonance and avoided level crossing (ALC) resonance spectroscopy. In the first method a static

magnetic field is applied transversely to the muon spin direction and the resulting evolution of the muon spin direction is measured. The spin relaxation method measures the relaxation with time of the initial muon polarization in a longitudinally applied magnetic field. The muon spin resonance experiment also uses a longitudinally applied magnetic field but in addition applies a transverse radio (RF) frequency field. The resonance signal is observed as a decrease in the longitudinal asymmetry (A) as the field is varied. Where A is the difference in the number of decay positrons emitted in forward and backward directions relative to the initial muon spin direction. The decrease in the initial polarization is the result of a coupling of the transitions between different muon hyperfine states and the RF field. ALC is the most recent form of μSR spectroscopy, first proposed by Abragam in 1984 [4]. It is similar to the resonance experiment, but in ALC the observed reduction in polarization arises due to coupling of the hyperfine states of the muon with some other nuclear states rather than a RF field. The ALC technique has already been successfully applied at PSI, TRIUMF and RAL [5, 6, 7].

1.3 Chemical States of μ^+

1.3.1 Muonium

The formation of the different chemical states containing μ^+ in gaseous or condensed matter usually occurs before direct observation of the species using μSR. Through momentum selection the muons are stopped in the sample of interest, after which they interact with their medium during thermalization or shortly afterwards. The processes of thermalization are rapid on the muon timescale and are electronic in

origin, therefore having no affect on the initial muon polarization. The simplest possible chemical state of μ^+ is that of muonium (Mu), which is the bound state of a positive muon and an electron ($\mu^+ e^-$). Two possible methods for muonium formation have been proposed. In the first mechanism known as the hot atom model [8], Mu is formed during the period of thermalization. The alternative method of muonium formation is the spur model, which proposes that the muon binds with an electron after thermalization [9]. Due to the similarity in structure of muonium and atomic hydrogen, Mu is often considered to be an isotope of hydrogen. A comparison of the physical properties of muonium, hydrogen and deuterium are given in Table 1.2.

Table 1.2 Selected physical properties of muonium, hydrogen and deuterium [3, 10]

Property	Mu	H	D
Mass / m_H	0.1131	1.00	1.998
Ionization potential / eV	13.539	13.598	13.601
Bohr radius / pm	53.17	52.94	52.93
Hyperfine Coupling Constant / MHz	4463	1420	218
Lifetime / s	2.1971×10^{-6}	—	—

The ionization potential and Bohr radius of the three atoms are nearly identical. The small differences can be attributed to the difference in the centre-of-mass of each atom. The large mass difference between the different atoms implies that muonium can be considered to be light isotope of hydrogen.

1.3.2 Muonic Diamagnetic States

Diamagnetic states containing μ^+ can either be formed directly from the implanted muons or through interactions of muonium with the medium. One of the simplest possible diamagnetic states to consider is that of muonium substituted water. The formation of this state is thought to occur by a two stage process [9].

$$H_2O + \mu^+ \rightarrow H_2OM\dot{u}^+ \qquad (1.3)$$

$$H_2OM\dot{u}^+ + H_2O \rightleftarrows MuOH + H_2O \qquad (1.4)$$

In liquids, such as water, it is often found that the majority of the muons form such diamagnetic states. The earlier forms of μSR spectroscopy were unable to distinguish between free μ^+ and muons in diamagnetic environments or to characterize the different possible diamagnetic states. The first successful assignment of μ^+ in a diamagnetic state was recently made by Cox et al. using the technique of avoided level crossing resonance μSR [7, 11].

1.3.3 Muonium Substituted Radicals

The third possible chemical state of the implanted muon is formed by the formal addition of muonium to an unsaturated organic substrate. The paramagnetic species formed is described as a muonium substituted free radical. Such radicals have been extensively studied since their first direct observation using the technique of transverse field muon spin rotation spectroscopy [12, 13]. This technique has been successfully applied to

the study of conformational analysis, kinetic isotope effects and regioselectivity of muonium addition for a wide range of organic free radicals [14, 15, 16, 17]. The wide applications of these studies has led to several comprehensive reviews [18, 19, 20] and one book [10] on the subject.

The mechanism of formation of muonium substituted radicals has also been extensively studied [21, 22]. There are several different possible mechanistic routes that lead to the formation of these radicals. Some possible formation schemes are the direct addition of hot or thermal muonium or the abstraction of an electron from its surroundings by a μ^+ diamagnetic precursor. The formation of muonium substituted radicals has led to the possibility of studying radicals for which the analogous protonated species have not been observed [23].

1.4 Transverse Field Muon Spin Rotation (TF-μSR) Spectroscopy

1.4.1 Experimental Aspects

All experimental observations reported in this thesis were carried out at the Paul Scherrer Institute, Villigen, Switzerland using the technique of transverse field muon spin rotation spectroscopy. At PSI a pion flux of 2×10^{-9} πs^{-1} is produced by focusing high energy protons (ca. 590 eV) onto a beryllium production target. The positive pions produced from the resultant nuclear interactions decay in flight, along an 8 m superconducting solenoid. Backward decay muons with a momentum of about 115 MeV/c and a spin polarization of around 70 % in the forward direction are selected for implantation in the sample. The continuous muon beam directed onto the sample has a muon flux of approximately

10^7 $\mu^+ s^{-1}$. The sample (S) to be studied is placed at the centre of the μSR spectrometer which consists principally of a pair of Helmholtz coils which can produce a magnetic field (B) of between 0 and 0.6 T and a series of scintillation counters positioned about the sample. A schematic representation of the μSR spectrometer is given in Figure 1.1.

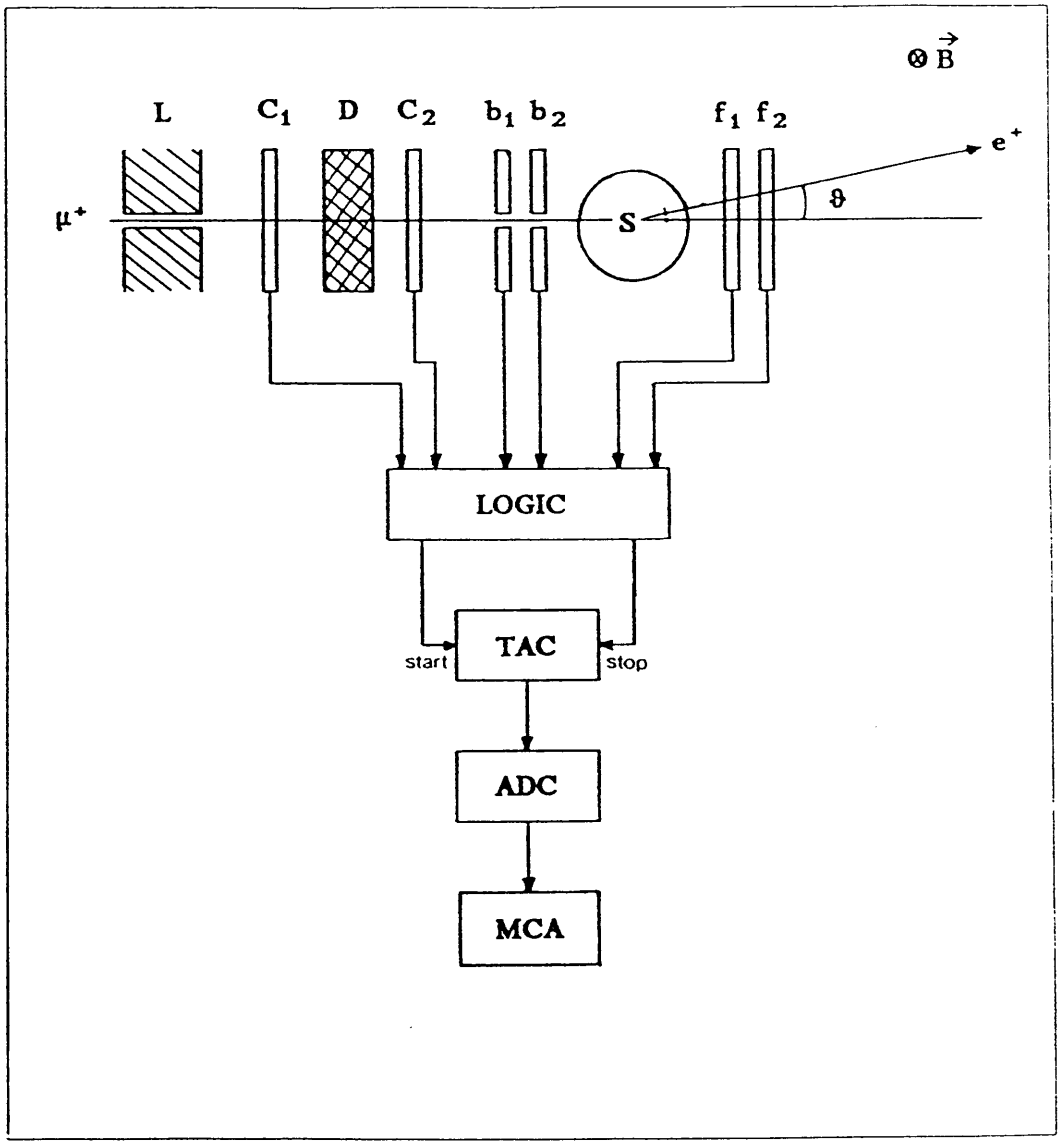

Figure 1.1 Schematic representation of the TF-μSR spectrometer at PSI.

The muons implanted in the sample decay according to equation (1.2). As mentioned previously the positron emission is an asymmetric process. The angular distribution, $P(\vartheta)$, of the positron intensity is expressed by the relationship

$$P(\vartheta) = 1 + \tilde{a}\cos\vartheta \qquad (1.5)$$

where ϑ is the angle between the muon spin direction and the direction of the emitted positron and $\tilde{a}$ is an asymmetry factor. The asymmetry factor is dependent upon the energy of the emitted positrons and has a maximum value of one for positrons emitted with the highest possible energy. For the μSR experiment the asymmetry factor has a value of $\sim 1/3$ as a consequence of averaging over all possible positron energies. This asymmetry in the muon decay enables any change in the initial muon spin polarization through interactions with an externally applied magnetic field, or local magnetic fields to be observed. The evolution of the muon polarization is followed by counting the number of decay positrons detected at a fixed value of ϑ.

The essential features of the TF-μSR technique are that initially the incident μ^+-beam passes through a lead collimator (L) which reduces the beam to the desired diameter (15-20 mm). The muons are then slowed down by passage through a polyethylene window at the end of the beam line and a degrader (D) of water or polyethylene. The thickness of the degrader D can be adjusted to maximise the number of muons stopped in the sample. The particle detectors used to detect the incoming muons (C_1, C_2) and the emitted positrons (f_1, f_2, b_1, b_2) comprise scintillators, lightguides and photomultiplier tubes. There are actually two other sets of detectors used to detect emitted positrons located above and below

the sample which are not shown in Figure 1.1 for reasons of clarity. The time difference between the arrival of each muon and the detection of its emitted positron is determined from the electrical-pulses triggered by the passage of a particle through the detectors. This form of counting is described as a muon-positron coincidence counting method and each time interval is known as an event. This technique ensures that the signal arising from an emitted positron can be associated with its parent muon. A limitation of this technique is that it necessitates the presence of only a single muon in the sample at any instant and is therefore a single particle counting technique. The counting of the events is controlled by complex electronic logic circuits which also distinguish between good and bad events. A good event corresponds to the time interval between the arrival of the muon and the detection of the associated emitted positron. A bad event can result from the arrival of a second muon before the positron corresponding to the initial muon has been detected or some other such spurious event. The electronic signals corresponding to good events are passed, to a time to amplitude converter (TAC), an analogue to digital converter (ADC), and finally to a multichannel analyser (MCA). The MCA is a storage device which records a histogram relating the number of events detected (H) with time. The time scale of the histogram is usually divided into time bins (or channels), the bin width is dependent on the signal or signals under examination.

If there is no externally applied magnetic field the recorded histogram for each counter will display a single exponential that decays with the muon lifetime τ_μ . In a transversely applied magnetic field the spin vector of the muon will precess at its Larmor frequency, $\nu = 135.537$ MHz T^{-1}, and this precession will be superimposed onto the lifetime histogram with a phase dependent on the position of each counter as

shown in Figure 1.2.

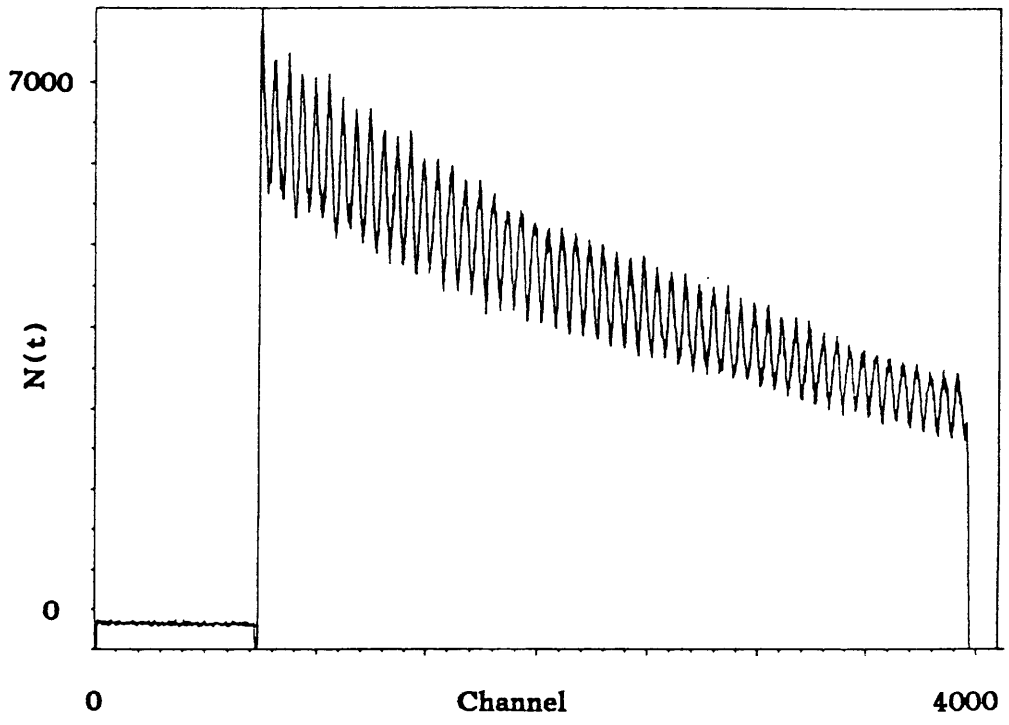

Figure 1.2 μSR histogram of the muonium substituted radical formed by muon implantation in liquid propan-2-one.

In a transverse field the general form of the histogram is given by [24, 25],

$$H(t) = N_o \exp(-t/\tau_\mu)\,[1 + F(t)] + BG \qquad (1.6)$$

where N_o is a normalization factor dependent upon the total number of counts , BG arises from the accidental background fraction and F(t) expresses the time dependence of the muon spin polarization. F(t) is summed over each different muon state, j ,within the sample and the frequencies associated with each state. The general form of F(t) is

$$F(t) = \sum_j F_j(t) = \sum_j A_j \exp(-\lambda_j t) \cos(\omega_j t + \vartheta_j) \qquad (1.7)$$

where A_j is the asymmetry, dependent upon the beam polarization, the asymmetry coefficient $\tilde{a}$ and other experimental factors, ω_j is the precession frequency, λ_j is a damping constant and ϑ_j is the initial phase. λ_j is a measure of the rate of depolarization and can reflect reactions or relaxation process. Analysis of the experimental data is carried out by firstly transforming the μSR histogram into Fourier space [26] and then fitting the resultant signals to the theoretical expression (1.6) using the MINUIT [27] fitting procedure, enabling the determination of the parameters A_j, λ_j, ω_j and ϑ_j. A Fourier transformed μSR histogram is displayed in Figure 1.3 and shows clearly the characteristic frequencies of a muonium substituted radical.

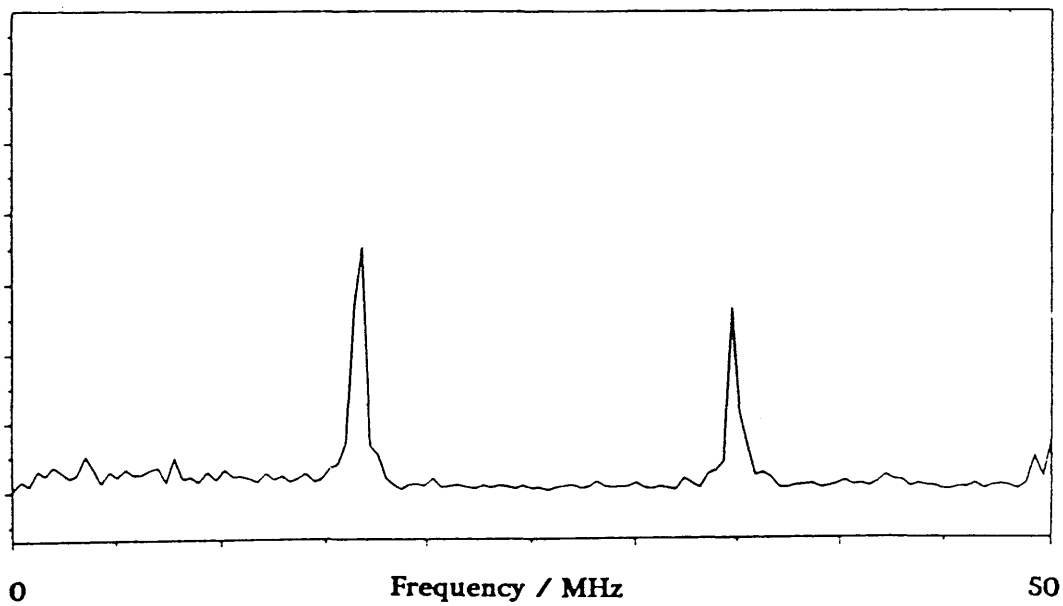

Figure 1.3 Fourier transformed μSR spectrum of the muonium substituted radical formed in liquid propan-2-one.

All experiments performed in this work were carried out using liquid samples. The liquids were prepared by degassing using a series of freeze-pump-thaw cycles on a vacuum line to remove dissolved oxygen which would otherwise have a depolarizing effect. The samples were then sealed, under vacuum, in thin-walled spherical glass bulbs, 25-35 mm in diameter. All samples were of the highest grade of purity commercially available. For experiments where it was necessary for the sample temperature to be varied a cryostat was employed. The sample was placed in the insulated cryostat which enabled the temperature to be lowered by the control of a flow of cold N_2 gas or raised using an electrical resistance. The temperature of the samples could be monitored at all times using two thermocouples attached to the sample bulb. The number of good events recorded for each experiment was about 5×10^7, requiring approximately two hours of continuous beam time. The number of events can be varied depending on the position and strength of the signals being studied. At PSI the μSR spectrometer has available about 8000 bins, which are divided equally amongst the four detectors. The width of the bins is selected according to the time or frequency resolution required. The upper and lower limits of observable TF-μSR frequencies are constrained by several experimental limiting factors. The lowest frequency is restricted to the order of 100 KHz by the time interval of the data gate. Where the data gate is the time interval allowed to elapse for the detection of a good event before the electronic circuitry is reset. The data gate usually extends over several muon lifetimes (~ 10 μs). The highest frequency to be resolved is dependent upon the time resolution of the intrinsic electronics which limits the highest frequencies to several hundred MHz.

The μSR experiments at PSI were controlled and the data collected

using a DEC computer system. The collected data were then transferred to a DEC VAX 8650 for complete analysis, involving transformation of the histograms into Fourier space and fitting of the frequency signals to the theoretical form H(t) using the MINUIT fitting routine. A number of books [28, 29, 30] and several papers [31, 32, 33] have comprehensively reported the theoretical and experimental aspects of transverse field μSR.

1.4.2 Theoretical Background to TF-μSR

The evolution of the muon spin polarization is dependent upon the magnetic state of the muon after implantation within the sample. Magnetic interactions between the muon and internally generated or externally applied magnetic fields, or a combination of both, determine the observed evolution of the polarization. For muonium substituted radicals formed in the liquid phase, which are the principal species of interest in this thesis, the spin Hamiltonian describing the magnetic interactions experienced by the muon is

$$\hat{H} = \hat{H}_z^{\mu} + \hat{H}_z^{e} + \sum_i \hat{H}_z^{i} + \hat{H}_{\mu e} + \sum_i \hat{H}_{\mu i} + \sum_i \hat{H}_{ei} \qquad (1.8)$$

where the first three terms are the Zeeman terms representing the interaction of the muon, the unpaired electron and the magnetic nuclei with a magnetic field. The remaining terms are the Fermi contact interactions arising from the coupling between the different magnetic species present within the system. The expression neglects the negligably small internuclear term, $\sum_{ij} \hat{H}_{ij}$. The form of the Hamiltonian presented assumes that the radical can be considered to be an isolated species and therefore neglects all intermolecular interactions. Further, due to the

rapid tumbling motions experienced by the radical in the liquid phase, the direct dipole-dipole interactions average to zero and are also neglected in equation (1.8).

The Hamiltonian is more usually written in the form

$$\hat{H} = \omega_e \hat{S}_z - \omega_\mu \hat{I}_z^\mu - \sum_i \omega_i \hat{I}_z^i + A_\mu \hat{S}.\hat{I}^\mu + \sum_i A_i \hat{S}.\hat{I}^i \qquad (1.9)$$

where it is assumed that the radical is in a non-viscous liquid and experiences an applied field B, in the z-direction. The Zeeman interactions are expressed in terms of the Larmor precession frequencies, ω_e, ω_μ and ω_i, of the muon , the electron and the i^{th} nuclei respectively and the spin operators, $\hat{S}_z$, $\hat{I}_z^\mu$ and $\hat{I}_z^i$, of each of these particles. The Fermi contact terms have been rewritten in terms of the hyperfine coupling constants A_μ and A_i and the corresponding spin operators. The hyperfine coupling constants provide a measure of the unpaired electron spin density at the site of the muon and the magnetic nuclei. For magnetic fields of about 0.02 T the coupling between the nuclei and the unpaired electron becomes very small [32] and the Hamiltonian is simplified to

$$\hat{H} = \omega_e \hat{S}_z - \omega_\mu \hat{I}_z^\mu - \sum_i \omega_i \hat{I}_z^i + A_\mu \hat{S}.\hat{I}^\mu \qquad (1.10)$$

The above Hamiltonian is used to describe the magnetic interactions experienced by a muon in a muonium substituted radical under a high transverse magnetic field.

1.4.3 Evolution of Muon Spin Polarization under a Transverse Magnetic Field

The theoretical method for evaluating the evolution of the muon spin polarization with time in different chemical states has been developed by several authors [31, 32, 34, 35, 36], in particular for muonium substituted radicals by Roduner and Fischer [31, 32]. A short outline of the theoretical description of muonium substituted radicals in transverse magnetic fields is presented here. It is assumed in this description that the timescale for radical formation is short compared to the inverse of the hyperfine and Zeeman interaction frequencies. This assumption implies that there is no loss of polarization during radical formation and that the initial polarization of the radical system is equivalent to the beam polarization P.

The evolution of the spin polarization is detected in an arbitrary direction q defined by the observation axis of the positron detector. The observed polarization is defined as the expectation value of the Pauli spin operator $\hat{\sigma}_q$ [37, 38].

$$P_q(t) = \langle \hat{\sigma}_q \rangle \tag{1.11}$$

The polarization can also be expressed as a Heisenberg expression in terms of the density operator $\hat{\rho}(0)$ of the system

$$P_q(t) = Tr\{\hat{\rho}(0).\ \hat{\sigma}_q(t)\} \tag{1.12}$$

where $\hat{\sigma}_q(t)$ has the form [38],

$$\hat{\sigma}_q(t) = \exp(i\hat{H}t/h)\hat{\sigma}_q\exp(-i\hat{H}t/h) \qquad (1.13)$$

and $\hat{H}$ is the spin Hamiltonian given by expression (1.9). Equation (1.12) can therefore be evaluated directly using the eigenfunctions $|n\rangle$ of $\hat{H}$, which are linear combinations of product spin functions.

$$|n\rangle = \sum_j c_{nj}|\chi_j\rangle \qquad (1.14)$$

where $|\chi_j\rangle$ represents a basis of product spin functions

$$|\chi_j\rangle = |\chi_j{}^{\mu}\rangle\,|\chi_j{}^{e}\rangle \prod_i |\chi_j{}^{i}\rangle \qquad (1.15)$$

Using the formulation of Roduner and Fischer [32], which essentially assumes that the electron and nuclei are unpolarized and uncoupled from the muon, $\hat{\rho}(0)$ is then expressed in a basis corresponding to quantization of spins in the direction of the beam polarization b.

$$\begin{aligned}\hat{\rho}(o) &= \hat{\rho}^{\mu}(0) \otimes \hat{\rho}^{e}(0) \otimes \prod_i \hat{\rho}^{i}(0) \\ &= 1/2\begin{pmatrix} 1+P & 0 \\ 0 & 1-P \end{pmatrix} \otimes \frac{1}{2}1^{e} \otimes \prod_i \frac{1}{2I^i+1}1^{i}\end{aligned} \qquad (1.16)$$

and $\hat{\sigma}_q$ is expressed in a basis corresponding to quantization along q, the axis of observation.

$$\begin{aligned}\hat{\sigma}_q &= \hat{\sigma}_q^{\mu} \otimes \hat{\sigma}^e \otimes \prod_i \hat{\sigma}_q^i \\ &= \begin{pmatrix} 1 & 0 \\ 0 & 1 \end{pmatrix} \otimes 1^e \otimes \prod_i 1^i \end{aligned} \tag{1.17}$$

Taking

$$\hat{\sigma}_b = \begin{pmatrix} 1 & 0 \\ 0 & -1 \end{pmatrix} \tag{1.18}$$

and

$$N = 4 \prod_i (2I^i + 1) \tag{1.19}$$

Then equation (1.16) can be written as

$$\hat{\rho}(0) = N^{-1}\left\{ 1^{\mu} + P.\hat{\sigma}_b \right\} \otimes 1^e \otimes \prod_i 1^i \tag{1.20}$$

The expression obtained by substituting (1.20) into (1.12) and noting that $Tr(\hat{\sigma}_q) = 0$ leads to an easily evaluated expression for $P_q(t)$.

$$\begin{aligned} P_q(t) &= Tr\left\{ N^{-1}\hat{\sigma}_q(t) + N^{-1}P\hat{\sigma}_b\hat{\sigma}_q(t) \right\} \\ &= \frac{P}{N} Tr\left\{ \hat{\sigma}_b.\hat{\sigma}_q(t) \right\} \end{aligned} \tag{1.21}$$

For the case of a transverse magnetic field b=q=x and therefore (1.21) becomes

$$P_q(t) = \frac{P}{N} \mathrm{Tr} \left\{ \hat{\sigma}_q \ \hat{\sigma}_q(t) \right\} \tag{1.22}$$

As $\hat{H}$ and $\hat{\sigma}_q$ are Hermitian operators and if $|m\rangle$ and $|n\rangle$ are orthonormal eigenvectors of $\hat{H}$ with eigenvalues $h\omega_m$ and $h\omega_n$ respectively; equation (1.22) can be expressed as

$$P_q(t) = \frac{P}{N} \sum_m \sum_n \langle m|\hat{\sigma}_q \hat{\sigma}_q(t)|n\rangle \tag{1.23}$$

Substituting expression (1.13) into (1.23)

$$P_q(t) = \frac{P}{N} \sum_m \sum_n \langle m|\hat{\sigma}_q \exp(i\hat{H}t/\hbar)\hat{\sigma}_q \exp(-i\hat{H}t/\hbar)|n\rangle$$

$$= \frac{P}{N} \sum_m \sum_n |\langle m|\hat{\sigma}_q|n\rangle|^2 \exp(i\omega_{mn}t) \tag{1.24}$$

Since $P_q(t)$ is an observable property

$$P_q(t) = \frac{P}{N} \sum_m \sum_n |\langle m|\hat{\sigma}_q|n\rangle|^2 \cos(\omega_{mn}t) \tag{1.25}$$

by expressing the eigenfunctions $|m\rangle$ and $|n\rangle$ in terms of the basis spin functions (1.14) and assuming that the magnetic field is applied transversely (q=b=x), then

$$\langle m|\hat{\sigma}_x|n\rangle = \sum_j \sum_k c^*_{mj} c_{nk} \langle \chi_j|\hat{\sigma}_x|\chi_k\rangle \tag{1.26}$$

and since $\hat{\sigma}_x$ is a muon spin operator

$$\langle m | \hat{\sigma}_x^{\mu} | n \rangle = \sum_j \sum_k c_{mj}^* c_{nk} \langle \chi_j^{\mu} | \hat{\sigma}_x^{\mu} | \chi_k^{\mu} \rangle \delta_{jk}^{e} \prod_i \delta_{jk}^{i} \qquad (1.27)$$

Therefore the final expression for the evolution of the muon spin polarization in a transverse magnetic field is obtained by substitution of equation (1.27) into (1.25) to give

$$P_x(t) = \frac{P}{N} \sum_m \sum_n \left| \sum_j \sum_k c_{mj}^* c_{nk} \langle \chi_j^{\mu} | \hat{\sigma}_x^{\mu} | \chi_k^{\mu} \rangle \delta_{jk}^{e} \prod \delta_{jk}^{i} \right|^2 \cos(\omega_{mn} t) \qquad (1.28)$$

Experimental studies of muonium substituted radicals using the technique of transverse field μSR have indicated that there is incomplete transfer of the initial beam polarization to the chemical states formed on muon implantation [9, 16, 39]. The lost polarization, P_L, is defined as

$$P_L = 1 - P_D - \sum_R P_R \qquad (1.29)$$

where P_D is the fraction of the polarization corresponding to muons in diamagnetic environments and $\sum_R P_R$ is the fraction corresponding to muons in muonium substituted radicals. It has been proposed that in aqueous systems the lost polarization is a consequence of spin exchange processes occuring between muonium formed within 1 ps of muon implantation and paramagnetic species in the radiation spur caused by the passage of the energetic muon through the medium [9, 39]. It has however been recently shown that the lost polarization observed in certain TF-μSR experiments can be accounted for using the level crossing resonance μSR [40]. These results indicate that the loss of spin

polarization is not through a spin-exchange mechanism but provide no explanation as to loss of polarization observed in the corresponding TF-μSR results.

1.4.4 Selection Rules for μSR Transitions

From equation (1.28) it can clearly be seen that contributions to the muon polarization arise only from transitions between the states $|m\rangle$ and $|n\rangle$ corresponding to product spin functions $|\chi_j\rangle$ and $|\chi_k\rangle$ of the form of (1.15). It is also obvious from this expression that these spin functions differ in the muon but not in the electron or nuclear components. For low to intermediate transverse magnetic fields the Hamiltonian (1.9) mixes eigenfunctions of equal total magnetic quantum number M, $M = m^{\mu} + m^{e} + \sum_{i} m^{i}$, which leads immediately to the μSR selection rule.

$$\Delta M = \pm 1 \tag{1.30}$$

Alternatively this selection rule can be derived through consideration of the intensities of the transitions. The amount of muon polarization associated with a frequency ω_{mn}, corresponding to the intensity of the transition, is proportional to the transition moment $|\langle m|\hat{\sigma}_q|n\rangle|^2$. For the case of a transversely applied magnetic field (q=x)

$$\hat{\sigma}_x = 1/2\,(\sigma^+ + \sigma^-) \tag{1.31}$$

which implies that the transition is non-zero only when the total

magnetic moment of the states $|m\rangle$ and $|n\rangle$ obeys the selection rule (1.30).

As the experimental results reported in this thesis are mainly concerned with the study of muonium substituted radicals in high transverse magnetic fields it is important to consider the selection rules applicable to these species. In a high transverse field ($|B| \geq 0.02$ T) the eigenfunctions $|m\rangle$ and $|n\rangle$ become pure spin product functions since the spins of the muon, the electron and the magnetic nuclei are effectively decoupled. Therefore the coefficients of (1.14) are usually one or zero and the states are then characterized by the magnetic quantum numbers m^{μ}, m^{e} and all m^{i}. Hence from equation (1.28) it follows that the selection rules for muonium substituted species in high transverse magnetic fields are

$$\Delta m^{\mu} = \pm 1, \quad \Delta m^{e} = 0, \quad \Delta m^{i} = 0 \qquad (1.32)$$

A more complete description of the theory of TF-μSR for a general paramagnetic muonium substituted species in a high transverse magnetic field is given in the next section.

1.5 High Transverse Fields: Muonium and Muonium Substituted Radicals

1.5.1 Muonium

The simplest paramagnetic species that can be considered is that of muonium. The Hamiltonian describing the magnetic interactions of this system under a transversely applied magnetic field is

$$\hat{H} = \omega_e \hat{S}_z - \omega_\mu \hat{I}_z + A_\mu \hat{S}.\hat{I} \qquad (1.33)$$

where it is assumed that the field is applied along the z-direction and that $\hat{S}$ and $\hat{I}$ are the electron and muon spin operators, respectively. The hyperfine coupling term can be expressed in terms of raising and lowering operators.

$$\hat{S}.\hat{I} = 1/2\,(\hat{S}^+\hat{I}^- + \hat{S}^-\hat{I}^+) + \hat{S}_z\hat{I}_z \qquad (1.34)$$

where

$$\begin{aligned} \hat{S}^+ &= \hat{S}_x + i\hat{S}_y \\ \hat{S}^- &= \hat{S}_x - i\hat{S}_y \end{aligned} \qquad (1.35)$$

and similar expressions are used for $\hat{I}^+$ and $\hat{I}^-$. The Hamiltonian can be rewritten as

$$\hat{H} = \omega_e \hat{S}_z - \omega_\mu \hat{I}_z + A_\mu [1/2(\hat{S}^+\hat{I}^- + \hat{S}^-\hat{I}^+) + \hat{S}_z\hat{I}_z] \qquad (1.36)$$

which is solvable using the eigenfunctions of the spin operators $\hat{S}_z$ and $\hat{I}_z$ as initial basis functions.

$$|\alpha_\mu \alpha_e\rangle,\ |\alpha_\mu \beta_e\rangle,\ |\beta_\mu \alpha_e\rangle,\ |\beta_\mu \beta_e\rangle \tag{1.37}$$

The resulting eigenenergies of (1.36) are

$$\begin{aligned} E_1 &= \omega_- + A_\mu/4 \\ E_2 &= (\omega_+^2 + A_\mu^2/4)^{1/2} - A_\mu/4 \\ E_3 &= -\omega_- + A_\mu/4 \\ E_4 &= -(\omega_+^2 + A_\mu^2/4)^{1/2} - A_\mu/4 \end{aligned} \tag{1.38}$$

where

$$\omega_{\pm} = 1/2(\omega_e \pm \omega_\mu) \tag{1.39}$$

The eigenfunctions corresponding to these eigenenergies are,

$$\begin{aligned} |1\rangle &= |\alpha_\mu \alpha_e\rangle \\ |2\rangle &= S|\alpha_\mu \beta_e\rangle + C|\beta_\mu \alpha_e\rangle \\ |3\rangle &= |\beta_\mu \beta_e\rangle \\ |4\rangle &= C|\alpha_\mu \beta_e\rangle - S|\beta_\mu \alpha_e\rangle \end{aligned} \tag{1.40}$$

here

$$\begin{aligned} S &= 1/\sqrt{2}\,[1 - 2\omega_+/(A_\mu^2 + 2\omega_+^2)^{1/2}]^{1/2} \\ C &= 1/\sqrt{2}\,[1 + 2\omega_+/(A_\mu^2 + 2\omega_+^2)^{1/2}]^{1/2} \end{aligned} \tag{1.41}$$

Using the eigenenergies (1.38) and the selection rule (1.32) the allowed μSR transition frequencies of muonium are

$$\begin{aligned}
\omega_{12} &= E_1 - E_2 = \omega_- - (\omega_+^2 + A_\mu^2/4)^{1/2} + A_\mu/2 \\
\omega_{23} &= E_2 - E_3 = \omega_- + (\omega_+^2 + A_\mu^2/4)^{1/2} - A_\mu/2 \\
\omega_{14} &= E_1 - E_4 = \omega_- + (\omega_+^2 + A_\mu^2/4)^{1/2} + A_\mu/2 \\
\omega_{34} &= E_3 - E_4 = -\omega_- + (\omega_+^2 + A_\mu^2/4)^{1/2} + A_\mu/2
\end{aligned} \tag{1.42}$$

The variation of the energy levels of muonium with magnetic field strength is displayed in Figure 1.4, in the form of a Breit-Rabi diagram [41]. The four allowed transitions are marked on the Figure. In low fields only the ω_{12} and ω_{23} transitions are observed and are effectively degenerate. The frequencies of the ω_{14} and ω_{34} transitions are too large to be easily resolved over all field strengths.

1.5.2 Muonium Substituted Radicals

In the case of muonium substituted radicals the unpaired electron couples with a number of other magnetic nuclei in addition to coupling with the muon. The spin Hamiltonian describing the magnetic interactions of the radical is

$$\hat{H} = \omega_e \hat{S}_z - \omega_\mu \hat{I}_z + A_\mu \hat{S}.\hat{I} - \sum_i \omega_i \hat{I}_z^i + \sum_i A_i \hat{I}^i.\hat{S}^i \tag{1.43}$$

where $\hat{I}^i$ is the nuclear spin operator and A_i is the nucleus-electron hyperfine coupling constant. At high transverse fields the nuclear

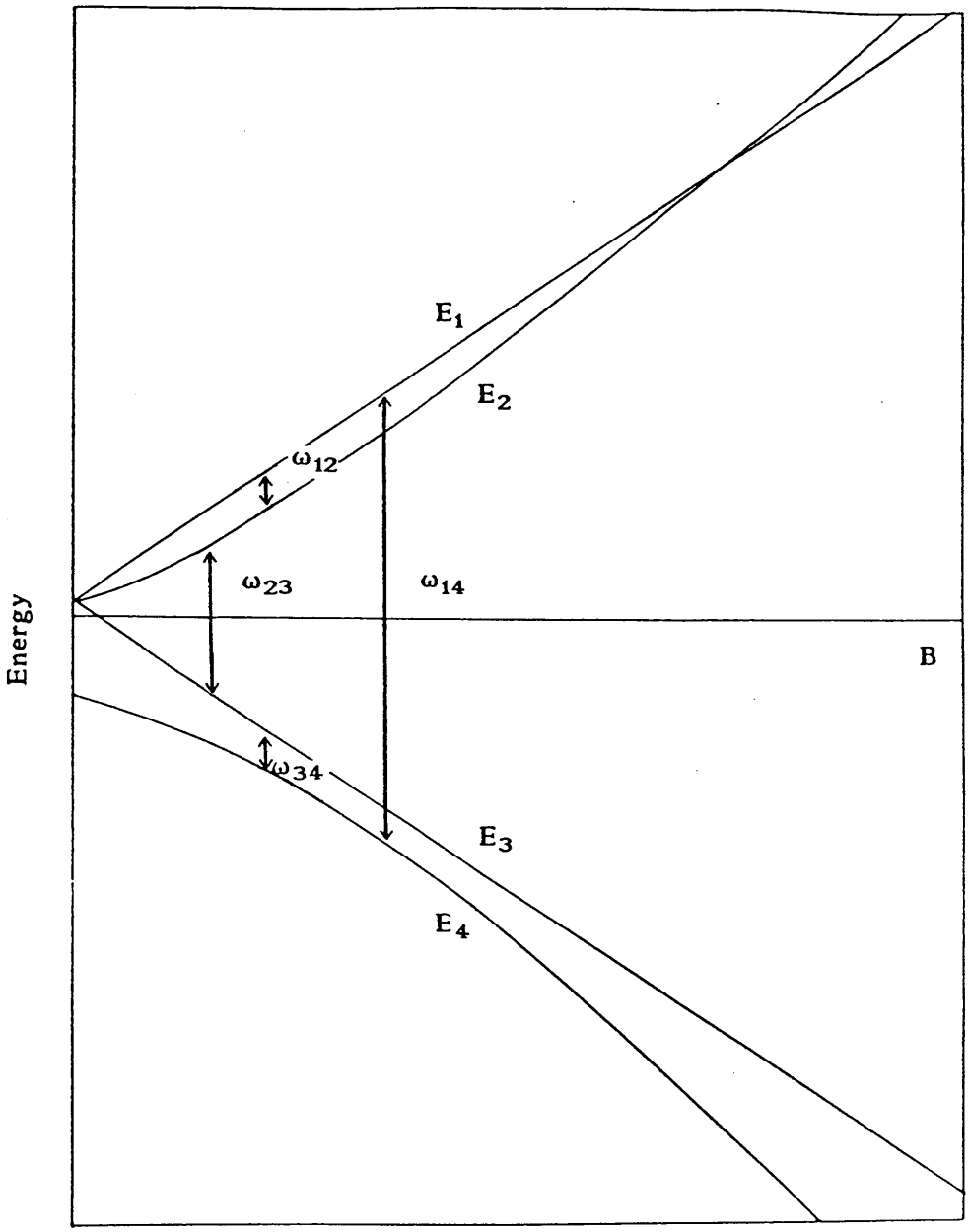

Figure 1.4 Breit-Rabi diagram for muonium.

interactions are small and can therefore be treated as a perturbation of the zero-order Hamiltonian.

$$\hat{H}^{(0)} = \omega_e \hat{S}_z - \omega_\mu \hat{I}_z + A_\mu \hat{S}.\hat{I} \qquad (1.44)$$

which is the spin Hamiltonian describing the interactions of the muon and the electron and is equivalent to the muonium Hamiltonian (1.33). Using as an initial basis set the spin product functions

$$\begin{aligned} &|\alpha_\mu \alpha_e\rangle \prod_i |F_i M_i\rangle, \quad |\alpha_\mu \beta_e\rangle \prod_i |F_i M_i\rangle \\ &|\beta_\mu \beta_e\rangle \prod_i |F_i M_i\rangle, \quad |\beta_\mu \alpha_e\rangle \prod_i |F_i M_i\rangle \end{aligned} \qquad (1.45)$$

where F_i and M_i are spin quantum numbers used to characterize the spin states of nucleus i, it is possible to determine the first-order eigenenergies.

$$\begin{aligned} E_1^{(1)} &= 1/2 \sum_i A_i M_i - \sum_i \omega_i M_i \\ E_2^{(1)} &= 1/2 \sum_i A_i M_i (C^2 - S^2) - \sum_i \omega_i M_i \\ E_3^{(1)} &= -1/2 \sum_i A_i M_i - \sum_i \omega_i M_i \\ E_4^{(1)} &= -1/2 \sum_i A_i M_i (C^2 - S^2) - \sum_i \omega_i M_i \end{aligned} \qquad (1.46)$$

where the terms C and S are defined as in equation (1.41). The first-order corrected allowed μSR transition frequencies are therefore.

$$\begin{aligned}
\omega_{12} &= \omega_{12}^{Mu} + S^2 \sum_i A_i M_i \\
\omega_{23} &= \omega_{23}^{Mu} + C^2 \sum_i A_i M_i \\
\omega_{14} &= \omega_{14}^{Mu} + C^2 \sum_i A_i M_i \\
\omega_{34} &= \omega_{34}^{Mu} + S^2 \sum_i A_i M_i
\end{aligned} \qquad (1.47)$$

here ω_{12}^{Mu}, ω_{23}^{Mu}, ω_{14}^{Mu} and ω_{34}^{Mu} are the transition frequencies observed in muonium and can be expressed by equations (1.42). In high transverse magnetic fields of about 0.02 T Roduner and Fischer [32] have shown that second-order corrections to the eigenenergies and transition frequencies are small and can be neglected.

In the high magnetic fields used in TF-μSR experiments only two transitions ω_{12} and ω_{34} are observed. This is a consequence of the intensities of the transitions ω_{12} and ω_{34} being proportional to C^2; since $C \rightarrow 1$ and $S \rightarrow 0$ as $B \rightarrow \infty$ only ω_{12} and ω_{34} are observed. The μSR spectrum of a muonium substituted radical in a high transverse field is therefore characterized by two precession signals as shown in Figure 1.3. The muon-electron hyperfine coupling constant, A_μ, can be derived from the observed frequencies using the relationship

$$|A_\mu| = |\omega_{12}| \pm |\omega_{34}| \qquad (1.48)$$

The negative sign in this equation applies to fields above $|B| = 3.672|A_\mu|$ mT [42] due to the crossing of the E_1 and E_2 energy levels. A direct comparison of the muon-electron coupling constant, A_μ, and the analogous proton-electron coupling constant, A_p, can be made by considering the reduced hyperfine coupling constatnt A_μ^* . A_μ^* is defined as the observed muon-electron coupling scaled by the ratio of the muon and proton magnetic moments, ($A_\mu^* = A_\mu \times \mu_p / \mu_\mu$).

1.6 Conformational and Internal Rotation Studies of Muonium Substituted Radicals

1.6.1 Analysis of μSR Spectra

For muonium substituted radicals formed in the liquid phase it is implicitly assumed that the intermolecular radical-solvent interactions are small with respect to the intramolecular interactions. In the analysis of the μSR spectra of muonium substituted radicals the intermolecular interactions are neglected and it is therefore assumed that the radical can be treated as an isolated species. Each good event recorded in a TF-μSR histogram corresponds to the detection of a single radical in the sample. The restriction to the presence of a single radical in the sample is imposed by the single counting detection method used in TF-μSR. The sum over each of the transient radicals formed on muon implantation is equivalent to the standard canonical ensemble. This model is supported by the wide success of TF-μSR in the study of muonium substituted radicals in the liquid phase.

To understand the analysis of the data obtained from the μSR experiments presented in this thesis it is necessary to consider the effects of nuclear motions on observed molecular properties, in particular the muon-electron hyperfine coupling constant. The effect of the vibrational motion of the nuclei in a molecule on molecular properties is the subject of later chapters. In this section the influence of internal rotation on molecular properties is considered. Internal motions are normally described in terms of internal coordinates; which are the bond lengths, bond angles and torsion angles used to specify the conformation of the radical. Two classes of internal motions are possible. The first

class known as small amplitude motions involve small displacements of the internal coordinates from their equilibrium values. Typical small amplitude motions are bond stretching and angle bending. The second type of internal motion arises from large amplitude motions which result in large deviations of the internal coordinates from their values at the equilibrium conformation of the radical. Torsional and inversion motions are examples of large amplitude motions.

At the temperatures at which TF-μSR data are usually obtained there is a Boltzmann distribution among the radical's vibrational manifold. Transitions between vibrational states of the radical are rapid on the μSR timescale. Therefore any observed property of the radical will be averaged over the populated vibrational states. These vibrational states include both the large and small amplitude motions of the radical. For certain muonium substituted radicals the observed muon-electron coupling is strongly isotope dependent [14, 43, 44]. ESR studies of alkyl radicals show a similar temperature dependence in the β-hyperfine coupling [45]. This temperature dependence must arise from the difference in the populations of the vibrational states at the different temperatures studied.

1.6.2 Temperature Dependence of the β–Hyperfine Coupling Constant

It is believed that the principal internal motion governing this temperature dependence is the large amplitude torsional motion about the central bond at which muonium substitution occurs. This motion is illustrated for the muonium substituted ethyl radical in Figure 1.5.

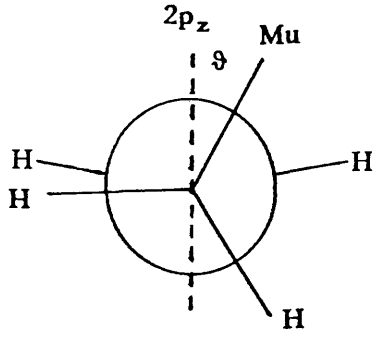

Figure 1.5 Newman projection of the muonium substituted ethyl radical.

where ϑ is the torsion angle between the C - Mu bond and the z-axis of the $2p_z$ orbital centred on the α-carbon. The torsional motion is described by considering the variation of ϑ, while keeping the remaining internal coordinates fixed. Muonium substitution occurs at the β-carbon and the torsional motion of interest therefore occurs about the C_α - C_β bond.

The dependence of the isotropic β–hyperfine coupling constant of certain muonium substituted radicals and their isotopomers can be expressed, due to their symmetry, in the form of a Fourier expansion of even terms.

$$A_\beta(\vartheta) = A_o + A_2\cos 2\vartheta + A_4\cos 4\vartheta + \ldots\ldots\ldots \qquad (1.49)$$

It is assumed that the higher order terms are small and that the expression can be truncated after the second term and rewritten in the Heller-McConnel [46] form.

$$A_\beta(\vartheta) = A + B\cos^2\vartheta \qquad (1.50)$$

where A is an angle independent term thought to arise from spin polarization and the term B describes the angle dependence of the spin density at the β—nucleus.

For simple radicals it is possible to describe the temperature dependence of the β-hyperfine couplings in terms of relationship (1.50). This expression can be used in a quantum mechanical averaging technique [47, 48, 49, 50] that fits experimentally observed couplings to theoretical values. From this procedure it is possible to derive information on the dependence of the total molecular energy on the torsional motion and hence on the barrier to internal rotation about the C_α - C_β bond. In addition further information on factors influencing the equilibrium conformation of the radical can be extracted.

1.6.3 Theory of Rotational Averaging

The treatment of internal rotation assumes that the large amplitude torsional motion can be separated from solvent interactions; and rotational and vibrational motions. In this approximation the molecule must at any instant be in one of the torsional states obtained by solution of the torsional Hamiltonian.

$$\hat{H} = -\left(\hbar^2/2I\right)\frac{\partial^2}{\partial\vartheta^2} + V(\vartheta) \qquad (1.51)$$

Here I is the reduced moment of inertia of the molecule, defined as

$$I = \frac{I_1 I_2}{I_1 + I_2} \qquad (1.52)$$

where I_1 and I_2 correspond to the moments of inertia of the two contra-rotating groups about the axis of rotation, at the equilibrium conformation of the radical. The term $V(\vartheta)$ describes the potential energy hindering the internal rotation. Equation (1.51) can be solved by treating the potential barrier as a perturbation of the free-rotation Hamiltonian, $\hat{H}^{(o)}$.

$$\hat{H}^{(o)} = \frac{-h}{2I} \frac{\partial^2}{\partial^2 \vartheta} \qquad (1.53)$$

The internal rotation Hamiltonian can therefore be re-expressed as

$$\hat{H} = \hat{H}^{(o)} + \hat{H}^{(1)} \qquad (1.54)$$

where

$$\hat{H}^{(1)} = V(\vartheta) \qquad (1.55)$$

The eigenfunctions, ψ_n, of the free internal rotation Hamiltonian are of the form

$$\psi_n = \frac{1}{\sqrt{2\pi}} e^{\pm im\vartheta} \qquad (1.56)$$

and can be used as a set of basis functions from which the eigenfunctions, ψ_j, of the torsional Hamiltonian can be calculated. The resulting eigenfunctions are expressed as linear expansions of the free rotation eigenfunctions.

$$\psi_j = \frac{1}{\sqrt{2\pi}} \sum_n c_n e^{\pm i m \vartheta} \qquad \begin{matrix} n = -\infty, \ldots, \infty \\ j = 1, \ldots, 2n+1 \end{matrix} \qquad (1.57)$$

For molecules in which the torsional motion has a periodic nature, the potential energy can be expressed as a Fourier series of even terms.

$$V(\vartheta) = \sum_m \frac{V_m}{2} (1 + \cos m\vartheta) \qquad (1.58)$$

where V_m is the barrier to internal rotation. The eigenenergies and eigenfunctions of the torsional Hamiltonian are therefore obtained by diagonalization of the secular determinant, $\langle \psi_k \mid \hat{H} \mid \psi_j \rangle$. The elements of the secular determinant are

$$H_{nn} = \frac{-\hbar}{2I} n^2 + \sum_m \frac{V_m}{2}$$

$$H_{nn'} = -\frac{V_m}{4} \qquad n' = n + m,\ n - m \qquad (1.59)$$

$$H_{nn'} = 0 \qquad n' = n + m,\ n - m$$

In the μSR experiment the transitions between different torsional states can not be observed, therefore the observed β-muon-electron hyperfine coupling constant, $A_\beta(\gamma)$, will be averaged over all populated torsional states. This can be accounted for by calculating a

population-weighted expectation value of $A_\beta(\gamma)$, which will have the form

$$\langle A_\beta(\gamma)\rangle_i = A + B \langle \cos^2\gamma \rangle_i \qquad i = 1, \ldots, 2n+1 \qquad (1.60)$$

where the term $\langle \cos^2\gamma \rangle_i$ can be computed from,

$$\langle i \mid \cos^2\gamma \mid i \rangle \qquad (1.61)$$

and i corresponds to the different torsional states. The angle γ is defined as

$$\gamma = \vartheta + \vartheta_o \qquad (1.62)$$

where ϑ_o defines the equilibrium conformation of the molecule; ϑ_o is the value of the dihedral angle defined in Figure 1.5 at the equilibrium conformation.

The terms $\langle \cos^2\gamma \rangle_i$ can be expressed in the form

$$\langle \cos^2\gamma \rangle_i = \int_o^{2\pi} \sum_{n'} \frac{1}{\sqrt{2\pi}} c_{n'}^* e^{-in'\vartheta} \mid \cos^2(\vartheta + \vartheta_o) \mid \sum_n \frac{1}{\sqrt{2\pi}} c_n e^{in\vartheta} d\vartheta \qquad (1.63)$$

and since the expression represents an observable property it can be simplified to

$$\langle \cos^2\gamma \rangle_i = 1/2 \sum c_n \left[c_n + \frac{1}{2} c_{n+2}(\cos 2\vartheta_o - \sin 2\vartheta_o) \right.$$

$$\left. + \frac{1}{2} c_{n-2}(\cos 2\vartheta_o + \sin 2\vartheta_o) \right] \qquad (1.64)$$

Dependence of the β-hyperfine coupling on temperature can be obtained by assuming a Boltzmann distribution between the torsional states. The β-hyperfine coupling can therefore be expressed in the temperature dependent form

$$A_\beta(T) = \frac{\sum_i \langle A_\beta \rangle_i \exp(-E_i/kT)}{\sum_i \exp(-E_i/kT)} \qquad (1.65)$$

where k is Boltzmann's constant.

For the case of free rotation, $V(\vartheta) = 0$, the eigenenergies are obtained by solution of the free rotation Hamiltonian (1.53). The resulting energies are found to occur in degenerate pairs and have a quadratic dependence on the quantum number n. In the limit of a very high barrier to internal rotation, the eigenenergies become equivalent to those of a harmonic oscillator and are defined by the expression.

$$E_\nu = (\nu + 1/2)\, h\omega \qquad (1.66)$$

where ν is the appropriate quantum number for the harmonic oscillator and ω is the frequency of oscillation. The eigenenergies of intermediate barriers can be labelled using either the quantum numbers n or ν. Figure 1.6 displays the correlation between the eigenenergies obtained for a zero and very high two-fold potential barrier.

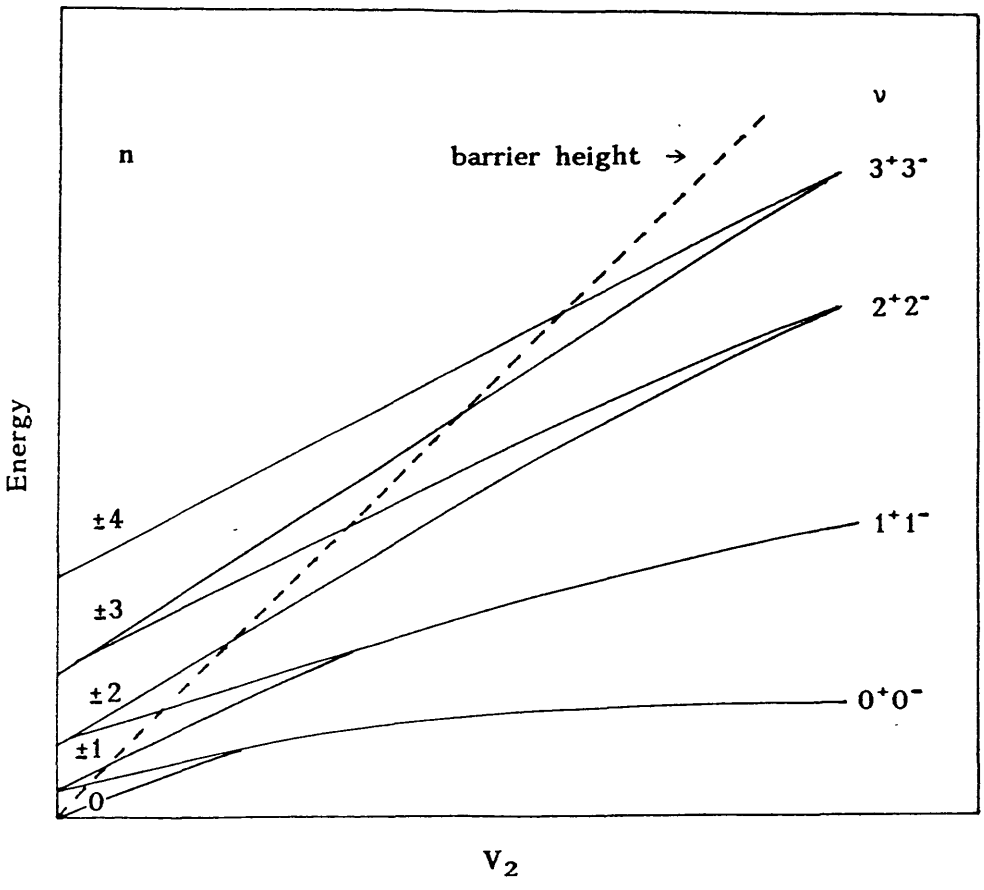

Figure 1.6 Variation of the energy levels associated with a two-fold potential barrier to internal rotation.

The populations of the torsional states become equal at the high temperature limit. There is essentially free rotation at this limit and therefore the term $\langle i | \cos^2\gamma | i \rangle$ can simply be written

$$\sum_i \langle \cos^2\gamma \rangle_i = \frac{2n + 1}{2} \qquad (1.67)$$

This when substituted into the equation defining the high temperature limit of $A_\beta(T)$, which is

$$\underset{T\to\infty}{A_\beta(T)} = A + B \sum_i \frac{\langle \cos^2\gamma \rangle_i}{2n + 1} \qquad (1.68)$$

simplifies the expression to

$$\underset{T\to\infty}{A_\beta(T)} = A + \frac{1}{2} B \qquad (1.69)$$

The theory outlined enables values for the barrier to internal rotation, and the parameters A and B to be evaluated. This is achieved by fitting experimentally observed temperature dependent β-hyperfine couplings to the theoretical values expressed by equations (1.60) and (1.65) using a simplex fitting routine. The parameters A, B and V_m obtained provide an insight into the conformation of the radical and its torsional motion.

CHAPTER 2

2 Experimental Studies of Muonium Substituted Free Radicals

2.1 Solvent Effects on the Muon-Electron Hyperfine Coupling Constant and Barrier to Internal Rotation of the 2-Muoxyprop-2-yl Radical

2.1.1 Introduction

The 2-muoxyprop-2-yl radical is formed by the formal addition of muonium to the carbonyl group of propan-2-one.

$$(CH_3)_2C{=}O + Mu \longrightarrow (CH_3)_2\dot{C}OMu \qquad (2.1)$$

Since its first observation by Roduner et al. [12] the 2-muoxyprop-2-yl radical has been comprehensively studied using the techniques of transverse field μSR [33, 44, 51, 52, 53, 54, 55] and avoided level crossing resonance μSR [5, 56]. These studies were mainly concerned with the measurement of the muon-electron β-hyperfine coupling constant, the effect of solvent interactions on this coupling and the mechanism of formation of the muoxy radical. The 2-muoxyprop-2-yl radical is particularly suitable for such studies due to the large quantity of comparable EPR data that exists on the analogous 2-hydroxyprop-2-yl radical [57, 58, 59].

The 2-hydroxyprop-2-yl radical, $(CH_3)_2\dot{C}OH$, was first observed by Gibson and co-workers from EPR studies of radicals formed in rigid solutions of hydrogen peroxide subjected to ultra-violet irradiation [60]. The resolution of the experimental apparatus used, however, prevented the determination of a value for the small hydroxy hyperfine coupling

constant. The first measurement of the hyperfine hydroxy coupling constant was made by Zeldes and Livingston [57] from an EPR study of liquids during photolysis. The hydroxy coupling of $(CH_3)_2\dot{C}OH$ formed by the photolysis of propan-2-ol containing 0.4 % H_2O_2 was determined to be 1.9 MHz at 299 K decreasing to zero at 250 K. In a later study by the same workers [58] the variation in the value of the coupling constant with temperature was attributed to a negative, temperature independent contribution to the coupling from spin density on the oxygen and a positive, temperature dependent contribution from the spin density on the radical centre. Further, the studies of Zeldes and Livingston showed that the magnitude of the hydroxy coupling constant is solvent dependent. For example it was found that for an aqueous solution containing 10 % propan-2-one and 5 % methanol the hydroxy coupling was 0.9 MHz at 300 K. This represents about a 50 % reduction in the magnitude of the hyperfine coupling with respect to that reported for liquid propan-2-one. A more recent EPR study on the hyperfine coupling constants of the 2-hydroxyprop-2-yl radical and the influence of different solvents on the magnitude of the coupling has been performed by Lehni [59]. In this study measurement of the hydroxy coupling was restricted to temperatures at which the hyperfine coupling has a positive value. Lehni notes that when the linewidths obtained from the EPR spectra are plotted against T/η, where η is the viscosity of the solvent, that the mixtures studied can be separated into two distinct classes. The first class corresponds to mixtures in which some degree of hydrogen-bonding between the 2-hydroxyprop-2-yl radical and the solvent is possible. The second class of mixtures are those containing solvents, such as n-decalin, that do not form hydrogen-bonds with the hydroxy radical.

In this section the muon-electron β-hyperfine coupling constant of the

2-muoxyprop-2-yl radical formed in samples consisting of propan-2-one and water in the volume ratios 100:1, 40:1 and 10:1 are reported. Unlike the earlier μSR studies where the measurement of the coupling was limited to a small temperature range, here the measurements are made over the full liquid range of each of the mixtures. Also reported are some preliminary measurements of the muon-electron β-hyperfine coupling of the 2-muoxyprop-2-yl radical formed in a mixture of propan-2-one and n-hexane in the volume ratio 1:1. These experiments are an extension of earlier work performed by R. M. Macrae [55], previously of this group. Comparison of these μSR results with the EPR measurements on the analogous 2-hydroxyprop-2-yl and the earlier μSR studies enables an interpretation relating the temperature dependence of the muon-electron hyperfine coupling to the radical structure, to the barrier hindering internal rotation and to solvent interactions to be presented.

2.1.2 TF-μSR Measurements

All experiments were performed at the Paul Scherrer Institute, using the μE1 and μE4 beamlines. Propan-2-one:water mixtures in the volume ratios 100:1, 40:1 and 10:1 and a propan-2-one:n-hexane mixture in the volume ratio 1:1 were studied. All the reagents used were of the highest grade commercially available. Each sample was degassed using the normal feeze-pump-thaw procedure before being sealed under vacuum in thin-walled spherical glass vessels. In each experiment a magnetic field of 0.2 T was applied transversely to the muon spin direction in the polarized beam and about 5×10^7 good events were recorded. The radical formed is characterized by a pair of lines in the Fourier transformed spectrum as shown by Figure 1.3. Figure 2.1 shows a selection of the Fourier transformed spectra obtained from the 100:1 mixture. The strong signal corresponding to muons in diamagnetic environments at ca. 27 MHz has been excised from the spectrum using a fitting procedure based upon the minimisation package MINUIT [27]. The Figure shows that the position and strength of the radical signals are temperature dependent. Similar spectra were obtained on analysis of the data from the other mixtures studied. The muon-electron hyperfine coupling constant, $|A_\mu|$, at this field is equal to the difference in the frequencies of the two observed signals. The reduced muon-electron coupling constants, A'_μ, defined as the coupling constant scaled by the ratio of the proton's magnetic moment to the muon's magnetic moment are listed in Table 2.1 for the 2-muoxyprop-2-yl radical formed in the 100:1, 40:1 and 10:1 mixtures. Also included in the Table are the results obtained by Macrae

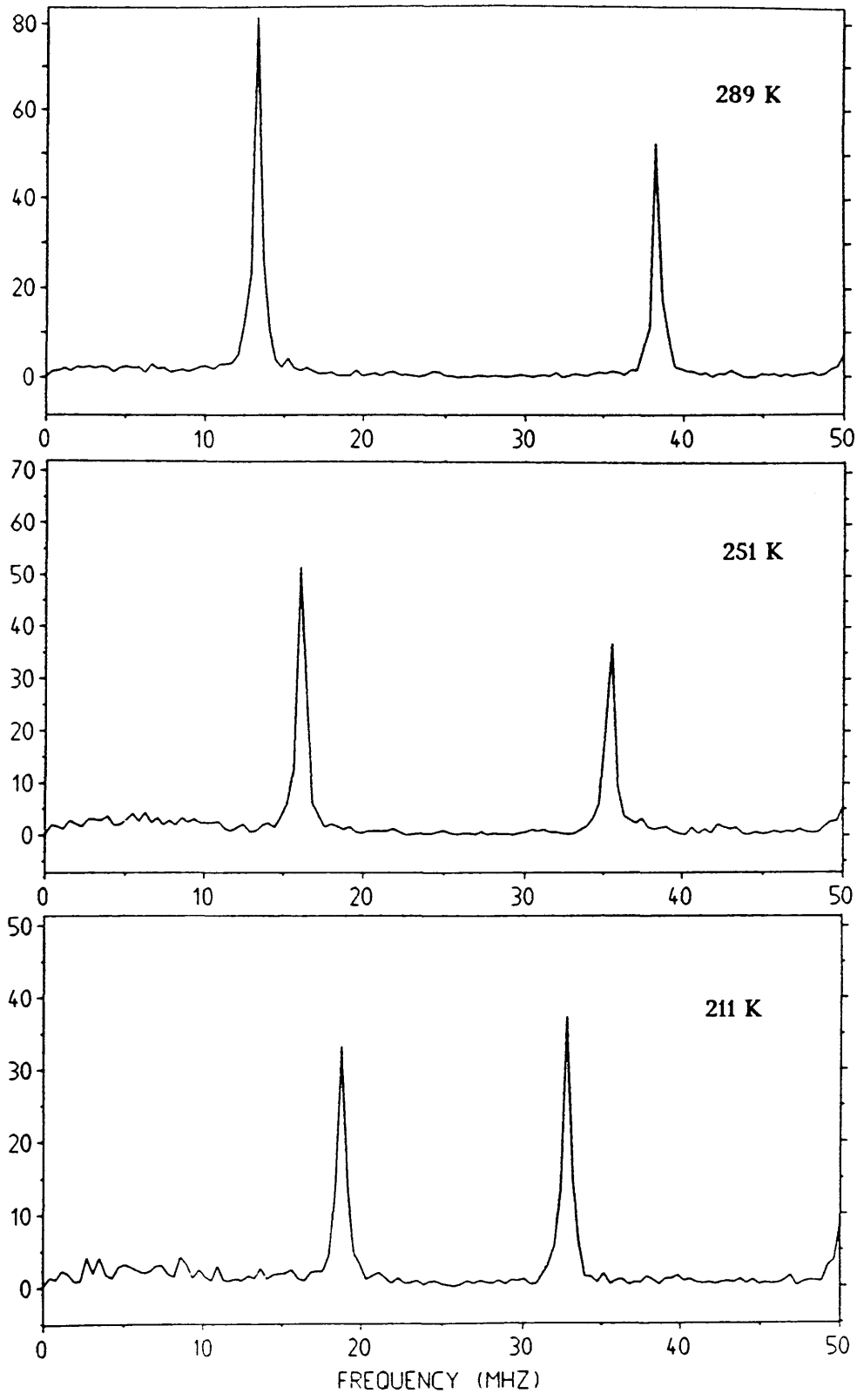

Figure 2.1 Fourier transformed spectra of the 2-muoxyprop-2-yl radical formed in the 100:1, by volume, propan-2-one:water solution.

[55] from studies of a sample of propan-2-one composed of equiportions of d6-propan-2-one and propan-2-one and propan-2-one:water mixtures in the volume ratios 20:1 and 15:1.

Table 2.1 The temperature, T / K, and solvent dependence of the reduced muon-electron hyperfine coupling constant $A_\mu^\cdot$ / MHz of the 2-muoxyprop-2-yl radical in various H_2O mixtures

Pure[a]		100:1		40:1		20:1[a]		15:1[a]		10:1	
T	$A_\mu^\cdot$	T	$A_\mu^\cdot$	T	$A_\mu^\cdot$	T	$A_\mu^\cdot$	T	$A_\mu^\cdot$	T	$A_\mu^\cdot$
180	3.64	181	3.30	170	2.97	183	2.91	193	3.25	182	3.07
203	4.49	211	4.42	201	3.72	203	3.47	207	3.73	200	3.57
228	5.48	228	5.13	225	4.62	223	4.20	233	4.70	226	4.45
251	6.44	251	6.08	248	5.64	243	5.06	250	5.39	239	4.93
277	7.59	277	7.28	290	7.62	263	5.97	269	6.26	258	5.77
300	8.56	289	7.88	314	8.74	283	6.98	277	6.51	280	6.70
319	9.38	316	9.11			303	7.85	291	7.24	317	8.47
						323	8.86	313	8.32		

[a] Ref. [55], T ± 0.1 K

All the couplings listed in Table 2.1 show the expected temperature dependence [44]; a lowering in the magnitude of the hyperfine coupling as the temperature is raised. Therefore the coupling constants are described as having a positive temperature coefficient. The temperature dependence of the couplings can be directly related to the radical conformation. The equilibrium conformation (I) and the barrier conformation (II), corresponding to internal rotation about the central

C-O bond, of the analogous 2-hydroxyprop-2-yl radical are shown in Figure 2.2.

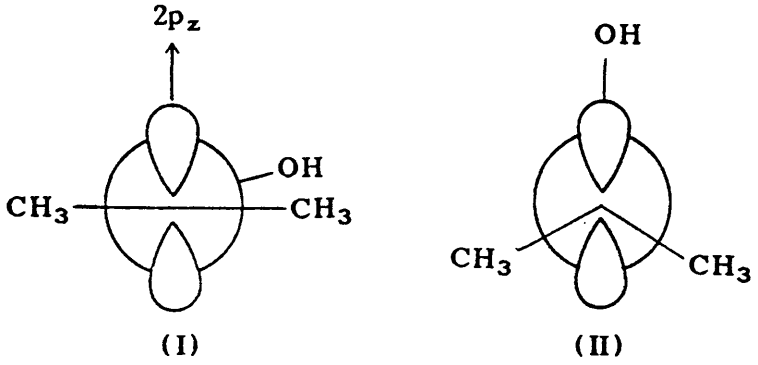

Figure 2.2 Equilibrium and barrier conformations of the 2-hydroxyprop-2-yl radical.

The conformations shown in Figure 2.2 were obtained from theoretical studies of the 2-hydroxyprop-2-yl radical [44, 55, 61]. These studies have also shown that for the 2-hydroxy radical conformation (II) has the maximum hydroxy hyperfine coupling and conformation (I) the minimum hydroxy hyperfine coupling. EPR studies [58, 59] of the 2-hydroxyprop-2-yl radical have shown that the hydroxy hyperfine coupling has a positive temperature coefficient, as does the corresponding 2-muoxyprop-2-yl radical. Therefore, it is expected that the barrier and equilibrium comformations of the 2-muoxyprop-2-yl radical are analogous to those shown in Figure 2.2.

The variation of the hydroxy and muoxy hyperfine coupling constants with temperature can be associated with the torsional motion of the O-H(Mu) group about the C-O bond. The muon-electron hyperfine coupling constant is larger, over all temperatures, than the corresponding proton-electron hyperfine coupling constants. This isotope effect must be a consequence of the difference in the zero-point vibrational energies of

the muon and the proton. Due to its higher zero-point vibrational energy the muonic isotopomer undergoes larger librational motions about the central C-O bond. Consequently the experimentally measured β-hyperfine coupling of the 2-muoxyprop-2-yl radical is influenced by the barrier conformation (II) to a greater extent than the coupling constant of the 2-hydroxyprop-2-yl radical. The difference in the amplitudes of the librational motion of the two isotopomers considered therefore explains the difference in the magnitude of the experimentally measured β-hyperfine coupling constants and the associated temperature dependence of the coupling.

The temperature dependent coupling constants listed in Table 2.1 are nearly linear with only a slight deviation from linearity at low temperatures. The couplings for the 100:1 mixture are found to be slightly lower than those of pure propan-2-one, decreasing from 9.11 MHz at 316 K to 3.30 MHz at 181 K. The couplings for the 10:1 mixture are the lowest measured, decreasing from 8.47 MHz at 317 K to 3.07 MHz at 182 K. The results in Table 2.1 show that the hyperfine coupling constants are dependent on the water concentration of the solution as found by Hill and co-workers [33, 52]. Figure 2.3 shows the temperature dependence of the hyperfine couplings of the 2-muoxyprop-2-yl radical in pure, 100:1 and 20:1 propan-2-one:water solutions. The hyperfine couplings of all mixtures listed in Table 2.1 follow the same temperature dependence, deviating only slightly from linearity at low temperatures. At all temperatures the observed couplings of the binary aqueous mixtures are smaller than those obtained in pure propan-2-one. However, closer inspection of the results reveals that whereas near room temperature the value of the coupling constant decreases with increasing water concentration, at around 220 K there appears to be a crossing of the

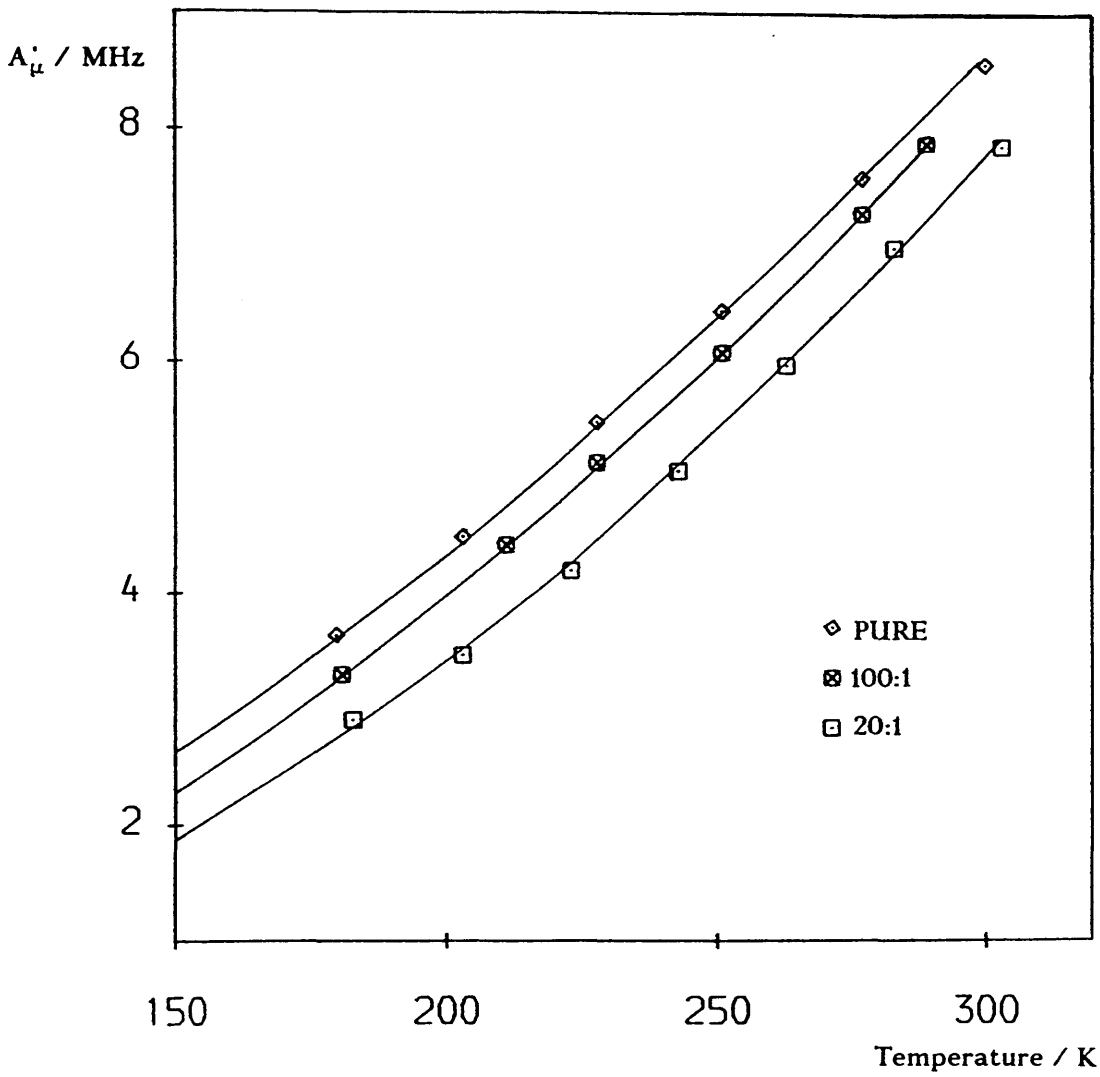

Figure 2.3 Temperature and solvent dependence of the reduced hyperfine coupling constant, $A_\mu^\cdot$, of the 2-muoxyprop-2-yl radical.

results obtained from the 15:1 and 20:1 solutions. This behaviour is observed to a greater extent in the 10:1 solution.

The solvent interactions which affect the measured β-hyperfine coupling constants of the 2-muoxyprop-2-yl radical are probably of a similar nature to those affecting the 2-hydroxyprop-2-yl radical. In each case the coupling constants could be influenced by spin delocalization which follows from the resonance structures shown in Figure 2.4.

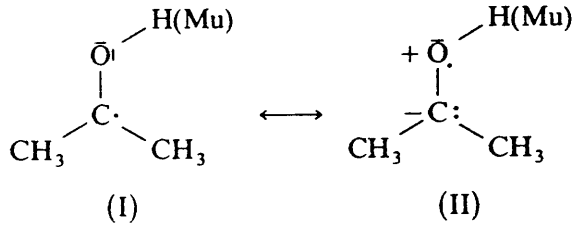

Figure 2.4 Possible resonance structures of the 2-hydroxy and 2-muoxy prop-2-yl radicals.

Figure 2.4 shows two of the possible resonance structures that occur as a result of the librational motion of the O-H(Mu) group against the rest of the radical. In polar solvents, such as water, resonance structure (II) could have a greater significance than in non-polar solvents. In this structure spin polarization of the unpaired electron at the oxygen leads to a negative contribution to the spin density at the hydroxy proton or muon site. The lowering of the muon coupling constant on addition of water could therefore result from the increasing role of structure (II) through an increase in hydrogen bonding, over that of pure propan-2-one, in the solutions.

The further lowering of the coupling constants on increasing the concentration of water present in the solution is thought to reflect an

increase in hydrogen-bonding within the mixtures. In pure propan-2-one there is only one possible muonium-bonded structure that can be formed and is shown as structure (I) in Figure 2.5. With the introduction of small quantities of water into the sample other muonium-bonded and hydrogen-bonded structures can be formed as illustrated by structures (II) and (III) in Figure 2.5 .

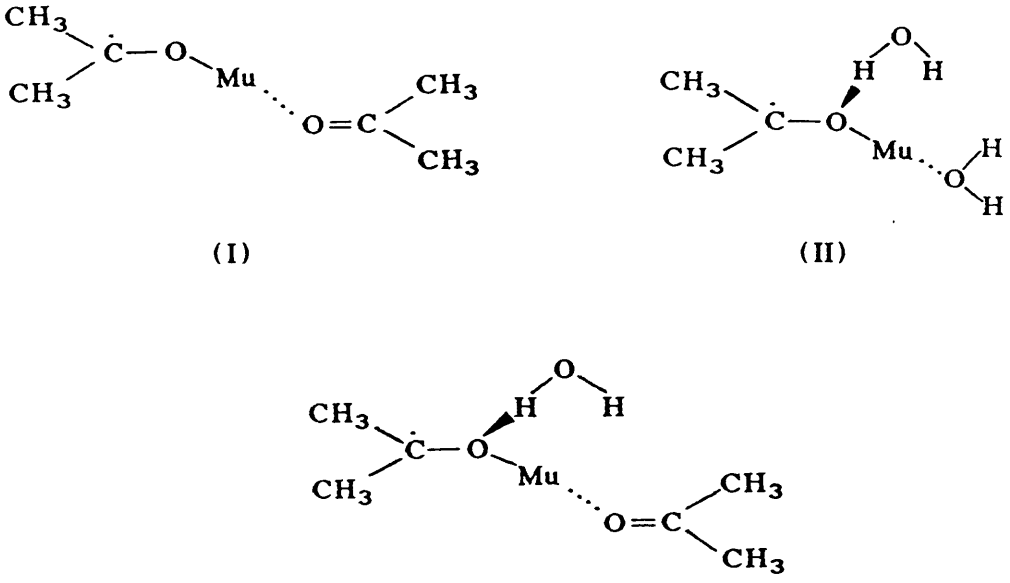

(I) (II)

(III)

Figure 2.5 Hydrogen and muonium bonded structures of the 2-muoxyprop-2-yl radical.

It has been noted in previous μSR studies of solvent effects on the hyperfine coupling constant of the 2-muoxyprop-2-yl radical that the introduction of small quantities of water to a solution of propan-2-one switches on additional hydrogen-bonding [33].

In a study of a binary mixture of propan-2-one:D_2O in the volume ratio of 20:1 by Macrae [55] the reduced muon-electron hyperfine

coupling was found to be 7.5 MHz at 298 K. This value shows no significant difference from that of the coupling constant measured for the 20:1 propan-2-one:water mixture at a similar temperature. The correspondence between the coupling constants indicates that the increased contribution to the hydrogen-bonding in the aqueous muoxy radical systems is through bonding by muonium to the oxygen of the water molecule.

Venkateswaran et al. [56] have studied the 2-muoxyprop-2-yl radical formed in solutions of propan-2-one in water and hexane using the method of avoided level crossing resonance μSR. For a 30 % by volume solution of propan-2-one in water the resonance signal was observed to be shifted upfield by 28 mT relative to the signal observed in a sample of pure propan-2-one. Using a value for A_μ of 22.0 MHz, as measured by Hill et al. [33] from a TF-μSR experiment on a comparable propan-2-one:water mixture, the methyl proton coupling constants were given the value A_{H_β} = 55.5 MHz. This value is equal, within the limits of experimental error, to the methyl proton coupling constants of the 2-muoxyprop-2-yl radical formed in pure propan-2-one [56]. This result indicates that the solvent effects that influence the muoxy hyperfine coupling constant of the prop-2-yl radical have relatively little effect on the spin density located at the methyl protons. Further the value of the methyl proton coupling constant is close to the literature value of the analogous 2-hydroxyprop-2-yl radical of 55.9 MHz [58]. This shows that muonium substitution of the hydroxy proton does not significantly affect the spin density located at the radical centre or the methyl protons. For a 30 % by volume solution of propan-2-one and hexane Venkateswaran et al. [56] observe a downfield shift of 11.5 mT in the position of the resonance. The muon-electron hyperfine coupling of the 2-muoxyprop-2-yl

radical in this solution was measured to be 29.4 MHz. Although the temperature at which these experiments were performed is not reported, it is assumed that all experiments were carried out at room temperature. The opposite direction of the shifts in the ALC resonance on dilution of pure propan-2-one by water and hexane supports the hydrogen bonding interpretation of the transverse field μSR results.

No transverse field μSR results were available for comparison with the avoided level crossing resonance studies of the propan-2-one:hexane mixture. Therefore in order to study the affect of introducing a hydrocarbon solvent which reduces the degree of hydrogen-bonding in the system a preliminary study on a solution of propan-2-one:n-hexane in the volume ratio 1:1 was performed, using TF-μSR. Preparation of the sample was essentially equivalent to the method used to prepare the propan-2-one:water mixtures. The experiment was performed under a magnetic field of 0.2 T applied transversely to the muon spin direction and about 1×10^6 good events were recorded. The relatively low number of events recorded for this experiment was a consequence of the muon beam being produced without the use of the muon channel. The muon-electron β-hyperfine coupling constant of the 2-muoxyprop-2-yl radical formed in this solution was measured at two temperatures. The reduced muoxy hyperfine coupling constant was found to be 5.66 MHz at 232 K decreasing to 3.56 MHz at 183 K. Comparison of these couplings with the couplings of the sample of pure propan-2-one listed in Table 2.1 indicate that over this temperature range there appears to be a crossing of the couplings measured in the 1:1 propan-2-one:n-hexane mixture and the pure propan-2-one solution. The reduced muon-electron hyperfine coupling of the 2-muoxyprop-2-yl radical is 0.08 MHz lower than the corresponding coupling in pure propan-2-one at about 180 K. This shift in

the hyperfine coupling on the addition of n-hexane is in the opposite direction to that expected for a solvent which forms no hydrogen-bonded complexes with the solute and is also in the opposite direction to the shift observed by Venkateswaran et al. at a higher temperature. The value of $A_\mu^{'}$ at 232 K for the 1:1 propan-2-one:n-hexane mixture is, however, nearly equivalent to that in pure propan-2-one indicating that the shift in the magnitude of the muoxy hyperfine coupling is temperature dependent. This temperature dependence could arise from a difference in the sign and magnitude of the low lying torsional energy levels of the 2-muoxyprop-2-yl radical in different solutions. Macrae [55] has already shown that it is possible to explain the difference in the temperature dependence of the β-hyperfine coupling of the 2-muoxy and 2-hydroxy prop-2-yl radicals by considering the sign and magnitude of the low lying torsional states. However, to examine this effect in the propan-2-one:n-hexane mixture the hyperfine couplings over the full liquid range of the sample would have to be measured. The dependence of the value of the β-hyperfine coupling constant on the sign and magnitude of the torsional energy levels will be discussed further in the next section, when solvent effects on the barrier to internal rotation are considered.

The experimental data obtained on the 2-muoxyprop-2-yl radical in different solvents by TF-μSR and avoided level crossing μSR indicate that solvent interactions on the methyl proton hyperfine couplings are small and have negligible influence on the observed coupling. Further through comparison of the μSR results with comparable EPR data on the analogous 2-hydroxyprop-2-yl radical it has been shown that muon substitution does not significantly affect the methyl proton hyperfine coupling [55]. These results suggest that isotope-dependent

hyperconjugation processes must be small and are not the origin of the observed isotope effect in the β-hyperfine coupling as proposed by Hill et al. [33, 52, 53]. The isotope effect must arise from the difference in the zero-point energies of the muon and the proton. This difference determines the librational motion of the O-H(Mu) group about the central C-O bond of the radical and consequently results in the observed isotope dependence of the temperature dependent hyperfine couplings.

2.1.3 Internal Rotation Studies

The hydrogen-bonding present in the propan-2-one:water mixtures is expected to hinder the internal rotation of the O-Mu group against the rest of the molecule [33]. It is possible to develop this argument quantitatively by considering the barrier height, V_2, to internal rotation of the 2-muoxyprop-2-yl radical. V_2 can be extracted from the temperature dependent β-hyperfine coupling constants using the rotational averaging technique described in chapter one. This procedure involves fitting of the experimentally measured coupling constants to theoretical values using a quantum mechanical averaging technique and has already been applied in a study of the internal rotation of muonium substituted ethyl isotopomers [43, 65]. It is assumed that in this method the major contribution to the temperature dependence of the coupling constants is the difference in the average torsional angle (γ) about the C-O internuclear axis. Also here it is assumed that the potential barrier hindering internal rotation is principally of a two-fold nature and can be represented by the truncated Fourier series.

$$V(\gamma) = \frac{1}{2} V_2(1 - \cos 2\gamma) \qquad (2.2)$$

Using the theory of rotational averaging the barrier height for the 2-muoxyprop-2-yl radical has been ascertained by fitting the theoretically calculated coupling constants obtained from equation (1.65) to the observed couplings, listed in Table 2.1, through simultaneous variation of the three parameters A, B and V_2 in equations (1.60) and (1.58). The

calculated values of the parameters A, B and V_2 for each mixture are collated in Table 2.2. The reduced moment of inertia of the radical was taken to be 1.393 x 10^{-48} Kg m^2. This value was derived from an *ab initio* study of the 2-hydroxyprop-2-yl radical performed by Macrae [55]. The equilibrium torsion angle, γ_o, of the 2-muoxyprop-2-yl radical was assumed to be $\pi/2$.

Table 2.2 Values for the parameters A/MHz, B/MHz and V_2/J mol^{-1} for the 2-muoxyprop-2-yl radical in various H_2O mixtures

Solution	A	B	V_2
Pure[a]	-117.0	315.3	3828.0
100:1	-105.0	298.1	4572.1
40:1	-94.9	283.7	5307.0
20:1[a]	-76.7	259.3	7037.0
15:1[a]	-69.6	262.9	8816.8
10:1	-70.4	246.7	7554.9

[a] Ref. [55]

The barrier to internal rotation increases from 4572 J mol^{-1} in the 100:1 propan-2-one:water mixture up to 8816 J mol^{-1} in the 15:1 mixture. In all cases, the value of the barrier exceeds that of 3828 J mol^{-1} for the 2-muoxyprop-2-yl radical in pure propan-2-one. The dependence of the barrier to internal rotation of the radical on the water concentration is shown in Figure 2.6. Two results appear anomalous; the expected trend is that the torsional barrier should increase in value as the water concentration is raised as a consequence of greater hydrogen-bonding in

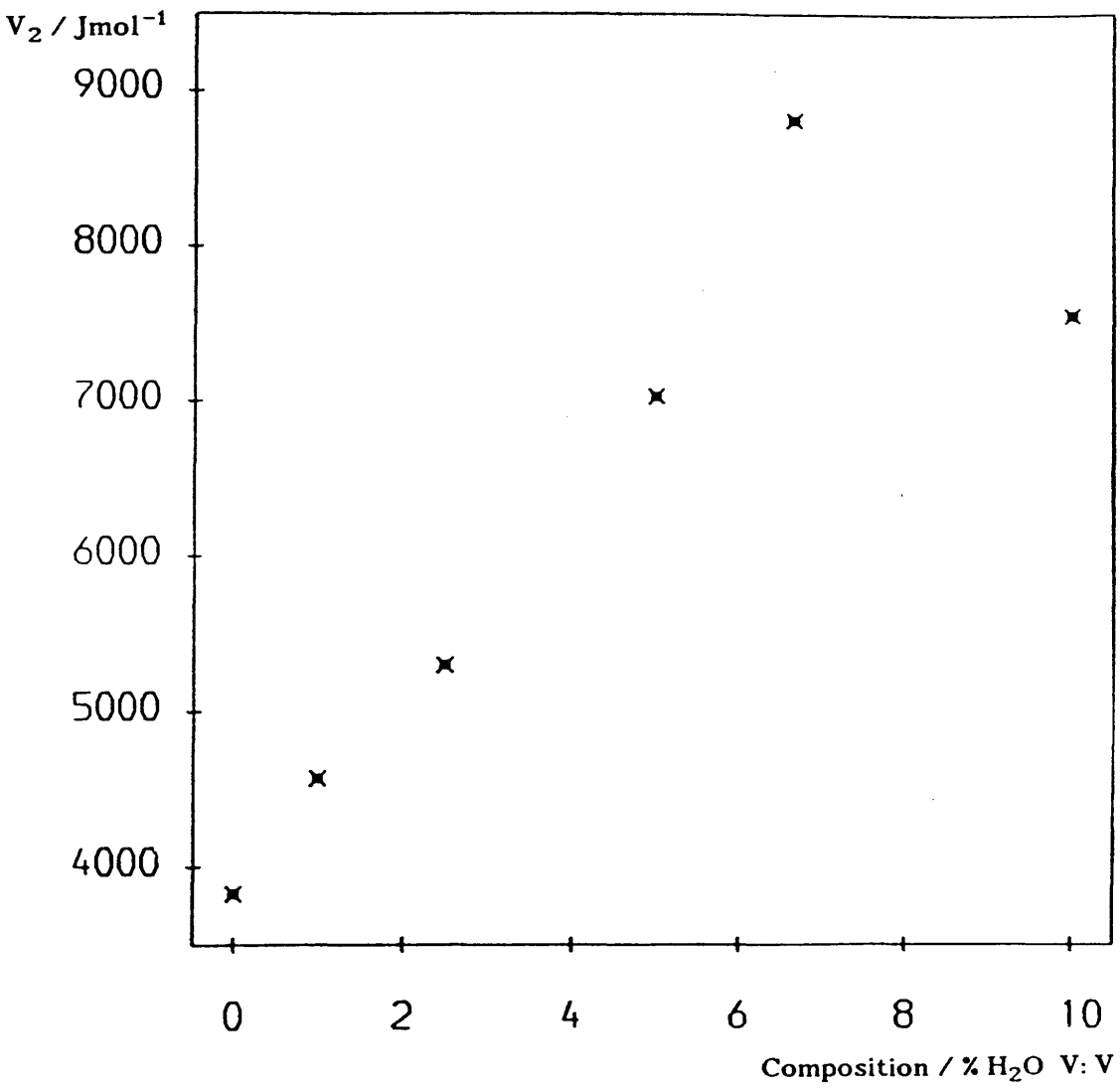

Figure 2.6 Dependence of the barrier height, V_2, to internal rotation of the 2-muoxyprop-2-yl radical on the composition of the mixture.

the solutions. The barrier of the 15:1 mixture is actually about 1000 J mol^{-1} higher than that of the 10:1 mixture. This anomaly is not apparent in Figure 2.7 which shows the dependence of the parameters A and B on the water concentration. At present there is no obvious explanation as to the nature of this anomaly, although it could arise from the experimental data reported for the pure, 20:1 and 15:1 solutions being collected during a different beam period to that of the 100:1, 40:1 and 10:1 mixtures.

The EPR study of the analogous 2-hydroxyprop-2-yl radical performed by Lehni [59] allows the barrier height of this radical to be determined. Using the reported β-proton hyperfine couplings the barrier to internal rotation of the hydroxy radical in a dilute solution of butan-2-ol was calculated as 10467 J mol^{-1}, with A = -7.89 MHz and B = 56.40 MHz, respectively. A value of 1.231 x 10^{-47} Kg m^2 was used for the reduced moment of inertia for the internal rotation about the C-O bond [55]. The study of Lehni reports splitting parameters for the radical in several different solvents and in each case the barrier derived from the couplings is higher than that of the 2-muoxyprop-2-yl radical and the values of the fitting parameters are similar to those reported. The difference in the torsional barriers of the 2-muoxy and 2-hydroxy prop-2-yl radicals can be explained from consideration of ancillary motions of the radical. In particular the difference in the librational motion of the O-H and O-Mu groups is thought to be the major factor influencing the difference in the rotational barriers.

Figure 2.8 displays the values of $\langle A_\mu^{'}(\gamma)\rangle_i$, the mean muon-electron hyperfine coupling constants, for the six lowest torsional energy levels of the 2-muoxyprop-2-yl radical formed in propan-2-one and the 100:1 and 20:1 mixtures. The corresponding torsional eigenvalues, E_i, obtained

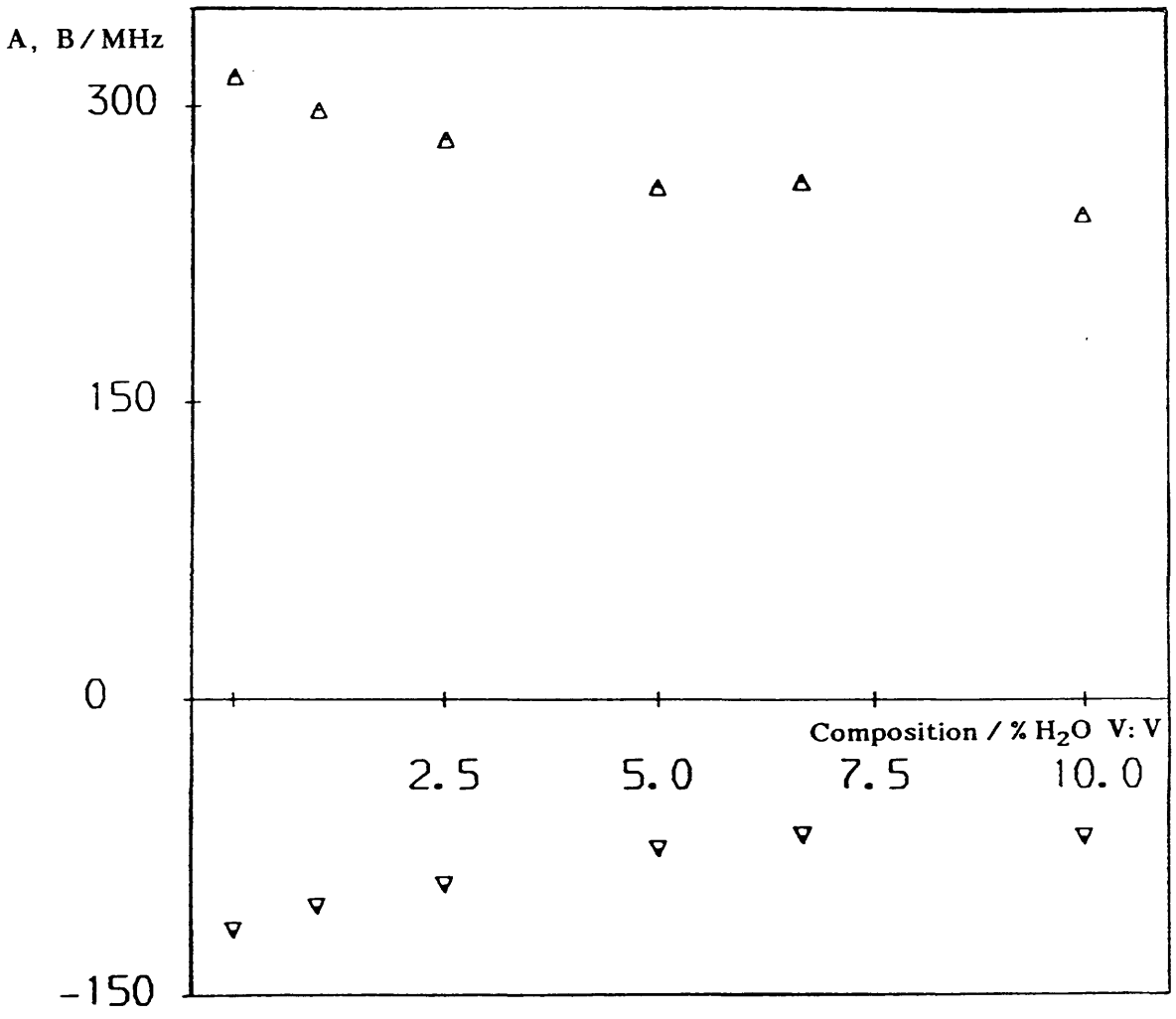

Figure 2.7 Solvent dependence of the parameters A: ∇ and B: △.

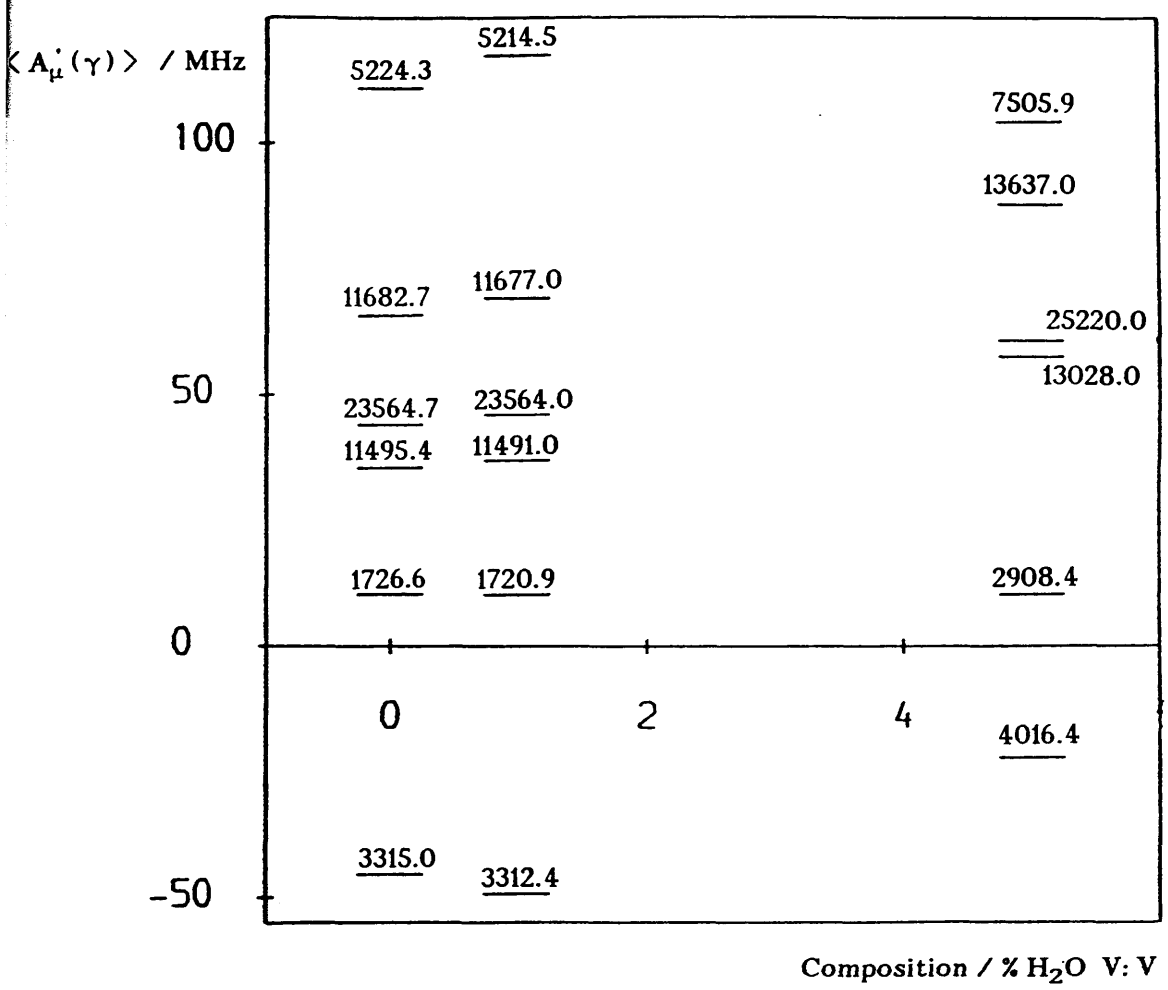

Figure 2.8 Values of $\langle A_\mu^\cdot(\gamma)\rangle_i$ for the six lowest torsional eigenstates of the 2-muoxyprop-2-yl radical in pure propan-2-one and the 100:1 and 20:1 mixtures. The corresponding torsional eigenvalues, E_i / J mol^{-1}, for each state are also shown.

by solution of the torsional Hamiltonian (1.51) are also shown. It is found that for all mixtures listed in Table 2.1 only one torsional level, that of i = 2, yields a negative coupling constant. In the temperature range of the experiment only the lowest five torsional energy levels are significantly populated, and as a consequence of the contribution of the level i= 2, the theoretical temperature dependence of the hyperfine coupling, of all mixtures, shows a minimum at around 150 K. This can be observed in Figure 2.9 which shows the temperature dependence of the theoretical hyperfine couplings of the 2-muoxyprop-2-yl radical in the 100:1 mixture, also shown are the experimentally measured muon-electron hyperfine coupling constants. Similar curves are obtained for pure propan-2-one and the other mixtures considered. The difference in the value of the coupling constant yielded by the low lying torsional levels, for each mixture, could explain the small deviation from linearity observed in the experimentally measured couplings at temperatures about 220 K.

The theoretical temperature dependence of the 2-hydroxyprop-2-yl radical is displayed in Figure 2.10. The theoretical hyperfine coupling was derived from the results of the EPR study of the 2-hydroxyprop-2-yl radical in a dilute butan-2-ol solution performed by Lehni [59]. The temperature dependence shown in Figure 2.10 is qualitatively different to the temperature dependence of the hyperfine coupling of the corresponding muoxy radical shown in Figure 2.9. Unlike the muoxy radical the theoretical hyperfine coupling curve of the hydroxy radical does not have a minimum at about 150 K. Further the hydroxy coupling appears to be able to take a negative value at low temperatures. Unfortunately there is no available low temperature EPR data on the

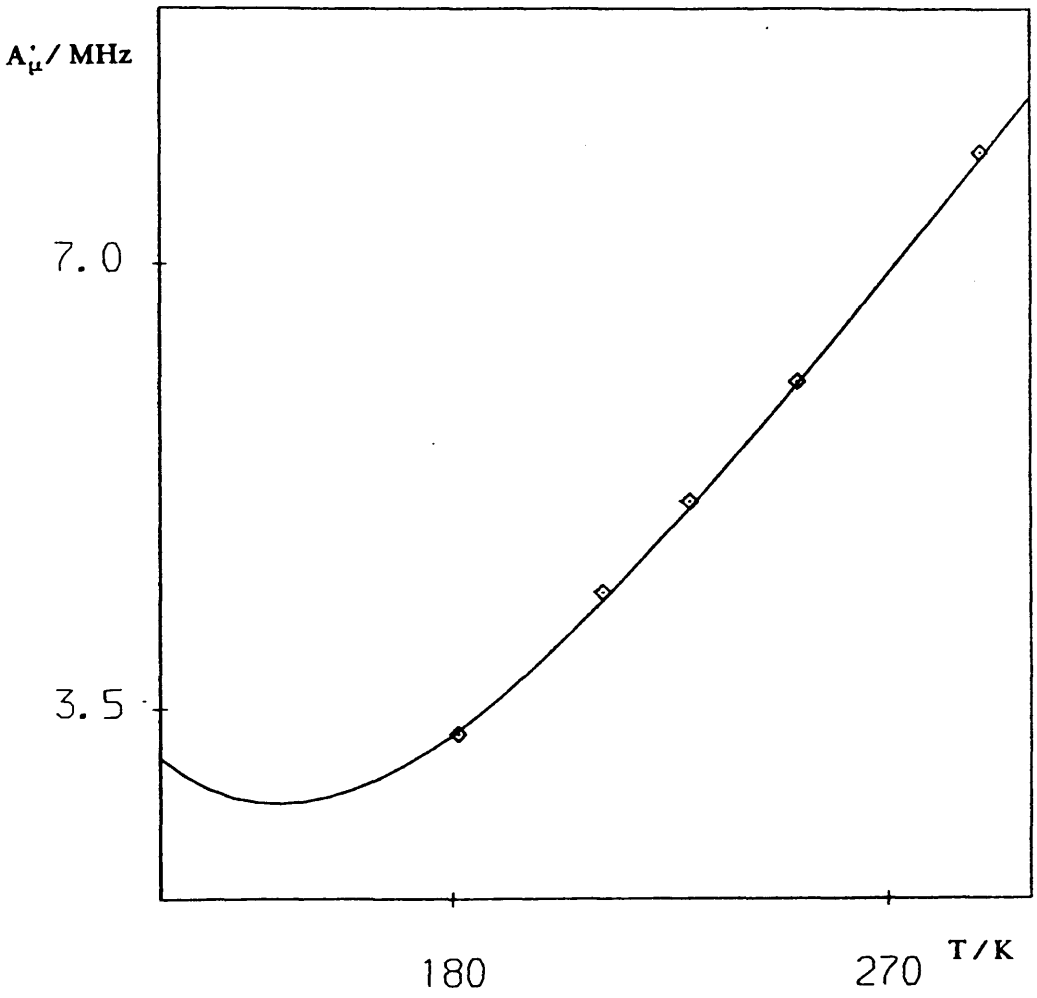

Figure 2.9 Theoretical temperature dependence of $A_\mu^\cdot$, together with the experimental results, for the 2-muoxyprop-2-yl radical.

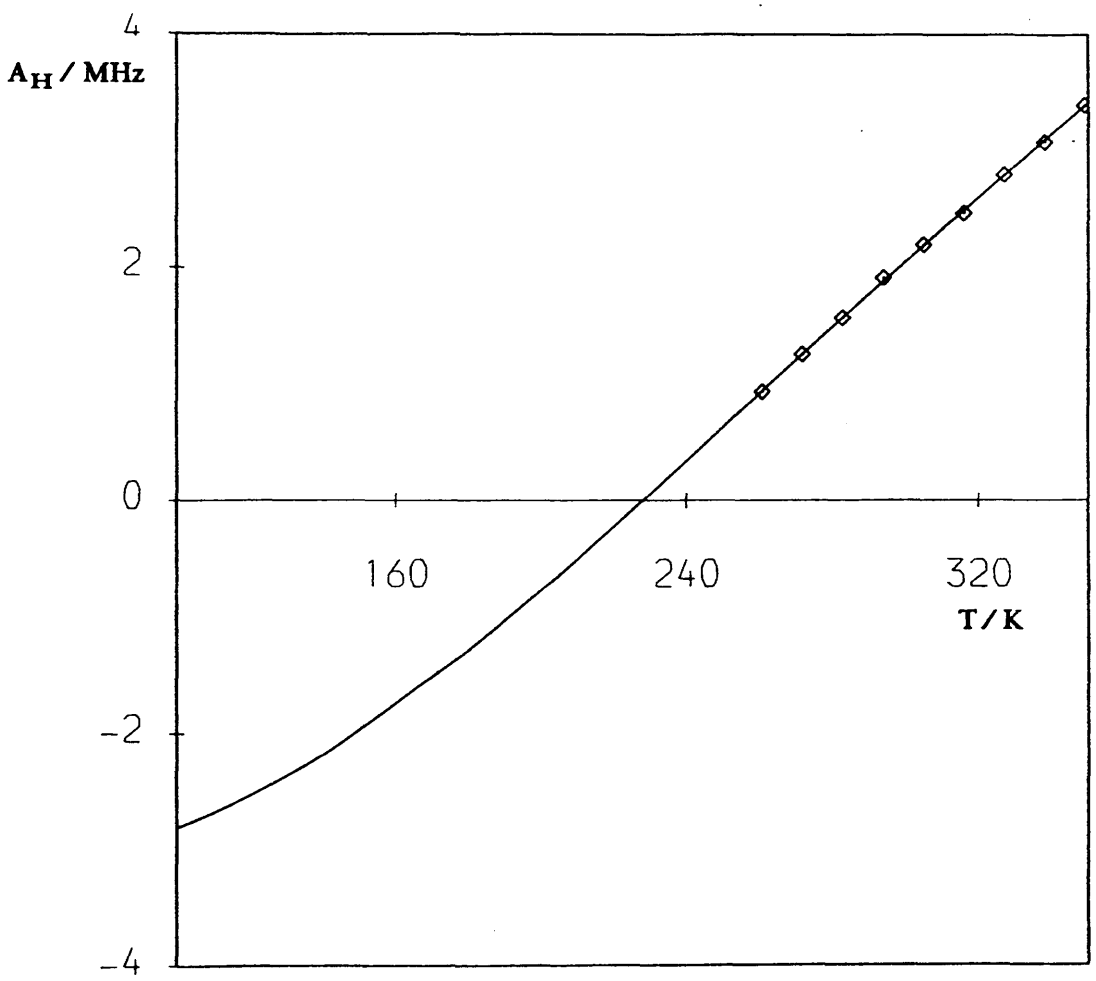

Figure 2.10 Theoretical temperature dependence of A_H, together with the experimental results, for the 2-hydroxyprop-2-yl radical.

2-hydroxyprop-2-yl radical for comparison. Zeldes and Livingston [58], however, found that the hyperfine coupling of the 2-hydoxyprop-2-yl radical was zero at 250 K and expected the proton coupling to decrease through zero as the temperature is lowered.

This difference in the temperature dependence of the 2-hydroxy and 2-muoxy prop-2-yl radicals can be attributed to the difference in the low lying torsional states of each radical. Table 2.3 lists the torsional eigenvalues, E_i, and the theoretical proton hyperfine coupling, $\langle A_H(\gamma) \rangle_i$, for the six lowest torsional states of the 2-hydroxprop-2-yl radical.

Table 2.3 Selected torsional energy levels, E_i / J mol^{-1}, and calculated proton hyperfine couplings, $\langle A_H(\gamma) \rangle_i$ / MHz, of the 2-hydroxyprop-2-yl radical

i	E_i	$\langle A_H(\gamma) \rangle_i$
1	1540.2	-3.1165
2	1540.4	-3.1236
3	4456.6	6.6386
4	4465.1	6.4144
5	6956.8	17.8725
6	7076.0	15.4204

For all states, $i > 2$, the associated hyperfine coupling is positive. The lowest lying states, $i \leq 2$, are both associated with a negative hyperfine coupling which therefore explains the constant decrease in the coupling as the temperature is lowered. The hypothetical limiting value of $\langle A_H(\gamma) \rangle_i$ is -3.11 MHz, at absolute zero. It can also be seen that the low lying torsional eigenvalues of the 2-hydroxyprop-2-yl radical are

nearly two-fold degenerate, as is expected due to its high barrier to internal rotation. In contrast, such degeneracy is not observed in the low lying torsional eigenenergies of the 2-muoxyprop-2-yl radical shown in Figure 2.8 due to its lower barrier to internal rotation. For this radical however, the two-fold degeneracy of the torsional eigenvalues is observed in states higher in energy than the barrier to internal rotation. In these states the system can be considered to have free internal rotation.

The theoretical values of the muon-electron hyperfine coupling constants and the barrier to internal rotation of the 2-muoxy and 2-hydroxy prop-2-yl radicals have been distinguished by the assumption of a simple model to represent the solvent system. This model neglects the possibility that the bonding that occurs in the system could affect the moment of inertia of the rotating group, and that the addition of a small volume of water to a solution of propan-2-one produces a homogeneous mixture. A more complete study would also have to consider the affect of internal rotation on the hydrogen and intermolecular bonds formed during the timescale of the experiment used to study the radical. Nevertheless, it is believed that given the complex nature of the solvent system, the model used provides a first step in the explanation of solvent effects on the barriers to internal rotation and the hyperfine coupling constants of muonic radicals.

2.2 Competitive Muonium Addition to 3-Methyl-2-Butenal

2.2.1 TF-μSR Studies of αβ-Unsaturated Carbonyl Compounds

In this section the first clear observation of competitive muonium addition to an αβ-unsaturated carbonyl compound, 3-methyl-2-butenal is reported. The presence of the two functional groups C=O and C=C in 3-methyl-2-butenal, $(CH_3)_2C=CHCHO$, introduces the possibility of competitive muonium addition. Figure 2.11 displays the three possible radical products that can be formed on muon implantation in liquid 3-methyl-2-butenal.

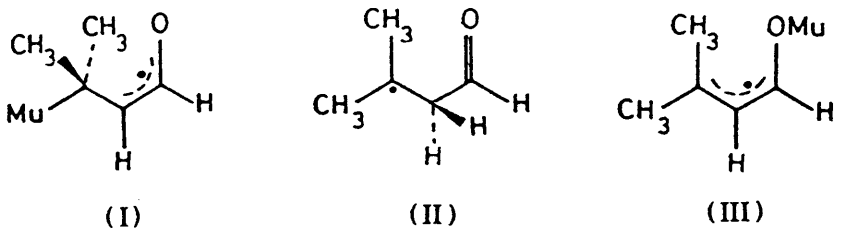

Figure 2.11 Radical products from muonium addition to inequivalent sites of 3-methyl-2-butenal.

There is also the possibility of muonium addition at the carbonyl carbon, but this is known not to occur to any observable extent in aldehydes or ketones. Radical (I) is an allyl type radical similar to the partially delocalized α-carbonyl radicals studied by Strub et al. [62]. Radical (II) is formed by muonium addition at C_2 and the unpaired electron is essentially localized on C_3. As a consequence of the difference in the capacity to delocalize the unpaired electrion of radicals (I) and (II), these species should be easily distinguishable from the magnitudes of

their respective muon-electron hyperfine coupling constants. The third possible radical is formed by muonium addition to the oxygen atom of the carbonyl group. The α-muoxy radical formed is expected to exhibit properties somewhat different to the α-muoxy radical considered in the previous section due to the possibility of spin delocalization through the carbon framework. Such delocalization would be expected to induce a lower β-muon-electron hyperfine coupling than that observed in the saturated α-muoxy radical.

No clear experimental observation of competitive muonium addition to an αβ-unsaturated ketone has been reported prior to this study. Macrae [55] performed a TF-μSR study on *trans*-2-butenal, $CH_3CH=CHCHO$, and observed strong signals corresponding to a radical formed by muonium addition to the C=C group. Very weak signals corresponding to muonium addition to the carbonyl group were also detected, but were too weak to enable an accurate determination of the muon-electron hyperfine coupling constant of the muoxy radical.

The data obtained from the study of 3-methyl-2-butenal, reported here, were collected at the Paul Scherrer Institute using the μE4 beamline. The sample was degassed using the standard freeze-pump-thaw procedure before being sealed and placed in the cryostat of the μSR spectrometer. A field of 0.2 T was applied transversely to the muon spin direction in the polarized beam. The muon-electron hyperfine coupling constants of the radicals formed were determined from the resulting μSR histograms. In order to characterize the radicals the hyperfine couplings were measured over the full liquid range of the sample. About 5×10^7 events were collected at each temperature to enable accurate determination of the coupling constants.

2.2.2 Results and Discussion

Figure 2.12 shows selected Fourier-transformed μSR spectra for the radicals formed from 3-methyl-2-butenal and the affect of temperature upon the position and linewidth of the signals. The diamagnetic signal at ca. 27 MHz has been excised from the spectra using a fitting procedure based on the minimization package MINUIT [27]. The signal C_y derives from the cyclotron frequency. The spectra consist of a pair of doublets R_1 and R_2, and each doublet can be attributed to a muonium-substituted free radical. The reduced muon-electron hyperfine coupling constants, A_μ^*, for each of the radicals observed, over the complete liquid range of the sample are listed in Table 2.4.

Table 2.4 Muon-electron hyperfine coupling constants, A_μ^* / MHz, for the muonic radicals formed in 3-methyl-2-butenal

	Radical (R_1)	Radical (R_2)
T / K	A_μ^*	A_μ^*
197.0	1.3	58.2
218.0	1.6	58.8
246.0	2.3	59.5
273.0	2.9	59.9
298.0	3.5	60.3
324.0	4.2	60.6
347.0	4.7	60.9

T ± 0.1 K

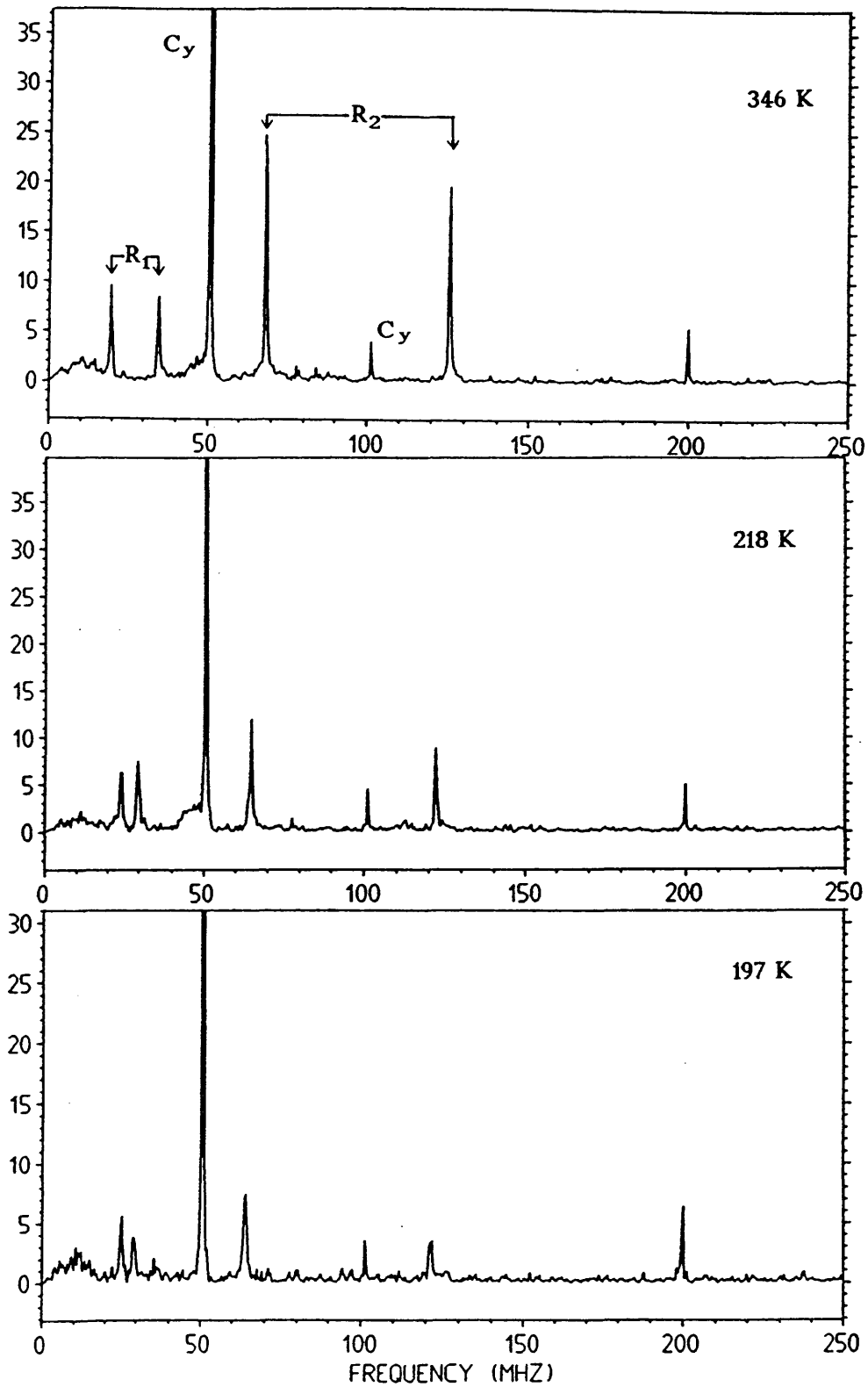

Figure 2.12 Fourier transformed μSR spectra for 3-methyl-2-butenal at three temperatures and with an applied field of 0.2 T.

The strong signals, R_1, correspond to a radical with a reduced muon-electron hyperfine coupling constant of 1.3 MHz at 197 K, increasing slightly to 4.7 MHz at 347 K. These low coupling constants and the associated temperature dependence are characteristic of muonium addition to a carbonyl group; R_1 is therefore assigned to the delocalized muoxyalkyl radical (Figure 2.11(III)).

Table 2.5 presents a comparison of reduced muon-electron hyperfine coupling constants for a series of muoxyalkyl radicals at around 295 K. It can be observed from the table that the coupling constants of the muoxyalkyl radicals formed from αβ-unsaturated carbonyl compounds are significantly lower than those of radicals such as 2-muoxyprop-2-yl. The lower coupling constants are the result of delocalization of the unpaired electron as expected.

Table 2.5 Reduced hyperfine coupling constants, A_μ', of selected muoxy radicals at ambient tempeartures[a]

Substrate	Radical	A_μ' / MHz
1, 1, 1-trifluoropropan-2-one	$CF_3\dot{C}(OMu)CH_3$	9.78[b]
hexane-2, 5-dione	$CH_3\dot{C}(OMu)CH_2CH_2COCH_3$	8.57[c]
propan-2-one	$CH_3\dot{C}(OMu)CH_3$	8.56[b]
ethanal	$CH_3\dot{C}H(OMu)$	6.82[c, d]
trans-2-butenal	$CH_3CH=CH\dot{C}(OMu)H$	2.9[c, e, f]
3-methyl-2-butenal	$(CH_3)C=CH\dot{C}(OMu)H$	2.89[e]

[a] 295 ± 5 K unless noted otherwise, [b] Ref. [44], [c] Ref. [55],

[d] 288 ± 5 K, [e] 273 ± 5 K,

[f] Approximate value estimated from weakly observed signals.

The major doublet denoted R_2 is due to the presence of a second muonium-substituted radical with a reduced hyperfine coupling constant of 58.2 MHz at 197 K increasing to 60.9 MHz at 347 K. By comparison with muonium-substituted dienes [16], in particular 2, 5-dimethyl-hexa-2, 4-diene, it is thought that R_2 arises from muonium addition at the C=C bond, yielding the thermodynamically more stable allyl type radical (Figure 2.11(I)).

This assignment is in accordance with the values measured for the αβ-unsaturated carbonyl compound, *trans*-2-butenal, studied by Macrae [56]. In this case only a single radical doublet is clearly observed corresponding to reduced hyperfine coupling constants decreasing from 94.8 MHz at 209 K to 82.8 MHz at 353 K. By comparison wth the coupling constants of the terminal alkene, vinylacetate [14], the radical corresponding to these signals was identified as an allyl type radical formed from muonium addition to the C=C bond. As with 3-methyl-2-butenal the product is the delocalized allyl type radical. The radical signals corresponding to muonium addition to the carbonyl group of *trans*-2-butenal were observed to be very weak and accurate data were difficult to obtain.

The opposite temperature dependence of the hyperfine coupling constants of the allyl type radical formed in 3-methyl-2-butenal and *trans*-2-butenal could arise from the radicals having different equilibrium conformations. The values of the hyperfine couplings of the allyl radical (R_1) listed in Table 2.3 indicate that the equilibrium geometry of the allyl radical formed in 3-methyl-2-butenal has the C-Mu bond in the nodal plane of the notional $2p_z$ orbital centred at C_2. Consequently the observed coupling constant increases in value with rising temperature. The observed temperature dependence of the hyperfine coupling constants

of the the allyl radical formed in *trans*-2-butenal indicate that, for this radical, the C-Mu bond lies out of the nodal plane of the $2p_z$ orbital located on C_2, as proposed by Macrae [55].

The polarizations, corrected for experimental time resolution [15], corresponding to muons in the muonic radicals formed from 3-methyl-2-butenal are found to be 0.109 for radical (I) and 0.064 for radical (III) at 298 K. If it is assumed that each radical has undergone proportionally the same depolarization, we can convert the fractional muon polarizations into fractional rate constants for radical formation [16]. The fractional rate constant for muonium addition to the C=C bond is 0.63 for 3-methyl-2-butenal at 298 K, which is substantially lower than the fractional rate constant for *trans*-2-butenal which is believed to be close to unity. It is surprising to find that the fractional rate constant for Mu attachment to the C=O group in 3-methyl-2-butenal is as high as 0.37. Methyl substitution of *trans*-2-butenal clearly has a strong effect on the regioselectivity of muonium addition. Whether the effect on the regioselectivity, arising from methyl substitution, occurs from an electronic or steric effect can only be determined from further experimental and theoretical studies of αβ-unsaturated carbonyl compounds.

CHAPTER 3

3 Molecular Orbital Methods for the Calculation of Selected Molecular Properties

3.1 Prelude

Comparison of the molecular properties of muonium substituted species with the corresponding properties of protonated species, reveals in some cases the existence of a large isotope effect. In particular the reduced muon-electron β-hyperfine coupling of muonium substituted radicals is significantly greater than the synonymous proton-electron coupling. The origin of this isotope effect has been the subject of some controversy since its initial observation by Roduner et al. [12]. The controversy arises from whether the observed isotope effect is due to an isotope dependent hyperconjugation interaction [63, 64] or to differences in the vibrational amplitudes and other internal degrees of freedom of the isotopomers [32]. The isotope effect on the hyperfine coupling has been interpreted to some extent by considering the conformational preference of the isotopomers arising from the isotope dependent barriers to internal rotation [43, 65]. Relation of the isotope effect to the single normal mode describing the internal rotation is however an inadequate explanation of the isotope effect observed in relatively rigid radicals such as muonated cyclohexadienyl [32] and triple-bond muonium adducts [66]. In addition the difference in the high temperature limit of the muonated and protonated ethyl radical [67] indicates that the isotope effect can

not simply be attributed to the difference in the torsional motions of the radicals.

Comparison of experimental and theoretically calculated molecular properties is restricted by the averaging over the populated vibrational states of the experimental results. Recent calculations show that a good comparison of the hyperfine couplings of the ethyl radical can be achieved if the *ab initio* results are corrected for vibrational and correlation effects [68]. In this chapter a brief description of *ab initio* molecular orbital theory is presented and a method for computing vibrational corrections to *ab initio* molecular properties is introduced. The calculated vibrational corrections enable the effects of isotopic substitution on molecular properties to be studied. The difference between the *ab initio* properties and the vibrationally averaged properties, of the species of interest, provides a measure of the effect on the molecular properties of the different vibrational amplitudes of the isotopomers. The calculations will therefore be important in the elucidation of the origin of the observed muonic isotope effect.

A comprehensive investigation by Raynes et al. [69, 70, 71, 72] on methane and its isotopomers has already shown the importance of including vibrational effects in considering *ab initio* magnetic susceptibilities and NMR coupling constants. Theoretical studies of the muonic isotope effect on the hyperfine coupling constant of muonium substituted radicals have been performed by Roduner and Reid [73], Lopes de Magalhaês and Ramos [74], Claxton et al. [75] and Chipman [76]. However in each of these studies a limited approach to the solution of the problem of vibrational averaging has been employed.

3.2 *Ab Initio* Molecular Orbital Theory

3.2.1 Theoretical Background

In principle, solution of the non-relativistic time independent Scrödinger equation [77]

$$\hat{H}\,\Psi = E\,\Psi \qquad (3.1)$$

should provide the energy (E) and many properties of a system of nuclei and electrons described by the wavefunction Ψ. The Hamiltonian, $\hat{H}$, of equation (3.1) is a differential operator representing the total energy. Unfortunately the Schrödinger equation can be solved directly only for simple one-electron systems. The solution of the differential equation (3.1) for many-electron systems is based upon a number of approximations.

First the motions of the electrons and the nuclei are separated through the Born-Oppenheimer approximation [78]. This separation is possible due to the large mass difference of the nuclei and electrons. Essentially in this approximation the electrons are regarded as moving in the field of fixed nuclei and the static nuclei therefore experience an average potential due to the surrounding electrons. The total Schrödinger equation (3.1) which describes the motion of both the electrons and nuclei in the system can consequently be separated into individual equations describing the electronic and nuclear motion, respectively. Under this separation the total wavefunction, Ψ, can be expressed as the

product of an electronic wavefunction (ψ) and a nuclear wavefunction (χ)

$$\Psi(R, r) = \psi(R, r)\, \chi(R) \qquad (3.2)$$

where the positions of the nuclei and the electrons are defined by the position vectors R and r, respectively. The electronic wavefunction explicitly depends on the electronic coordinates but also depends parametrically on the fixed nuclear coordinates.

The assumption of static nuclei enables the Hamiltonian of the Schrödinger equation for a N-electron, M-nuclei system to be expressed in atomic units as

$$\hat{H} = -\frac{1}{2} \sum_{i=1}^{N} \nabla_i^2 - \sum_{i=1}^{N} \sum_{A=1}^{M} \frac{Z_A}{r_{iA}} + \sum_{i=1}^{N} \sum_{j>i}^{N} \frac{1}{r_{ij}} \qquad (3.3)$$

where Z_A is the atomic number of nucleus A and ∇_i is the Laplacian operator which involves differentiation with respect to the coordinates of the i^{th} electron. In atomic units by an appropriate choice of physical quantities, the charge and the mass of an electron, $\hbar$ and $4\pi\varepsilon_o$ are equal to unity. This Hamiltonian operates only on the electronic coordinates of the system and is termed the electronic Hamiltonian. Solution of the Schrödinger equation involving the electronic Hamiltonian provides the electronic wavefunction $\psi(R, r)$ and the electronic energy E_e. The total energy of the system is obtained by adding the term

$$\sum_{A=1}^{M} \sum_{B>A}^{N} \frac{Z_A Z_B}{R_{AB}} \qquad (3.4)$$

describing the nuclear repulsion of the static nuclei to the electronic energy. The Born-Oppenheimer approximation therefore allows the simplification of the total Schrödinger equation to an electronic problem and neglects the effects of nuclear motion. Exact solutions to the electronic Schrödinger equation are possible only for simple one-electron systems such as the H_2^+ molecular ion. Approximate solutions can be obtained for many-electron systems using the Hartree-Fock approximation [79, 80]. The essence of the Hartree-Fock approximation is that it replaces the complicated many-electron problem by a one-electron problem in which the electron-electron repulsions are treated in an average way.

3.2.2 The Hartree-Fock Approximation

The simplest antisymmetric electronic wavefunction which can be used to describe the ground state of an N-electron system is a single Slater determinant [81] represented by

$$\psi(1, \ldots, N) = \frac{1}{\sqrt{N!}} \sum_{n=1}^{N!} (-1)^P P_n\{\chi_i(1)\,\chi_j(2) \ldots\ldots \chi_k(N)\} \qquad (3.5)$$

where N is a normalization factor, P_n is a permutation operator that generates the n^{th} permutation of electrons 1, 2, ..., N, P is the number of transpositions required to obtain this permutation and $\chi_i(1) \ldots\ldots \chi_k(N)$ are the spin orbitals describing the N-electron system. The spin orbitals are the wavefunctions for each electron and are the product of a spatial orbital, ψ, and one of the two possible spin functions α or β.

The Hartree-Fock approximation is based upon the variation method

of quantum mechanics. This states that the best possible electronic wavefunction of the form of (3.5) is that which gives the lowest possible expectation energy (E_o)

$$E_o = \langle \psi | \hat{H} | \psi \rangle / \langle \psi | \psi \rangle \qquad (3.6)$$

where $\hat{H}$ is the electronic Hamiltonian operator. The variational flexibility in the wavefunction is in the choice of the spin orbitals $\chi_i(j)$. The Hartree-Fock approximation assumes it is possible to obtain the optimum spin orbitals by minimizing the energy E_o with respect to the choice of spin orbitals.

The expectation value of the electronic energy is more usually written in the form

$$E_o = 2 \sum_{i=1}^{N/2} h_{ii} + \sum_{i,j=1}^{N/2} 2J_{ij} - K_{ij} \qquad (3.7)$$

After integration out of the spin functions the term h_{ii} can be expressed in terms of the spatial functions as

$$h_{ii} = \langle \psi_i(s) | -\frac{1}{2} \nabla_s - \sum_A \frac{Z_A}{r_{sA}} | \psi_i(s) \rangle \qquad (3.8)$$

and is known as the core-Hamiltonian. This term describes the kinetic and potential energies of a single electron in the field of the static nuclei. The remaining terms J_{ij} and K_{ij} in (3.7) are known as the coloumb and exchange integrals, respectively. The coloumb integral can be expressed as

$$J_{ij} = \langle \psi_i(s)\psi_j(p) | \frac{1}{r_{sp}} | \psi_i(s)\psi_j(p) \rangle \qquad (3.9)$$

which represents the classical coloumb repulsion between the charge clouds $|\psi_i(s)|^2$ and $|\psi_j(p)|^2$. The exchange integral is the result of exchange correlation which arises from the motions of electrons with parallel spins.

$$K_{ij} = \langle \psi_i(s)\psi_j(p) | \frac{1}{r_{sp}} | \psi_i(p)\psi_j(s) \rangle \qquad (3.10)$$

Minimization of E_o with respect to the choice of spin orbitals leads to the Hartree-Fock eigenvalue equation

$$\hat{F}_i \chi_i = \varepsilon_i \chi_i \qquad i = 1, \ldots\ldots, N \qquad (3.11)$$

where χ_i are the spin orbitals, ε_i is the corresponding orbital energy and $\hat{F}_i$ is effectively a one-electron operator called the Fock operator which has the form.

$$\hat{F} = \hat{h}_s + \sum_i^N (2\hat{J}_i - \hat{K}_i) \qquad (3.12)$$

where $\hat{J}_i$ and $\hat{K}_i$ are the coloumb and exchange operators expressed as

$$\hat{J}_i(s)\psi_i(s) = \langle \psi_i(p) | \frac{1}{r_{sp}} | \psi_i(p) \rangle \psi_j(s) \qquad (3.13)$$

and

$$\hat{K}_i(s)\psi_j(s) = \langle \psi_i(p) | \frac{1}{r_{sp}} | \psi_j(p) \rangle \psi_i(s) \qquad (3.14)$$

The expectation value of the operators $\hat{K}_i$ and $\hat{J}_i$ are equivalent to the previous definitions of the coloumb and exchange integrals given in equations (3.9) and (3.10). The Hartree-Fock equation (3.11) is an

eigenvalue equation with the spin orbitals as eigenfunctions and the energies of the spin orbitals as eigenvalues. The coloumb and exchange operators of the Fock operator describe the potential field experienced by the i^{th} electron. It is obvious from (3.13) and (3.14) that this field is dependent upon the eigenfunctions χ_i. Therefore the Fock operator is dependent upon its eigenfunctions. The procedure for solving the Hartree-Fock equation is known as the self-consistent-field (SCF) method. This involves making an initial guess at the spin orbitals and then solving the eigenvalue problem (3.11) to obtain a new set of spin orbitals. Using these new orbitals new fields can be obtained and the procedure repeated until self-consistency is achieved. The resultant spin orbitals and orbital energies enable the total electronic energy (E_o) and many molecular properties of the N-electron system to be determined.

The theory outlined for the solution of the Hartree-Fock equation has assumed that the N-electron system is a closed shell system. This imposes the restiction that each spatial orbital is doubly occupied and that identical spatial orbitals are used for different spin orbitals. The electronic wavefunction of a N-electron system composed of $n\alpha$ and $n\beta$ electrons in terms of spatial (ψ) and spin functions (α and β) is

$$\Psi = |\psi_1^{\alpha}(1)\alpha(1)\psi_1^{\beta}(2)\beta(2)\psi_2^{\alpha}(3)\alpha(3)\psi_2^{\beta}(4)\beta(4).....\psi_{2n}^{\beta}(2n)\beta(2n)| \qquad (3.15)$$

The method of solution of the electronic Schrödinger equation using a wavefunction of this form is known as the restricted Hartree-Fock (RHF) method [82]. This method can be extended to open-shell systems, where the number of α and β electrons is inequivalent. In practice open-shell

systems are usually treated using unrestricted Hartree-Fock (UHF) theory [83]. In the UHF procedure different spatial orbitals are used to describe electrons of α and β spin and the restiction of double occupancy of the spatial orbitals is lifted. The procedure used to solve the electronic Schrödinger equation using an unrestricted wavefunction is analogous to the RHF method. The minimization of the energy with respect to the choice of orbitals results in the derivation of two Hartree-Fock equations corresponding to the spatial orbitals of α and β electrons.

$$\hat{F}_i^{\alpha} \psi_i^{\alpha} = \varepsilon_i \psi_i^{\alpha} \tag{3.16}$$

$$\hat{F}_i^{\beta} \psi_i^{\beta} = \varepsilon_i \psi_i^{\beta} \tag{3.17}$$

Unlike the electronic wavefunction obtained from the RHF methods the UHF wavefunction is not a pure state and is therefore not an eigenfunction of the spin operators S_z and S_z^2. This is a result of the wavefunction containing contaminating components from states of higher multiplicities. Provided the spin contamination from higher spin states is small the UHF wavefunction results in a lower energy and improved values of molecular properties for open-shell systems due to the increased flexibility in the choice of spin functions.

The solution of the Hartree-Fock equations for molecules is usually performed by a method proposed almost simultaneously by Hall [84] and Roothaan [85] in which the basis spatial orbitals are expressed in terms of a linear combination of m basis functions φ.

$$\psi_i = \sum_{q=1}^{m} c_{iq} \varphi_q \tag{3.18}$$

The set of functions $\{\varphi_q\}$ is known as the basis set and by adopting this expansion technique, the Hartree-Fock equation can be solved for molecular systems. The larger and more complete the set of functions φ_q that is chosen the closer the approximate molecular spatial orbitals are to the orbitals that would be obtained by direct solution of the Hartree-Fock equations. The molecular energy obtained by direct solution of the Hartree-Fock equations is known as the Hartree-Fock limit. In practice any finite value of m will lead to an energy somewhat above the Hartree-Fock limit.

The primary deficiency of the Hartree-Fock theory is the inadequate treatment of the correlation between motions of electrons. The single-determinant wavefunction employed in this method takes no account of the correlation between electrons with opposite spin. Correlation of the motions of electrons of the same spin is partially accounted for by the virtue of the determinantal form of the wavefunction. The correlation limitation leads to calculated energies that are higher than the exact non-relativistic energy. The difference between the energy at the Hartree-Fock limit and the exact energy is known as the correlation energy. Several advaced quantum mechanical techniques have been developed to incorporate correlation effects in *ab initio* molecular orbital calculations. The principal methods used to study the contribution of the correlation energy to the total molecular energy are configuration interaction (CI), multi-configurational SCF (MCSCF) and many body perturbation theory (MBPT). A recent review by Simons [86] provides a good introduction to the subject of modern *ab initio* quantum chemistry. Several excellent books exist giving comprehensive descriptions of Hartree-Fock theory and the more advanced quantum mechanical

methods used to incorporate correlation effects. Three of which have been freely consulted in compiling this section are those by Szabo and Ostlund [87], Hehre et al. [88] and Dykstra [89].

3.2.3 Orbitals and Basis Functions

The solution of the electronic Schrödinger equation through the Hartree-Fock approximation, as outlined in the previous section, assumes that an initial set of spin orbitals are chosen to describe the electronic wavefunction. These spin orbitals comprise a product of spatial functions $\psi_i(R, r)$ and either an α or β spin function. The spin orbitals formed from the product describe both the spin and spatial coordinates of the i^{th} electron. The spatial functions of molecules are termed molecular orbitals. These molecular orbitals are in practice described as linear combinations of known one-electron functions, $\varphi_i(x, y, z)$. The formation of molecular orbitals from one-electron basis functions is known as the linear combination of atomic orbitals (LCAO) method. The molecular orbital is therefore expressed in terms of the atomic basis functions

$$\psi_i(x, y, z) = \sum_{u=1}^{N} c_{ui} \varphi_u \qquad (3.19)$$

where c_{ui} are the molecular orbital expansion coefficients. These coefficients provide the orbital description with a degree of flexibility that enables its use in the Hartree-Fock approximation.

Two types of basis functions (φ_u) are in widespread use. The first type of basis uses Slater type orbitals (STOs) [90]. These are functions which are analogous to the actual solutions of the Schrödinger equation

of the hydrogen atom but possess different nodal properties. These functions in the form of spherical coordinates are described by (3.20)

$$\varphi_{nlm}^{STO}(r, \vartheta, \varphi) = A_n r^{n-1} e^{-\zeta r} Y_{l,m}(\vartheta, \varphi) \qquad (3.20)$$

where n, l and m are the principal, azimuthal and magnetic quantum numbers respectively; r, ϑ and φ have their usual meaning in a radial coordinate system, A_n is a normalizing factor and $Y_{l,m}(\vartheta, \varphi)$ are the unnormalized spherical harmonics which introduce the required angular dependence. The term $r^{n-1} e^{-\zeta r}$ is the radial part of the wavefunction and ζ is the effective nuclear charge or more simply the orbital exponent.

The second, and more widely used, type of basis functions are gaussian type atomic orbitals (GTOs) which were first introduced into molecular orbital calculations by Boys [91].

$$\varphi_{nlm}^{GTO}(r, \vartheta, \varphi) = A_N r^{n-1} e^{-\alpha r^2} Y_{l,m}(\vartheta, \varphi) \qquad (3.21)$$

Gaussian functions are less satisfactory for the representation of atomic orbitals than Slater type orbitals because they do not have a cusp at their origin. However, they have the advantage that integrals involving gaussian basis functions are easier to evaluate than integrals involving STOs.

To improve the representation of molcular orbitals by gaussian functions, linear combinations of gaussian functions (g_i) are used as basis functions

$$\varphi_u = \sum_i d_{ui} g_i \qquad (3.22)$$

where g_i are individual gaussian functions and the coefficients d_{ui} are fixed. Basis functions of this type are called contracted gaussians, the individual gaussian functions being termed primitive gaussians.

The larger and more complete the set of basis functions $\{\varphi_u\}$ the greater the degree of flexibility in the expansion of the spin orbitals and the lower will be the expectation value of the molecular energy. Larger and larger basis sets will keep lowering the Hartree-Fock energy until the Hartree-Fock limit is reached. A large number of standard basis sets now exist for use in *ab initio* molecular orbital calculations. The choice of a basis set for any calculation is dependent upon the accuracy of the basis set in representing a particular molecular property and the computational time available. A study by Davidson and Feller [92] provides a comprehensive guide to the evolution of the commonly used basis sets and the inherent problems in chosing the correct set. A description of the basis sets required for very high quality *ab initio* calculations is given by Almlöf et al. [93].

3.3 *Ab Initio* One-Electron Properties

3.3.1 Hyperfine Coupling Constants

There are two main magnetic interactions between the unpaired electron and the magnetic nuclei in an organic radical. The first interaction is the classical dipolar interaction between the magnetic moments of the nuclei and the electron. This interaction is strongly anisotropic. It is not observed in liquids because due to the rapid and disordered motions of the molecules it averages to zero. The most

significant interaction is the isotropic or Fermi-contact hyperfine interaction. This interaction can be expressed by the spin Hamiltonian

$$\hat{H} = A_N \hat{S} . \hat{I} \qquad (3.23)$$

for the simplified case of an electron coupling with one magnetic nuclei. A_N is the hyperfine coupling constant, which is a measure of the unpaired spin density at the site of nucleus N and $\hat{S}$ and $\hat{I}$ are the electron and nuclear spin operators, respectively. A_N is related to the electronic wavefunction (ψ) describing the system by the equation

$$A_N = \frac{8\pi}{3h} g_e g_N \beta_e \beta_N \langle \psi | \hat{\rho}_N(r) | \psi \rangle \qquad (3.24)$$

where g_e and g_N are the electron and nuclear g-factors respectively; β_e is the Bohr magneton; β_N the nuclear magneton and $\langle \psi | \hat{\rho}_N(r) | \psi \rangle$ is the expectation value of the spin density at the position of nucleus N. The hyperfine coupling constant is therefore easily evaluated from the electronic wavefunction obtained from an *ab initio* calculation.

At the Hartree-Fock level for certain radicals, *ab initially* computed hyperfine coupling constants show poor agreement with experiment [94]. This problem can be overcome to some extent through the inclusion of correlation and vibrational corrections as shown by the work of Chipman et al. [76, 95] and Carmichael [68].

3.3.2 Nuclear Quadrupole Coupling

Quadrupole coupling arises from the interaction of a nuclear quadrupole moment (Q) with the electric field gradient (efg) generated at the nucleus by the surrounding electron and nuclear charge clouds. The quadrupole moment is a measure of the deviation of nuclear charge from spherical symmetry and is possessed by nuclei of spin $I > 1/2$. The energy arising from the quadrupole interaction is dependent upon the orientation of the quadrupole moment in the electric field. The Hamiltonian describing this interaction can be written

$$\hat{H} = \hat{I}.\hat{Q}.\hat{I} \qquad (3.25)$$

where $\hat{I}$ is the nuclear spin operator and $\hat{Q}$ is the quadrupole energy tensor, usually expressed in terms of components of the electric field gradient (q_{xx}, q_{yy}, q_{zz}). The quadrupole energy tensor has a principal axis system (x, y, z) in which it is diagonal. In this system the Hamiltonian can be written in the simplified form

$$\hat{H}_Q = \frac{1}{2} A [3I_z^2 - I(I+1) + \eta(I_x^2 - I_y^2)] \qquad (3.26)$$

where

$$\eta = \frac{q_{xx} - q_{yy}}{q_{zz}} \qquad (3.27)$$

with

$$|q_{zz}| \geq |q_{yy}| \geq |q_{xx}| \qquad (3.28)$$

η is an asymmetry parameter which vanishes in an axially symmetric field gradient ($q_{xx} = q_{yy} = q_{zz}$) and

$$A = \frac{e^2 q_{zz} Q}{2I(2I - 1)} \tag{3.29}$$

where Q is the nuclear quadrupole moment and q_{zz} is the zz-component of the electric field gradient at the nucleus. The product $e^2 q_{zz} Q$ is referred to as the quadrupole coupling constant.

The components of the electric field gradient at a nucleus can be evaluated using *ab initio* molecular orbital theory. In a molecule the efg at a particular nucleus N is given by the expectation value of the field gradient operator

$$e q_{zz} = \langle \psi | \frac{3\cos^2\vartheta - 1}{r^3} | \psi \rangle \tag{3.30}$$

where r is the radius vector from the nucleus to the electron, ϑ is the angle between r and the nuclear fixed z-axis and ψ is the elctronic wavefunction.

Studies of the quadrupole couplings in the water molecule by Keshari et al. [96] and in ammonia by Gejji and Lunnell [97] show the ability of current *ab initio* calcualtions in providing quadrupole couplings in good agreement with experiment.

3.4 Vibrational Corrections to *Ab Initio* Molecular Properties

3.4.1 Introduction

As mentioned in the prelude to this chapter vibrational corrections enables a study of the effect of isotopic substitution on *ab initio* calculated molecular properties to be performed. The calculations also enable the determination of the contribution of nuclear vibrational motion to isotope effects.

In this section a variation-perturbation technique that can be applied to the calculation of vibrational corrections is presented. This method has been fully developed by Kern and Matcha; and Ermler et al. [98, 99, 100, 101]. The initial stage of this technique is the calculation of *ab initio* potential energy and property surfaces of the species of interest. The computed surfaces are then fit to analytic expressions using a least-squares fitting routine. The derived analytic energy function is used in a standard normal mode analysis which enables the transformation matrix to normal coordinates to be computed [102, 103]. The property and energy expansions are then re-expanded as Taylor series functions of the normal coordinates. These expressions are then used in a perturbation theory analysis of the vibrational corrections. The computer program SURVIB has been developed by Harding et al. [104] to perform a least-squares fit to *ab initio* property surfaces and to compute values of the vibrationally averaged properties.

3.4.2 Theoretical Description

Within the Born-Oppenheimer approximation the electronic and nuclear motions of the system are uncoupled and the total wavefunction of the Schrödinger equation can be written as the product of a nuclear and electronic function. The electronic wavefunction can be derived using *ab* initio molecular orbital theory as described in the previous section. The nuclear wavefunction describing the vibrational motion of the nuclei in the system can be obtained by solution of the vibrational Hamiltonian

$$H_v = H_v^{(o)} + H_v^{(1)} + H_v^{(2)} \qquad (3.31)$$

where

$$H_v^{(o)} = \frac{1}{2} \sum_{i}^{N} \omega_i (p_i^2 + q_i^2) \qquad (3.32)$$

$$H_v^{(1)} = \sum_{ijk}^{N} k_{ijk} q_i q_j q_k \qquad (3.33)$$

and

$$H_v^{(2)} = \sum_{ijkl}^{N} k_{ijkl} q_i q_j q_k q_l \qquad (3.34)$$

The terms $H_v^{(o)}$, $H_v^{(1)}$ and $H_v^{(2)}$ are the harmonic cubic and quartic contributions to the vibrational energy of the system, respectively. The parameters ω_i, k_{ijk} and k_{ijkl} are the frequencies or force constants corresponding to the reduced normal coordinates q_i. The nuclear wavefunction χ_v obtained by solution of the vibrational wavefunction using Rayleigh-Schrödinger [105] perturbation theory enables the derivation of any molecular property in a given vibrational state. The

nuclear wavefunction describing the vibrational motion of the nuclei can be obtained by assuming convergence of

$$\chi_v = \chi_v^{(o)} + \lambda \chi_v^{(1)} + \lambda^2 \chi_v^{(2)} \tag{3.35}$$

and

$$E_v = E_v^{(o)} + \lambda E_v^{(1)} + \lambda^2 E_v^{(2)} \tag{3.36}$$

where λ is an ordering parameter and E_v is the vibrational energy associated with wavefunction χ_v. Substitution of equations (3.35) and (3.36) into the vibrational Schrödinger equation

$$H_v \chi_v = E_v \chi_v \tag{3.37}$$

leads to the zero-order, first-order and second-order perturbation equations

$$(H_v^{(o)} - E_v^{(o)}) \chi_v^{(o)} = 0 \tag{3.38}$$

$$(H_v^{(o)} - E_v^{(o)}) \chi_v^{(1)} + (H_v^{(1)} - E_v^{(1)}) \chi_v^{(o)} = 0 \tag{3.39}$$

and

$$(H_v^{(2)} - E_v^{(2)}) \chi_v^{(o)} + (H_v^{(1)} - E_v^{(1)}) \chi_v^{(1)} + (H_v^{(o)} - E_v^{(o)}) \chi_v^{(2)} = 0 \tag{3.40}$$

From (3.38), (3.39) and (3.40) the zero and first-order solutions to the vibrational Schrödinger equation can be obtained.

The solution $\chi_v^{(o)}$ to the zero-order equation (3.38) is a simple

product of harmonic oscillator functions of the form

$$\chi_v^{(o)} = \chi_{v_1}(q_1)\,\chi_{v_2}(q_2)\ldots\ldots\ldots\ldots\chi_{v_N}(q_N) \qquad (3.41)$$

where

$$\chi_{v_i}(q_i) = N_{v_i} H_{v_i}(q_i)\exp(-\frac{1}{2} q_i^2) \qquad (3.42)$$

N_{v_i} is a normalization factor and H_{v_i} are the Hermite polynomials of degree v_i in the variables q_i. Using the zero-order solutions as an expansion set for the first-order wavefunction

$$\chi_v^{(1)} = \sum_{u=v} a_{vu}^{(1)}\,\chi_u^{(o)} \qquad (3.43)$$

with each expansion coefficient $a_{vu}^{(1)}$ being associated with excitations or de-excitations of $\chi_u^{(o)}$, the first-order correction to the wavefunction can be obtained. As a consequence of the first-order energy vanishing due to all the terms in $H_v^{(1)}$ being odd in at least one displacement coordinate, the wavefunction $\chi_v^{(1)}$ is obtained using a variational approach. This method requires consideration of the second-order perturbation equation (3.40). Using the expansion (3.43) to represent the first-order corrected wavefunction $\chi_v^{(1)}$, the second-order energy functional ($\tilde{E}$) is given by [105]

$$\tilde{E}_v^{(2)} = \langle \chi_v^{(o)} | H_v^{(2)} | \chi_v^{(o)} \rangle + 2\langle \chi_v^{(o)} | H_v^{(1)} - E_v^{(1)} | \chi_v^{(1)} \rangle + \langle \chi_v^{(1)} | H_v^{(o)} - E_v^{(o)} | \chi_v^{(1)} \rangle \qquad (3.44)$$

To obtain the coefficients of expansion (3.43) the energy functional $\tilde{E}_v^{(2)}$ is minimized with respect to the first-order wavefunction $\chi_v^{(1)}$. Explicit expressions for the expansion coefficients of $\chi_v^{(1)}$ have been derived by Ermler et al. [101]. Although this method can be generalized to include second and higher-order perturbation corrections to the wavefunction, here low-lying vibrational states are considered and the perturbation corrections are restricted to first-order terms. The vibrational wavefunction is therefore approximated by

$$\chi_v = \chi_v^{(o)} + \chi_v^{(1)} \tag{3.45}$$

and is normalized through first-order. The inclusion of first-order corrections allows the effects of anharmonicity in the vibrational motion of a system to be studied. The wavefunction χ_v corrected through first-order also enables vibrational corrections to expectation values averaged over electronic wavefunctions of polyatomic molecules to be calculated. The vibrationally averaged expectation value is given by the equation

$$\langle P \rangle_v = \langle \chi_v | P_E | \chi_v \rangle / \langle \chi_v | \chi_v \rangle \tag{3.46}$$

where

$$P_E = \langle \psi | P | \psi \rangle / \langle \psi | \psi \rangle \tag{3.47}$$

and ψ and χ_v are, respectively, the electronic and vibrational wavefunctions. The operator P_E is the analytic form of the electronic property obtained from the least-squares fitting routine. In reduced

normal coordinates near the equilibrium configuration of the system the analytic function can be represented by a multidimensional power series of the form

$$P_E = P_o + \sum_{i=1}^{N} \alpha_i q_i + \sum_{i,j=1}^{N} \beta_{ij} q_i q_j + \sum_{i,j,k=1}^{N} \gamma_{ijk} q_i q_j q_k + \ldots\ldots\ldots \quad (3.48)$$

where α, β and γ are expansion coefficients and P_o is the value of P_E at the minimum energy conformation of the system. Substitution of equations (3.48) and (3.45) into (3.46) allows the calculation of the vibrationally averaged property. This procedure leads to the quantum number (ν) expansion for vibrational corrections to electronic properties of

$$\langle P \rangle_\nu = C + \sum_{i=1}^{N} A_i(\nu_i + 1/2) + \sum_{i \leq j}^{N} B_{ij}(\nu_i + 1/2)(\nu_j + 1/2) \quad (3.49)$$

where C, A and B are expansion coefficients derived from the normal frequencies (ω) obtained from the normal mode analysis and the property expansion coefficients of (3.48). The initial term C of equation (3.49) is independent of the vibrational state of the polyatomic system. The remaining terms which are dependent on the vibrational state provide a measure of the harmonic and anharmonic contributions to the vibrational averaging. The vibrational corrections to the computed molecular properties can be defined as the difference between the vibrationally averaged property $\langle P \rangle_\nu$ and the value of the property at the stationary point of the property function P_E. These corrections are therefore obtained by the combination of second-order perturbation theory with *ab initio* molecular orbital theory.

This technique provides a theoretical method for studying isotope effects on molecular properties. The isotope dependence of the properties is introduced in the transformation of the internal coordinate analytic property function to the mass dependent normal coordinate analytic function. The *ab initio* property surface of any molecule can therefore be used to compute the molecular properties of all possible isotopomers.

The errors arising from the application of any method of vibrational analysis are normally dominated by the inherent inaccuracies in the analytic functions representing the *ab initio* property surfaces. It is therefore important to have an estimate of the error associated with the fitting procedure. The error estimate from the program SURVIB assumes the harmonic force constants are exact and only the standard deviations in the cubic force constants are considered. The linear, quadratic and cubic coefficients in the property expansions are, however, all included. The error limits of the vibrationally averaged properties are found by adding the respective standard deviations to both the cubic force constants and to the property expansion coefficients, repeating the calculations of the property corrections and then designating three times the difference between the two results as the error in the corrected property.

Imposed on this method of vibrational averaging are the restrictions arising from truncation of the vibrational wavefunction after the first-order correction and the use of Hartree-Fock theory to compute the necessary property and energy surfaces. Further the vibrational analysis is limited to states that remain in the region of small vibrations. This is achieved by considering vibrational levels whose quantum numbers sum to less than three.

Calculations of *ab initio* properties are increasingly introducing corrections due to vibrational effects. These corrections can be made due to the availability of accurate potential energy surfaces for small molecules and the recent advances in the computation of higher-order derivatives. A comprehensive study by Clabo et al. [106] indicates the improved agreement between theoretical and experimental properties that can be achieved by the introduction of vibrational averaging. More recently Harding [107] has performed an extensive vibrational analysis of hydrogen peroxide and its deuterium isotopomers using an *ab initio* anharmonic force field. The results of which are in good agreement with available experimental data.

CHAPTER 4

4 Vibrational Corrections to Molecular Properties of the Water Molecule and Selected Isotopomers

4.1 Introduction

A large number of detailed theoretical vibrational analysis studies have been performed on the water molecule and its isotopomers [98, 99, 100, 101, 106, 108, 109, 110, 111, 112]. This is a reflection of the simplification of the vibrational problem for systems having a small number of normal modes of vibration. Additionally the potential energy and property surfaces necessary to compute the force constants and vibrational corrections are easier to calculate for small systems. In this chapter the vibrational corrections to selected molecular properties of the water molecule and its isotopomers, in particular MuOH and Mu_2O, are presented. The substitution of hydrogen by muonium is expected to result in large isotope shifts in the calculated vibrational corrections to molecular properties of the water molecule due to the large mass difference between the respective nuclei. The theoretical results should aid in the interpretation of the experimental observations made by Cox and co-workers on the diamagnetic state formed on muon implantation in ^{17}O doped ice [7, 11]. The computation of the vibrational corrections to the molecular properties of the isotopomers of water were performed using the computer program SURVIB [104]. This program uses a variation-perturbation approach as outlined in the previous chapter. The *ab initio* calculations necessary to carry out the theoretical studies were performed on the University of Glasgow MicroVax 3600 using the GAMESS molecular orbital package [113].

4.2 The Water Molecule

4.2.1 Computational Details

Initially a full geometry optimization of the water molecule was carried out at the SCF level using the Baker optimization routine [114] of the GAMESS molecular orbital program. The calculation was performed using the standard 6-31G** contracted gaussian basis set of Hariharan and Pople [115]. In the SCF calculation convergence was assumed to have been achieved when the change in the elements of the density matrix was less than 10^{-5} in absolute value in a single SCF cycle. The convergence criteria for the geometry optimization were that the largest component of the calculated gradient was less than 5 x 10^{-4} Hartree / Bohr and the root-mean-square gradient was less than 1.6 x 10^{-4} Hartree / Bohr. The calculated equilibrium geometry of the water molecule is given in Figure 4.1.

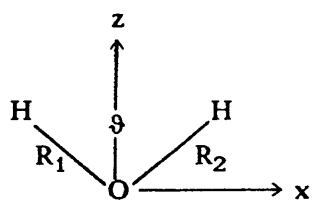

$R_1^e = R_2^e = 94.3$ pm

$\vartheta^e = 105.99^o$

Figure 4.1 Optimized geometry of the water molecule.

The total energy at this conformation and its electronic and nuclear components are given below

$$E_{Total} = -76.023615\ E_h$$
$$E_{el} = -85.353449\ E_h$$
$$E_{nuc} = 9.329834\ E_h$$

The z-component of the molecular dipole moment (μ_z) and the zz-component of the electric field gradient (q_{zz}), in the principal axis system, of the oxygen nucleus at this conformation were found to be 7.162×10^{-30} C m and 1.864 a.u., respectively. These results are in good agreement with comparable *ab initio* calculations [116]. Correlation effects have been neglected in this study of the water molecule to reduce the time required to compute the energy and property surfaces necessary for vibrational averaging. In addition the work of Rosenberg et al. [109] has shown that the computed vibrational corrections obtained from SCF and CI calculations on the water molecule are very similar, even for the cases where the SCF and CI values of a property vary significantly. The neglect of correlation effects will therefore not affect the trends observed in the computed isotope dependent vibrational corrections but will considerably reduce the computational effort required to calculate the corrections.

Electronic wavefunctions and properties were calculated, at the SCF level, at 120 points about the stationary point geometry. The surfaces were built up varying the three internal coordinates R_1, R_2 and ϑ from their equilibrium values R_1^e, R_2^e and ϑ^e over the ranges ± 6 pm, ± 6 pm and ± 6°, respectively. These ranges were chosen beacuse they correspond to the root-mean-square zero-point vibrational amplitudes of the

molecule [98, 99]. The computed surfaces are composed of 58 symmetric and 62 asymmetric configurations.

4.2.2 Vibrational Analysis

The computed SCF energy surface was fitted to a Taylor series expansion in terms of the internal coordinates R_1, R_2 and ϑ using a least-squares fitting routine. The internal coordinate function obtained from the fitting routine consists of a Simmons-Paar-Finlan (SPF) [117] expansion in terms of the bond lengths and a Taylor series expansion in terms of the bond angle. Taylor series functions in which the bond lengths are replaced by the corresponding SPF coordinate provide superior fits to the surface, especially for regions significantly removed from the equilibrium geometry. The Simmons-Paar-Finlan coordinate can be expressed as

$$R^{SPF} = (R - R^e) / R \qquad (4.1)$$

where R is an internal coordinate bond length and R^e is the equilibrium value of that internal coordinate. The computed energy function is expressed in the form

$$E = E_o + \sum_{i=1}^{3} K_i S_i + 1/2 \sum_{i,j=1}^{3} K_{ij} S_i S_j + \sum_{i,j,k=1}^{3} K_{ijk} S_i S_j S_k \qquad (4.2)$$

where the terms S_1, S_2 and S_3 are to be identified with the SPF coordinates $R_1^{SPF} = (R_1 - R_1^e)/ R_1$, $R_2^{SPF} = (R_2 - R_2^e) / R_2$ and the angle displacement coordinate $\Delta\vartheta = \vartheta - \vartheta^e$, respectively. The term E_o is the energy of the molecule at the SCF stationary point conformation. The

expansion coefficients K_i correspond to the first-order derivatives of the energy with respect to the internal coordinates and are therefore zero when E is expanded about the minimum energy configuration. The non-zero independent expansion coefficients K_{ij} and K_{ijk}, which correspond to the second and third order derivatives of the energy with respect to the internal coordinates, respectively, are listed in Table 4.1. The calculated force constants listed in Table 4.1 are in reasonable agreement with experimentally determined values of these parameters [118, 119].

Table 4.1 Calculated independent quadratic and cubic expansion constants of the analytic internal displacement coordinate enegy function (E) / a.u.

Quadratic Expansion Constants		Cubic Expansion Constants	
K_{11}	1.009	K_{111}	-0.1719
K_{12}	-0.01956	K_{112}	-0.02146
K_{13}	0.05443	K_{113}	0.04749
K_{33}	0.08933	K_{123}	-0.01196
		K_{133}	-0.02955
		K_{333}	-0.02824

Expression (4.1) was actually expanded to include fourth-order terms, although they are not explicitly required for the perturbation treatment used to calculate the vibrational corrections they are included as they result in reduced errors in the cubic expansion coefficients. Fourth-order expansions were used in all calculations on the water molecule to

minimize the errors in the computed results except for the isotopomer MuOH. For this isotopic variant the lowest errors in the results for the vibrational correction to the dipole moment were obtained using a third-order expansion. The computed energy function (E) reproduces the 120 calculated energies with a maximum error of 6.0×10^{-7} and a root-mean-square error of 2.5×10^{-7} a.u. The stationary point of the analytic function has an energy of -76.023615 E_h and internal coordinates $R_1 = R_2 = 94.3$ pm and $\vartheta = 105.97°$.

The calculated harmonic force constants are used to generate the harmonic frequencies ω_i and the transformation matrix to the reduced normal coordinate frame for the isotopic variants H_2O, HDO, D_2O, MuOH and Mu_2O. The harmonic frequencies and the zero-point energy of each of these species obtained from the theoretical *ab initio* energy surface are given in Table 4.2.

Table 4.2 Calculated harmonic frequencies (ω_i) / cm^{-1} and harmonic zero-point energies (E_{zp}) / cm^{-1} for H_2O, DOH, D_2O, MuOH and Mu_2O

Isotopomers	H_2O	DOH	D_2O	MuOH	Mu_2O
ω_1	4263.99	4208.54	3126.31	12184.00	12251.34
ω_2	1770.37	1551.87	1295.88	3767.36	5079.63
ω_3	4147.83	3055.51	2989.82	4252.90	12126.08
E_{zp}	5091.16	4407.96	3706.00	10102.13	14728.52

The subscripts 1, 2 and 3 refer to the symmetric stretch (ω_1), bend (ω_2) and asymmetric stretch (ω_3) for H_2O, D_2O and Mu_2O; and O-H(Mu) stretch (ω_1), O-D(H) stretch (ω_3) and bend (ω_2) for HDO and MuOH.

The internal coordinate analytic function (E) is re-expanded in terms of a normal coordinate expansion using the transformation matrix obtained from the normal mode analysis. The analytic normal coordinate energy function has the form

$$E = E_o + \sum_{i=1}^{3} \alpha_i q_i + \sum_{i,j=1}^{3} \beta_{ij} q_i q_j + \sum_{i,j,k=1}^{3} \gamma_{ijk} q_i q_j q_k \qquad (4.3)$$

where q_i are the reduced normal coordinates and α, β and γ are the expansion coefficients. Table 4.3 lists the normal coordinate expansion coefficients of expression (4.3) for the isotopic variants of the water molecule under consideration.

Table 4.3 Normal coordinate expansion coefficients / x 10^2 for the energy function (E) of the water molecule and its isotopomers / a.u.

	Isotopomer				
Coefficient (x 10^2) [a]	H_2O	HDO	D_2O	MuOH	Mu_2O
β_{11}	0.01887	0.01838	0.01014	0.15409	0.15580
β_{22}	0.00325	0.00250	0.00174	0.01473	0.02678
β_{33}	0.01786	0.00970	0.00928	0.01877	0.15263
γ_{111}	0.00000	0.00054	0.00000	0.01304	0.0000
γ_{112}	0.00010	0.00005	0.00004	-0.00113	0.00228
γ_{113}	0.00115	-0.00007	0.00045	0.00018	0.02763
γ_{122}	0.00000	-0.00011	0.00000	-0.00381	0.00000
γ_{123}	0.00000	0.00006	0.00000	0.00209	0.00000
γ_{133}	0.00000	-0.00004	0.00000	-0.00029	0.00000
γ_{222}	-0.00001	-0.00001	0.00000	0.00011	-0.00039
γ_{223}	-0.00010	0.00001	-0.00004	-0.00035	-0.00215
γ_{233}	0.00002	0.00002	0.00000	-0.00038	0.00102
γ_{333}	0.00037	-0.00020	0.00014	-0.00047	0.00921

[a] Expansion coefficients of adsolute value less than 1 x 10^{-7} are given as exactly zero.

The difference between the expansion coefficients listed in Table 4.3 results from the transformation to mass dependent normal coordinates. These coefficients and the computed harmonic frequencies (ω_i) enable the expansion constants of the quantum number (v) expansion for the energy

to be determined. This quantum number expansion is usually expressed in the form

$$E_v = G + \sum_{i=1}^{3} A_i(v_i + 1/2) + \sum_{1\le j}^{3} B_{ij}(v_i + 1/2)(v_j + 1/2) \quad (4.4)$$

and enables the vibrational corrections to the energy for each isotopomer to be calculated. The expansion constants of (4.4) for selected isotopic variants of the water molecule are listed in Table 4.4.

Table 4.4 Vibrational quantum number expansion constants for the energy expansion of H_2O, HDO, D_2O, MuOH and D_2O / cm^{-1}

	E / cm^{-1}				
Constant	H_2O	HDO	D_2O	MuOH	Mu_2O
G	2.67	-9.73	0.90	-76.63	30.09
A_1	4263.99	4208.54	3126.31	12184.00	12251.34
A_2	1770.37	1551.87	1295.88	3767.36	5079.63
A_3	4147.83	3055.51	2898.82	4252.90	12126.08
B_{11}	-36.86	-79.51	-21.10	-670.21	-286.44
B_{22}	-22.85	-13.03	-12.36	-98.87	-186.35
B_{33}	-40.84	-42.24	-21.21	-65.77	-352.03
B_{12}	-18.18	-20.14	-9.42	-134.74	-160.50
B_{13}	-162.53	-1.72	-84.38	-25.44	-1379.38
B_{23}	-12.82	-22.81	-6.24	-66.00	-113.40

The expansion coefficients for the isotopomers H_2O and D_2O are in good agreement with those calculated by Clabo et al. [106] and with the experimentally determined constants reported by Pliva et al. [120]. Using the theoretically determined harmonic frequencies (ω_i) and the expansion coefficients of (4.3) the first-order correction to the vibrational wavefunction was computed and the expectation values of the root-mean-square amplitudes and the bond and angle displacement coordinates over the zero-point vibrational wavefunction corrected to first-order were calculated. The expectation values of these properties for selected isotopic variants of the water molecule are given in Table 4.5.

Table 4.5 Expectation values of internal displacement coordinates $\langle \Delta R \rangle$ / pm and $\langle \Delta \vartheta \rangle$ / °

Molecule	$\langle \Delta R_1 \rangle$	$\langle \Delta R_2 \rangle$	$\langle \Delta \vartheta \rangle$	$\langle \Delta R_1 \rangle^{1/2}$	$\langle \Delta R_2 \rangle^{1/2}$	$\langle \Delta \vartheta \rangle^{1/2}$
H_2O	1.33	1.33	-0.031	6.51	6.51	8.68
HDO	1.05	1.20	-0.032	5.55	6.51	8.13
D_2O	0.96	0.96	-0.046	5.55	5.55	7.43
MuOH	2.81	1.58	0.113	11.07	6.51	12.73
Mu_2O	3.85	3.85	0.008	11.07	11.07	14.71

The zero-point energy of the light muonic species Mu_2O is ca. 190 % greater than the corresponding energy of H_2O and the other isotopic variants. It could therefore be predicted that the vibrational corrections to the muonic isotopomers will be larger than the corresponding protium or deuterium corrections. This is found to be the case for the expectation values of the internal displacement coordinates reported in Table 4.5. The size of the quantities in Table 4.5 gives an estimate of the

magnitude of the harmonic and anharmonic motion of the isotopic variants. The average bond length, O−X, obtained by including the vibrational corrections of Table 4.5 is 95.63, 95.26 and 98.15 pm for X = H, D and Mu in H_2O, D_2O and Mu_2O, respectively. The average bond angle for the isotopomers H_2O, HDO, D_2O, MuOH and Mu_2O is 105.94°, 105.94°, 105.92°, 106.08° and 105.98°, respectively. The vibrationally averaged internal coordinates of the water molecule are therefore $R_1 = R_2$ = 95.63 pm and ϑ = 105.94° which are in closer agreement with experiment ($R_1 = R_2$ = 95.72 pm, ϑ = 104.52° obtained by Benedict et al. [121]) than the *ab initio* results. Table 4.5 shows that for the protonated and deuterated species the mean bond length and angle is shifted by only 1 % or less, but for the muonic isotopomers this increases to about 4 %. The root-mean-square amplitudes are however nearly 7.5 % of their equilibrium value for H_2O, DOH and D_2O and about 10 % for MuOH and Mu_2O. These results clearly indicate that vibrational corrections to the muonium isotopomers are considerably larger than the corresponding proton or deuterium corrections.

Vibrational corrections to the z-component of the dipole moment and the electric field gradients at the oxygen nucleus have also been calculated. For the calculation of the electric field gradients the mass of the oxygen nucleus was taken to be that of the ^{17}O isotope (16.999131 u.). The vibrational quantum number expansions of the z-component of the dipole moment and the zz-component of the electric field gradient are given in Tables 4.6 and 4.7, respectively. The expansions take the same form as equation (4.4) and are derived from the *ab initio* property surfaces using the same method as that applied to the energy surfaces.

Table 4.6 Vibrational quantum number expansion constants for the z-component of the dipole moment / Debyes[a]

	μ_z (x 10^2)				
Constant	H_2O	HDO	D_2O	MuOH	Mu_2O
G	-0.00768	-0.00228	-0.00439	-0.05438	-0.05928
A_1	2.74991	1.96859	2.21435	5.45344	7.10772
A_2	-3.21417	-2.78851	-2.27867	-5.87469	-9.48136
A_3	0.99597	1.28567	0.54706	0.73579	3.53019
B_{11}	-0.01222	-0.02039	-0.00804	-0.17456	-0.07954
B_{22}	-0.03781	-0.01701	-0.02004	-0.06748	-0.31423
B_{33}	-0.00721	-0.01189	-0.00342	-0.00097	-0.06774
B_{12}	0.01940	0.02466	0.01209	0.33033	0.13215
B_{13}	-0.04329	-0.00269	-0.02357	-0.05105	-0.34940
B_{23}	0.04517	-0.01734	0.02256	-0.03965	0.39841

[a] (1 Debye = 3.3356 x 10^{-30} C m).

Table 4.7 Vibrational quantum number expansion constants for the zz-component of the electric field gradient at the ^{17}O nucleus / a.u.

	q_{zz} ($\times 10^2$)				
Constant	H_2O	HDO	D_2O	MuOH	Mu_2O
G	-0.00090	-0.01913	-0.00103	-0.10117	0.00228
A_1	4.62713	4.55077	3.47748	13.11252	12.95619
A_2	-1.20134	-1.04458	-0.85527	-1.66528	-3.52699
A_3	4.44231	3.29494	3.14607	3.47945	13.17505
B_{11}	-0.05157	-0.10261	-0.02785	-0.85822	-0.42327
B_{22}	-0.01314	-0.00700	-0.00740	-0.00544	-0.10411
B_{33}	-0.05176	-0.05082	-0.02713	-0.07328	-0.43754
B_{12}	0.02685	0.03988	0.01574	0.31289	0.20030
B_{13}	-0.20830	-0.00051	-0.11123	0.07230	-1.72984
B_{23}	0.02981	-0.00700	0.01771	-0.09521	0.22448

The vibrational corrections to the components of the ^{17}O quadrupole coupling constant (χ) of each isotopomer have been calculated from the computed electric field gradients using the relationship

$$\chi = (e^2 q_o Q) / h \qquad (4.5)$$

where $q_o = q_{xx}$, q_{yy} or q_{zz} and Q is the quadrupole moment of the ^{17}O nucleus. The quadrupole moment of the ^{17}O nucleus was taken to be -0.0265×10^{-28} m^2 [122]. Zero-point vibrational corrections to selected

properties of the water molecule and its isotopomers are given in Table 4.8.

Table 4.8 Zero-point vibrational corrections to properties of H_2O, HDO D_2O, MuOH and Mu_2O

		Zero-point Vibrational Corrections[a]				
Property	P_o	H_2O	HDO	D_2O	MuOH	Mu_2O
E / a.u.	-76.023615	-0.0229(2)	-0.0199(1)	-0.0167(1)	-0.0447(6)	-0.0648(1)
μ_z / D	2.14759	0.0024(1)	0.0021(1)	0.00231(9)	0.0010(4)	0.0044(5)
χ_{zz} / MHz	-1.0678	-0.098(5)	-0.086(5)	-0.076(3)	-0.17(1)	-0.25(3)
χ_{yy} / MHz	-10.322	-0.14(5)	-0.12(5)	-0.10(3)	-0.2(1)	-0.4(2)
χ_{zz} / MHz	11.3892	0.236(1)	0.204(1)	0.1739(7)	0.439(2)	0.655(5)
η [b]	0.89254	-0.2053	-0.1875	-0.1558	-0.2884	-0.3133

[a] The error limits in parentheses are three times the standard deviations

[b] The asymmetry parameter is dimensionless.

The vibrational corrections to the zz-component of the quadrupole coupling constant have been decomposed into harmonic and anharmonic contributions in Table 4.9.

Table 4.9 Harmonic and anharmonic corrections to the zz-component of the quadrupole coupling constant

	χ_{zz} / MHZ[a]				
	H_2O	HDO	D_2O	MuOH	Mu_2O
P_o	11.3892	11.3892	11.3892	11.3892	11.3892
G	-0.00005(2)	-0.0012(1)	-0.00006(1)	-0.0061(2)	0.00001(3)
Harmonic	0.2403(6)	0.2077(5)	0.1762(4)	0.455(1)	0.690(1)
Anharmonic	-0.0041(5)	-0.001(4)	-0.0021(2)	-0.009(1)	-0.035(4)
Total	11.625(1)	11.594(1)	11.5632(7)	11.829(2)	12.04(5)

[a]The error limits in parentheses are three times the standard deviations.

For all the isotopic variants considered the vibrational corrections to χ_{zz} show a cancellation between the harmonic and anharmonic terms, with the harmonic term predominating. The harmonic corrections are about 2 % of the equilibrium value of χ_{zz} for H_2O, D_2O and HDO and around 5 % for MuOH and Mu_2O. The anharmonic corrections are 0.03 %, 0.01 %, 0.02 %, 0.08 % and 0.31 % for H_2O, HDO, D_2O, MuOH and Mu_2O, respectively. Similar values are obtained on decomposition of the yy-component of the ^{17}O nuclear quadrupole coupling constant into its harmonic and anharmonic components. The xx-component however exhibits considerably larger vibrational corrections. The magnitude of the correction increases from 7 % for D_2O to 23 % for Mu_2O. This is a consequence of the anharmonic term reinforcing the harmonic correction. The vibrational corrections to the quadrupole coupling in Table 4.8 clearly show that the largest corrections arise from muonium substitution.

The vibrational corrections to the z-component of the dipole moment (μ_z) are positive for all isotopomers considered. The largest correction

of around 0.2 % occurs for the symmetric species Mu_2O. The vibrational corrections to μ_z for the asymmetric isotopomers are not directly comparable to the corrections to the symmetric species. This is a consequence of the dipole moment pointing along the bisector of the bond angle (ϑ) for the symmetric species, which in this instance corresponds to the z-axis. Therefore for the isotopic variants H_2O, D_2O and Mu_2O the x and z components of the molecular dipole monent are zero and the molecular dipole moment corresponds to the z-component. For the muonium and deuterium substituted asymmetric species MuOH and HDO the molecular dipole moment is not directed along the z-axis but is the vector sum of x and z-components. The small value of the vibrational correction to μ_z for MuOH reflects the large deviation from C_{2v} symmetry of this species.

The results reported in Tables 4.8 and 4.9 are concerned with vibrational corrections to the ground state of the molecule. The vibrational corrections to properties of H_2O in selected low lying excited vibrational states have been computed and the results are collated in Tables 4.10 and 4.11.

Table 4.10 Vibrational corrections to properties of H_2O in selected vibrational states

Vibrational State (ν_1 ν_2,ν_3)	E / cm^{-1}	μ_z / D	χ_{zz} / MHz	$\langle \Delta R_1 \rangle$ / pm	$\langle \Delta \vartheta \rangle$ / °
(0 0 0)	-5020.24	0.0024	0.236	1.33	-0.031
(1 0 0)	-9120.16	0.0296	0.507	2.85	-0.898
(0 1 0)	-6729.42	-0.0301	0.163	0.99	0.949
(0 0 1)	-8998.71	0.0123	0.496	2.80	-0.206
(1 1 0)	-10811.15	-0.0027	0.435	2.51	0.082
(1 0 1)	-12936.10	0.0390	0.753	4.32	-1.073
(0 1 1)	-10695.07	-0.0198	0.424	2.47	0.774
(1 1 1)	-14614.27	0.0071	0.684	3.98	-0.093
(2 0 0)	-13146.37	0.0565	0.771	4.36	-1.765
(0 2 0)	-8392.89	-0.0634	0.088	0.67	1.929
(0 0 2)	-12895.49	0.0219	0.749	4.28	-0.381
(0 1 2)	-14579.03	-0.0097	0.679	3.95	0.599
(0 2 1)	-12345.73	-0.0527	0.351	2.14	1.754
(1 0 2)	-16670.35	0.0483	0.994	5.79	-1.248
(1 2 0)	-12456.44	-0.0358	0.362	2.18	1.062
(2 0 1)	-16799.78	0.0654	1.006	5.83	-1.940
(2 1 0)	-14819.17	0.0243	0.701	4.03	-0.785
(3 0 0)	-17098.85	0.0831	1.030	5.88	-2.632
(0 3 0)	-10010.67	-0.0975	0.011	0.33	2.909
(0 0 3)	-16710.58	0.0315	0.996	5.75	-0.556

Table 4.11 Vibrational corrections to properties of MuOH in Selected states of vibration

Vibrational State (ν_1 ν_2 ν_3)	E / cm^{-1}	μ_z / D	χ_{zz} / MHz	$\langle \Delta R_1 \rangle$ / pm	$\langle \Delta R_2 \rangle$ / pm	$\langle \Delta \vartheta \rangle$ / °
(0 0 0)	-9760.24	0.001	0.439	2.81	1.58	0.113
(1 0 0)	-20523.72	0.053	1.148	11.31	1.73	-1.374
(0 1 0)	-13229.49	-0.058	0.344	0.08	1.98	1.903
(0 0 1)	-13835.89	0.008	0.643	2.67	4.18	0.368
(1 1 0)	-23858.22	-0.018	1.071	8.57	2.13	0.415
(1 0 1)	-24573.92	0.059	1.355	11.17	4.34	-1.451
(0 1 1)	-17239.13	-0.051	0.541	-0.06	4.58	1.826
(1 1 1)	-27842.42	0.004	1.273	8.43	4.74	0.339
(2 0 0)	-29946.78	0.102	1.751	19.81	1.89	-2.861
(0 2 0)	-16500.99	-0.1118	0.248	-2.66	2.38	3.692
(0 0 2)	-17780.00	0.0148	0.837	2.52	6.78	-0.039
(0 1 2)	-21117.24	-0.045	0.729	-0.21	7.19	1.750
(0 2 1)	-20444.63	-0.111	0.439	-2.80	4.98	3.616
(1 0 2)	-28492.59	0.066	1.553	11.02	6.94	-1.527
(1 2 0)	-26994.98	-0.058	0.994	5.84	2.53	2.20
(2 0 1)	-33971.53	0.108	1.963	19.67	4.49	-2.938
(2 1 0)	-33146.53	0.050	1.693	17.08	2.29	-1.072
(3 0 0)	-38029.40	0.148	2.249	28.31	2.05	-4.349
(0 3 0)	-19574.76	-0.179	0.151	-5.39	2.78	5.482
(0 0 3)	-21592.59	0.022	1.022	2.38	9.39	-0.116

The results in these Tables show that the magnitudes of the vibrational corrections are larger for the higher vibrational states. The largest corrections generally occur for uncoupled excitations [eg. (3 0 0)]. The sign of each correction can be correlated with the change in geometry of the molecule. Thus for H_2O when the stretching modes , such as (3 0 0), are excited, ΔR_1, ΔR_2 and $\Delta\vartheta$ change so as to increase μ_z. This can be compared with an excitation of a bending mode, such as (0 3 0), where the bond angle increases, which results in a negative dipole moment correction. The columns listing the corrections to the average bond length in Tables 4.10 and 4.11 show the difference that arises on the formation of an asymmetric species. For H_2O only the corrections $\langle \Delta R_1 \rangle$ are listed because the values for $\langle \Delta R_2 \rangle$ are identical, whereas for MuOH the corrections to the average O-Mu and O-H bond lengths are significantly different and are therefore both listed. This difference must arise from the variation in the vibrational energy of the different isotopomers.

In Table 4.9 both the harmonic and anharmonic terms are isotope dependent. Within the Born-Oppenheimer approximation all the isotopomers have the same equilibrium bond lengths and bond angle. The calculated isotope effects on the vibrational corrections must therefore arise from the different nuclei sampling different regions of the property surface. Figures 4.2, 4.3 and 4.4 show the variation of the energy, the z-component of the dipole moment and the zz-component of the electric field gradient at the oxygen nucleus of the water molecule with internal coordinates R_1 and ϑ, respectively. The figures clearly show that for displacements equivalent to those reported in Table 4.5 the region of the surface sampled by each isotopomer will be markedly different. The large

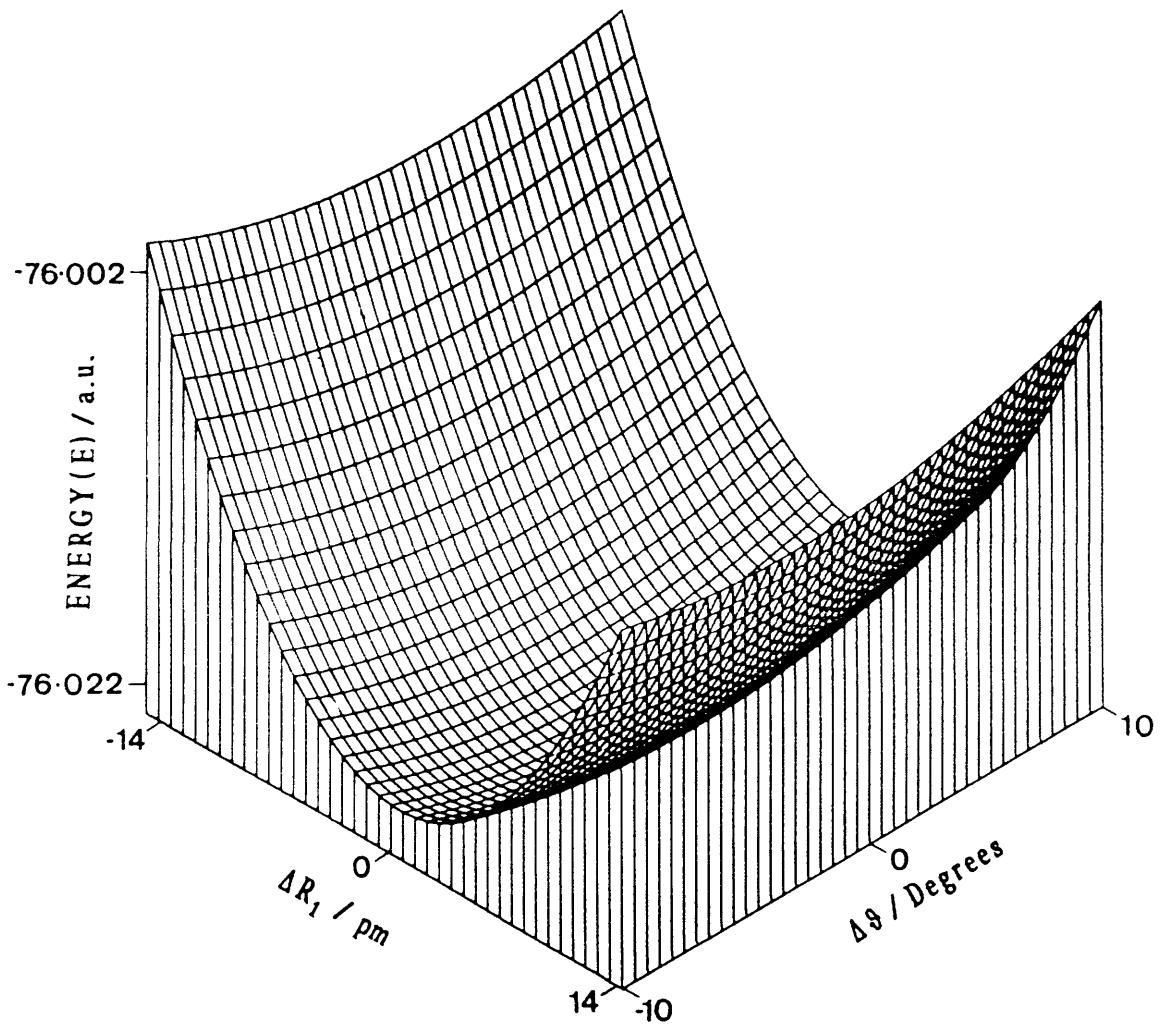

Figure 4.2 Variation of the energy of the water molecule with internal coordinates R_1 and ϑ.

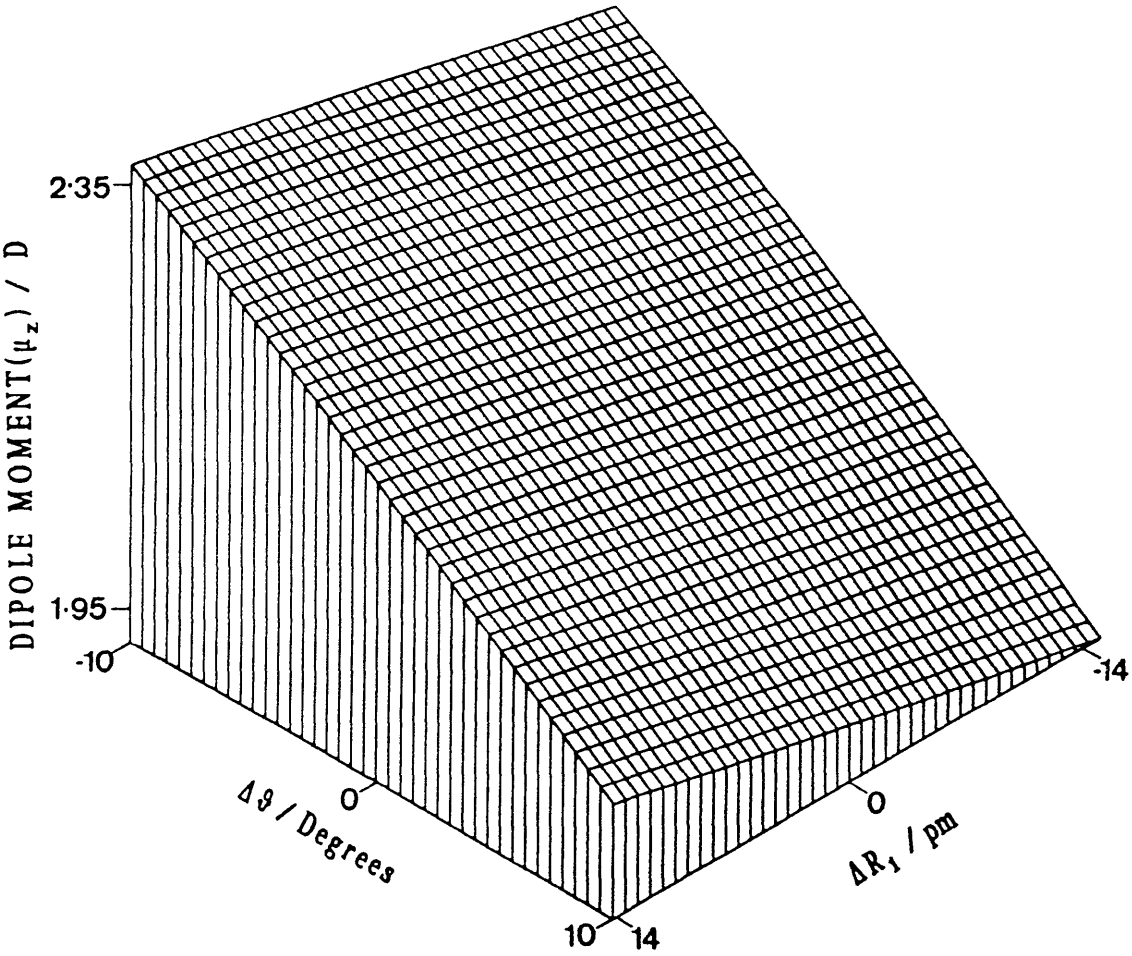

Figure 4.3 Variation of the z-component of the dipole moment of the water molecule with internal coordinates R_1 and ϑ.

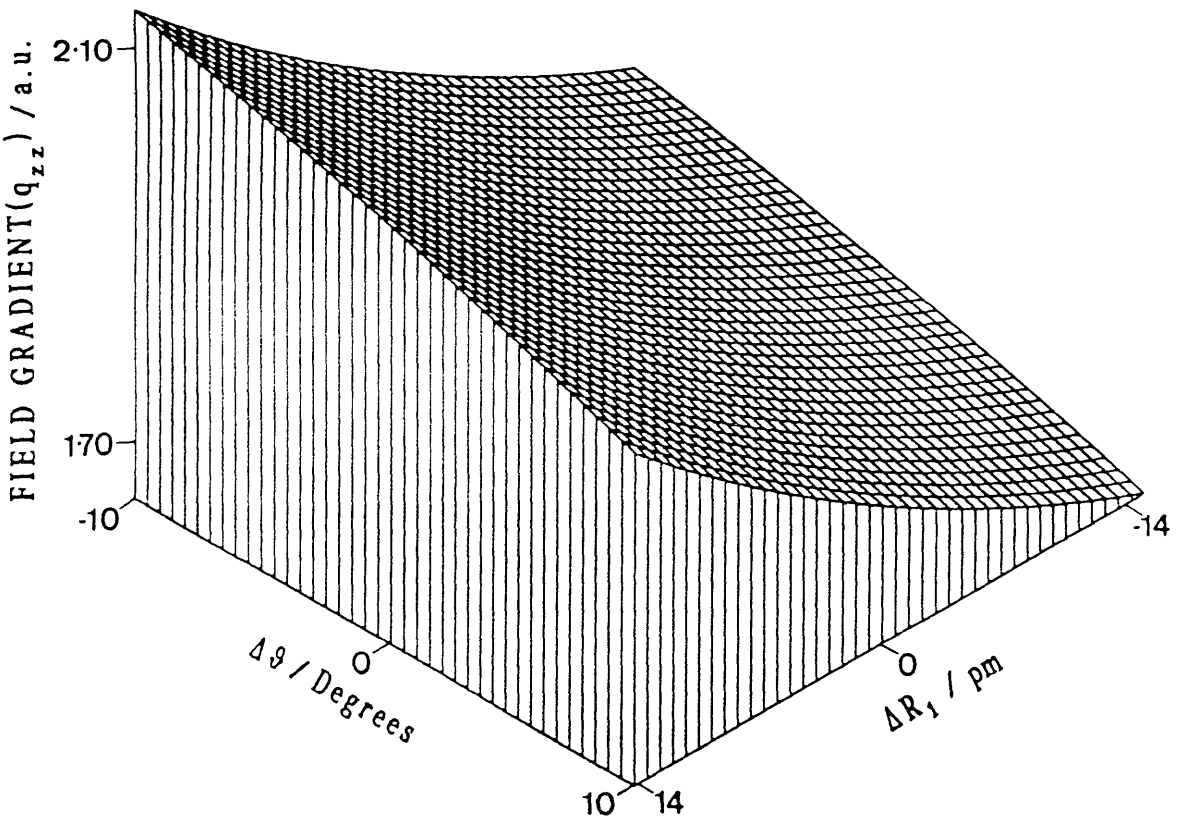

Figure 4.4 Variation of the zz-component of the electric field gradient at the oxygen nucleus of the water molecule with internal displacement coordinates R_1 and ϑ.

vibrational corrections to the muonium substituted species MuOH and Mu_2O can be attributed to the larger vibrational motion of the muon. The deuterium and protium isotopes experience a smaller vibrational effect due to their lower vibrational energies. The isotope shifts in the properties of the water molecule in the ground vibrational state are collated in Table 4.12.

Table 4.12 Isotope shifts of selected properties of the water molecule in the ground vibrational state

Property	$\langle P(H_2O)\rangle$ - $\langle P(D_2O)\rangle$	$\langle P(H_2O)\rangle$ - $\langle P(HDO)\rangle$	$\langle P(H_2O)\rangle$ - $\langle P(MuOH)\rangle$	$\langle P(H_2O)\rangle$ - $\langle P(Mu_2O)\rangle$
E / a.u.	-0.006	-0.003	0.0218	0.0419
μ_z / D	0.00009	0.0003	0.0014	-0.002
χ_{xx} / MHz	-0.022	-0.012	0.072	0.152
χ_{yy} / MHz	-0.04	-0.02	0.06	0.255
χ_{zz} / MHZ	0.062	0.032	-0.203	-0.419

In all cases, other than the z-component of the dipole moment, the isotope shift occuring on muonium substitution is in the opposite direction to the isotope shift resulting from deuterium substitution. As was stated earlier the largest isotope shifts are found to be those corresponding to the isotopic variants MuOH and Mu_2O. These results assume the isotopomer to be in the ground vibrational state (0 0 0). Tables 4.10 and 4.11 list the corrections to properties in higher vibrational states. In the higher states the isotopoe shifts can be considerably larger than those reported in Table 4.12. For example the isotope shift on

muonium substitution to the z-component of the dipole moment of an isotopomer in the vibrational state (0 0 3) is 0.0095 which is almost a 700 % increase on the ground state isotope shift. Similarly the isotope shift, on muonium substitution, to the zz-component of the quadrupole coupling of an isotopomer in the vibrational state (3 0 0) increases to 1.219 which is about a 600 % increase on the ground state value. These large increases in the isotope shifts can be attributed to the increased value of the root-mean-square displacements in the higher vibrational states. The larger displacements result in the muonium isotopomers sampling a larger region of the surface which therefore results in the increased isotope shifts observed.

4.2.3 Comparisons with Experiment

The greatest limitation on the accuracy of the results presented in the previous section is the Hartree-Fock approximation. The theoretical harmonic and cubic force constants of H_2O and D_2O given in Table 4.4 differ from experiment [120] by up to 20 %. Errors of a similar magnitude are expected to occur in the force constants of the other isotopomers considered. These errors are largely attributable to correlation effects in general and improper dissociation behaviour in particular. A more complete study of vibrational corrections would therefore include correlation effects. The work of Rosenberg et al. [109] however has shown that the inclusion of correlation effects does not significantly alter the trends observed in the calculated isotope shifts of the vibrational corrections at the SCF level.

Cox et al. [7, 11] have recently identified the diamagnetic fraction formed on muon implantation in ^{17}O doped ice using the technique of avoided level crossing resonance μSR. The diamagnetic state observed is proposed to be that of MuOH. This species was detected by matching the muon's Zeeman energy levels with the ^{17}O quadrupole energy levels in a longitudinally applied magnetic field and observing the reduction in the muon spin polarization that occurs when this condition is achieved. Hence it is possible to derive from this experiment the value of the ^{17}O quadrupole coupling constant of MuOH. The value of the coupling was found to be 6.1 MHz ($\eta = 1$) at 200 K. This can be compared with the corresponding values in normal ice at 77 K of 6.1 MHZ ($\eta = 0.93$) [123] and in D_2O ice, at about 260 K, of 6.66 MHz ($\eta = 0.94$) [124]. The observed experimental isotope shifts in the ^{17}O quadrupole coupling constant on muonium and deuterium substitution are therefore ca. 5 %

and 4 % of the H_2O value, respectively.

The magnitude of the quadrupole coupling of each of the ice isotopic variants is considerably less than the theoretical values listed in Table 4.8 calculated using *ab initio* molecular orbital theory. This is a consequence of the *ab initio* values assuming that the H_2O molecule can be treated as an isolated species and therefore the results neglect the effects of intermolecular interactions. The *ab initio* values are in closer agreement to the ^{17}O quadrupole coupling measured in the vapour phase. The value of the ^{17}O quadrupole coupling constant of HDO in the gas phase is reported to be 10.17 MHz ($\eta = 0.75$) [125]. The vibrationally averaged theoretical value of this property obtained from Table 4.8 is 11.59 MHz ($\eta = 0.70$). Several experimental studies [125, 126, 127, 128, 129] have established that the reduction in the ^{17}O quadrupole coupling constant on going from the vapour to the solid phase is the result of the increased importance of intermolecular interactions in the solid state. These interactions can reduce the ^{17}O quadrupole coupling by as much as 40 % relative to the vapour phase. Cummins et al. [130] have studied the origins of this reduction and conclude that the principal contribution to the shift in the ^{17}O quadrupole coupling is an electronic effect. The vibrational isotope shifts occuring in the properties of H_2O and its isotopic variants in the solid and gaseous states should however have the same origin.

The isotope shift in the ^{17}O quadrupole coupling constant resulting from muonium substitution is in the opposite direction relative to the corresponding deuterium shift in both the experimental and theoretical results. The experimental observations suggest that muonium substitution results in a lowering in the magnitude of the coupling, whereas the theoretical isotope shifts given in Table 4.12 predict shifts in the opposite

direction for these isotopomers. This difference could arise from the theoretical results neglecting the effects of intermolecular interactions and assuming the molecule to be in its ground rotational and vibrational state. The magnitudes of the experimentally and theoretically determined isotope shifts in the ^{17}O quadrupolar coupling constant are however of a similar magnitude. The experimentally observed isotope shifts can be understood in terms of vibrational effects analogous to those resulting in the theoretically calculated isotope shifts. Therefore the largest vibrational corrections are expected to occur for the diamagnetic MuOH and Mu_2O states due to their higher zero-point vibrational energies which result in these species sampling a larger region of the electric field gradient surface than their corresponding protium or deuterium isotopomers.

CHAPTER 5

5. Vibrationally Averaged β—Hyperfine Coupling Constants for the Muonium Substituted Ethyl Radical

5.1 Prelude

Experimental studies of the muonium substituted ethyl radical using the methods of transverse field muon spin rotation and level-crossing resonance spectroscopy have shown that the β-hyperfine coupling is strongly isotope dependent [43, 67]. The isotope effect is a consequence of the spin density on the β-muon being larger than that on the equivalent β-proton for any given conformation of the radical. This isotope effect is often referred to as a residual isotope effect. In this chapter vibrational corrections to the spin density of β-nuclei and selected molecular properties of the ethyl radical are calculated. These corrections should assist in the elucidation of the isotope dependent barrier to internal rotation of the radical [65].

A complete solution of the vibrational problem of the ethyl radical is hindered by the large number of normal modes of vibration which must be considered. Vibrational averaging over all possible normal modes would be an extremely complex and computationally expensive problem. A study of the vibrational corrections to the β-hyperfine coupling of the ethyl radical by Claxton et al. [75] limited its approach to averaging over selected normal modes separately. Chipman [76] has also calculated vibrational corrections to the hyperfine couplings by a systematic examination of the dependence of the couplings on the out-of-plane bending at the methylenic carbon, on the torsional motion around the central C-C bond and the coupling between them. A similar but more

complete approach has been utilised to compute the vibrational corrections presented here. As for the water molecule, the vibrational corrections were computed using the computer program SURVIB [104] and all necessary *ab initio* calculations were performed using the GAMESS [113] molecular orbital package on the University of Glasgow MicroVax 3600.

5.2. Computational Procedure

An unrestricted geometry optimization of the ethyl radical was performed at the UHF-SCF level using the split valence 6-31G* basis set [115]. The criteria for the convergence of the SCF energy cycles and the gradient of the energy are identical to those defined in chapter 4. The converged equilibrium geometry of the ethyl radical determined from this calculation is displayed in Figure 5.1.

Bond Lengths / pm	C_1-C_2 149.81, C_1-H_3 109.07, C_2-$H_{4(5)}$ 107.52, C_1-$H_{6(7)}$ 108.55
Bond Angles / °	H_3-C_1-C_2 111.75, H_6-C_1-C_2 111.32, H_5-C_2-C_1 120.39, H_4-C_2-C_5 117.25, H_3-C_1-H_6 107.13, H_7-C_1-H_6 107.95
Dihedral Angles / °	H_3-C_1-C_2-H_4 81.83, H_7-C_1-C_2-H_4 37.92

Figure 5.1 Optimized geometry of the ethyl radical.

The calculated equilibrium geometry is in good accord with *ab initio* studies of the ethyl radical performed by Claxton and Graham [131]; Pacansky and Dupuis [132] and Webster and Macrae [133]. The total energy corresponding to this geometry and its nuclear and electronic components are given below.

$$E_{Total} = -78.59715\ E_h$$

$$E_{el} = -115.58365\ E_h$$

$$E_{nuc} = 36.98650\ E_h$$

The spin density (ρ^s) at each of the nuclei in the radical and the corresponding isotropic hyperfine coupling constants (A), calculated using the method described in Chapter 3, at this conformation are listed in Table 5.1

Table 5.1 Nuclear spin densities (a.u.) and isotropic hyperfine coupling constants / A (MHz) of the ethyl radical

	ρ^s	A	A^{exp}[a]
C_1	-0.05347	-60.10	-38.10
C_2	0.22403	251.08	110.0
H_3	0.03022	135.08	75.4
H_4	-0.02879	-128.68	-62.8
H_5	-0.02879	-128.68	-62.8
H_6	0.00847	37.86	75.4
H_7	0.00847	37.86	75.4

[a] Ref. [45, 134].

Experimental values of the proton and ^{13}C hyperfine coupling constants are given in Table 5.1 to enable comparison. In all cases the *ab initio* couplings appear to show large deviations from experiment. The proton β-hyperfine coupling is however in good agreement with the experimental value of 75.4 MHz. This is a consequence of the experimental coupling being reported as the average coupling of the β-nuclei. Therefore, the experimental value of the coupling is given by the equation

$$\bar{A}_\beta = \frac{1}{3} A_p \qquad (5.1)$$

where A_p is the sum of the β-hyperfine proton coupling constants. The corresponding theoretical value of $\bar{A}_\beta$ obtained from the couplings in Table 5.1 is 70.27 MHz. The 6-31G* basis is therefore considered to provide an adequate description of the spin density located on the β-nuclei of the radical. The poor agreement between the experimental and *ab initio* couplings of the remaining nuclei indicates that the basis is inadequate for an accurate description of the spin density at these nuclei. Improved values of the spin density, at all nuclei, can be obtained through the inclusion of correlation and vibrational effects as shown by Chipman [76] and Carmichael [68]. In the calculations performed here correlation effects have been neglected as the work of Carmichael has shown that correlation effects are almost constant over the region of the energy hypersurface which influences the zero-point vibrational corrections.

The isotopically substituted ethyl radical, as shown in Figure 5.2, has the C-X bond eclipsing the singly occupied notional $2p_z$ orbital centred on the methylenic carbon. The vibrational motion of nucleus X can be described in terms of the variation of the internal coordinates R, ϑ_1 and

ϑ_2 illustrated in Figure 5.2; where R is the C-X bond length, ϑ_1 is the XCC bond angle and ϑ_2 is the $XCCH_\alpha$ torsion angle.

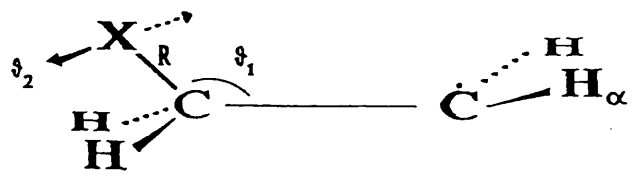

R^e = 109.07 pm

ϑ_1^e = 111.75°

ϑ_2^e = 81.83°

Figure 5.2 Internal coordinates R, ϑ_1, and ϑ_2 of the isotopically substituted ethyl radical (X=Mu, H, or D).

The equilibrium geometry of the protium and muonium substituted radicals is that of Figure 5.2; however, the equilibrium conformation of the deuterium substituted radical has D in the nodal plane of the $2p_z$ orbital. The principal concern of this chapter is the determination of the vibrational corrections to the β-hyperfine coupling constant of the muonium substituted ethyl radical, the deuterated and protonated radicals (X=D, H) have also been considered to show the isotope effect on the computed hyperfine couplings. For X=Mu the mass difference between the isotope and the remaining protons effectively decouples the vibrational motion of the C-Mu group from the rest of the radical. This decoupling is reflected in the *ab initially* calculated harmonic vibrational frequencies tabulated in Table 5.2 for the CH_2MuCH_2 and CD_2MuCH_2 isotopomers of the ethyl radical.

Table 5.2 Calculated harmonic vibrational frequencies of the muon in CH_2MuCH_2 and CD_2MuCD_2 / cm^{-1}

	Frequency / cm^{-1}	
Vibrational mode[a]	CH_2MuCH_2	CD_2MuCD_2
ω_1	9075.03	9074.54
ω_2	3754.82	3727.54
ω_3	3693.94	3610.39

[a] The subscripts 1, 2 and 3 refer to the C-Mu stretch (ω_1), the MuCC angle bend (ω_2) and the $MuCCH_\alpha$ torsional bend (ω_3).

Comparison of these frequencies indicates that the C-Mu stretch is completely decoupled from the rest of the radical. The small change, on isotopic substitution, to the harmonic frequencies corresponding to the bending and torsion modes indicates that these modes experience a small degree of coupling with the other vibrational modes of the radical. Similar calculations performed on the deuterium substituted radical, CH_2DCH_2, show that the C-D stretch is completely decoupled and the angle bending and torsion modes experience a degree of coupling with the rest of the radical. The size of the coupling of the bending and torsion modes of the C-D group is somewhat larger than that of C-Mu, however the results indicate for X = Mu or D the vibrational motion of the C-X group is effectively decoupled from the remaining vibrational modes of the radical. This result is supported by similar observations made by Claxton et al. [75], Webster and Macrae [133] and Pacansky and Dupuis [135]. Vibrational averaging for X = Mu or D can therefore be acheived using only three of the normal modes of vibration of the radical. The three normal modes can be described as the C-X bond

stretching mode (ω_1), the XCC angle bending mode (ω_2) and the $XCCH_\alpha$ torsional rotation mode (ω_3). These normal modes can be expressed in terms of the internal coordinates R, ϑ_1 and ϑ_2. Although the protonated (X = H) form of the radical can not be treated by simply considering these modes, the results obtained for $C_2H_5^{\cdot}$ are given for comparison with the muonium and deuterium calculations. When X=H, coupling with the remaining normal modes must be considered, unlike the situation where the C-X normal modes are decoupled by muonium or deuterium substitution.

Calculation of the vibrational corrections to the β-hyperfine coupling constant of nucleus X requires energy and spin density surfaces which describe the vibrational motion of this nuclei. As a consequence of the decoupling of the vibrational modes of the C-X group from the rest of the radical, these surfaces were built up by varying the three internal coordinates R, ϑ_1 and ϑ_2 from their equilibrium values R^e(109.07 pm), ϑ_1^e(111.75°) and ϑ_2^e(81.83°) over the ranges ±8 pm, ± 10° and ±10°, respectively. The calculated surfaces are composed of 252 points about the stationary point geometry of the radical. All calculations were performed at the 6-31G*, UHF-SCF level using the GAMESS [113] *ab initio* program. The computer program SURVIB [104] was used to perform a least-squares fit to the *ab initio* surfaces and to compute vibrational corrections to the energy and the β-hyperfine coupling constant.

Vibrational corrections to the β-hyperfine coupling constants of the ethyl radical and its isotopomers reported by Claxton et al. [75] were calculated by averaging over each of the three normal modes ω_1, ω_2 and ω_3 describing the vibrational motion of the C-X group separately. More recently Chipman [76] has computed vibrational corrections to the

β-hyperfine couplings by considering the effects of out-of-plane bending at the methylenic carbon and of torsion motion about the carbon-carbon bond. The vibrational corrections calculated here are computed using complete vibrational averaging over the three normal modes ω_1, ω_2 and ω_3 and therefore include the effects of coupling between the normal modes.

5.3 Results and Discussion

The computed *ab initio* energy and spin density surfaces were fitted to a fourth-order internal coordinate expansion. As for the study of the water molecule in chapter 4 the fourth-order terms are unnecessary for the perturbation treatment used to calculate the vibrational corrections but are included to minimize the errors in the third-order terms. The internal-coordinate functions obtained from the fitting procedure consist of a Simmons-Parr-Finlan [117] expansion in terms of the bond length and a Taylor series expansion in terms of the bond angle and torsion angle. The computed property function can be expressed in the form

$$P = P_o + \sum_{i=1}^{3} K_i S_i + 1/2 \sum_{i,j=1}^{3} K_{ij} S_i S_j + \sum_{i,j,k=1}^{3} K_{ijk} S_i S_j S_k \qquad (5.2)$$

where S_1, S_2 and S_3 are associated with the bond displacement $\Delta R^{SPF} = (R-R^e)/R$ and angle displacements $\Delta\vartheta_1 = \vartheta_1-\vartheta_1^e$ and $\Delta\vartheta_2 = \vartheta_2-\vartheta_2^e$, respectively. The term P_o is the value of the property at the SCF equilibrium geometry of the radical and K_i, K_{ij} and K_{ijk} are the expansion constants derived from the fitting procedure. The computed energy function reproduces the calculated energies with a maximum error of 7.9×10^{-6} a.u. and a root-mean-square error of 2.7×10^{-6} a.u. The

stationary point energy of the analytic function is -78.59715 E_h. The internal coordinates R, ϑ_1 and ϑ_2 at the stationary point of the energy function have the values R^s = 109.07 pm, ϑ_1^s = 111.75° and ϑ_2^s = 81.83°; which are equivalent to the SCF equilibrium values given in Figure 5.2. Tables 5.3 and 5.4 list the independent internal-coordinate displacement expansion parameters for the energy and spin density surfaces respectively. The computed analytic energy function is used to perform a standard normal mode analysis. The harmonic frequencies and harmonic zero-point energies obtained from this analysis for selected isotopomers of the ethyl radical are given in Table 5.5.

Table 5.3 Calculated quadratic and cubic expansion constants (a.u.) of the analytic internal displacement coordinate energy function

Quadratic Expansion Constants		Cubic Expansion Constants	
K_{11}	0.7577	K_{111}	-0.01043
K_{22}	0.1247	K_{222}	-0.00675
K_{33}	0.0978	K_{333}	0.00072
K_{12}	-0.01316	K_{112}	-0.00139
K_{13}	0.000029	K_{113}	-0.00003
K_{23}	-0.000051	K_{223}	-0.00130
		K_{133}	-0.03900
		K_{233}	-0.02720
		K_{123}	-0.00026

Table 5.4 Calculated expansion constants (a.u.) of the analytic internal displacement coordinate function describing the spin density at nucleus X

Expansion Constants			
K_1	0.05686	K_{111}	0.06602
K_2	0.00995	K_{222}	0.04090
K_3	-0.000004	K_{333}	0.00093
K_{11}	0.20910	K_{112}	0.03183
K_{22}	-0.00762	K_{122}	0.01377
K_{33}	0.01038	K_{113}	-0.01350
K_{12}	0.02472	K_{223}	0.00002
K_{13}	0.00128	K_{133}	0.0585
K_{23}	0.00008	K_{233}	-0.0107
		K_{123}	-0.0007

Table 5.5 Calculated harmonic frequencies (ω) / cm^{-1} and harmonic zero-point energies (E_{zp}) / cm^{-1}

	C-H	C-Mu	C-D
ω_1	3187.32	9136.32	2344.08
ω_2	1895.18	3819.56	1699.35
ω_3	1359.22	3725.59	1036.83
E_{zp}	3220.86	8340.73	2540.13

The subscripts 1, 2 and 3 refer to the bond stretch (ω_1), angle bend (ω_2) and torsional motion (ω_3).

From the normal-mode analysis the transformation matrix to normal coordinates is obtained which allows the spin density and energy functions to be re-expanded as Taylor series expansions in terms of the reduced normal-coordinates. These expressions are then used in a standard perturbation treatment of the vibrational corrections as outlined in chapter 3. The expansion coefficients of the analytic reduced normal coordinate (q_i), energy and spin density functions for the isotopomers C-X (X = D, H and Mu) are listed in Tables 5.6 and 5.7, respectively. The normal-coordinate analytic function has the form

$$P = P_o + \sum_{i=1}^{3} \alpha_i q_i + \sum_{i,j=1}^{3} \beta_{ij} q_i q_j + \sum_{i,j,k=1}^{3} \gamma_{ijk} q_i q_j q_k \quad (5.3)$$

where P_o is the value of the energy or spin density at the stationary point of the function and α, β and γ are the expansion coefficients.

Table 5.6 Normal-coordinate expansion coefficients (x 10^4) for the energy function of the isotopomers C-X (X = D, H, Mu) / a.u

	Coefficient (x 10^4) [a]		
Isotopomer	C-D	C-H	C-Mu
β_{11}	0.57036	1.05451	8.66448
β_{22}	0.29976	0.37282	1.51436
β_{33}	0.11159	0.19177	1.44076
γ_{111}	-0.01047	-0.02649	-0.62598
γ_{112}	0.00108	0.00097	0.00668
γ_{113}	0.00091	0.00155	0.01966
γ_{122}	-0.00094	0.00021	0.14861
γ_{123}	0.00007	0.00019	0.00902
γ_{133}	0.00240	0.00673	0.17745
γ_{222}	-0.00240	-0.00029	-0.00147
γ_{221}	-0.00025	0.00005	-0.00156
γ_{233}	-0.00004	0.00005	0.00437
γ_{333}	0.00000	0.00006	0.00242

[a] Expansion coefficients of absolute value less than 1 x 10^{-9} are given as exactly zero.

Table 5.7 Normal-coordinate expansion coefficients ($\times 10^4$) for the function describing the spin density at nucleus X (a.u.) for the isotopomers C-X (X = D, H, Mu)

	Coefficient ($\times 10^4$)		
Isotopomer	C-D	C-H	C-Mu
α_1	4.79269	6.60684	19.1578
α_2	-0.34385	-0.27199	-0.99184
α_3	-1.09422	-1.37124	3.47644
β_{11}	0.11122	0.20876	1.73556
β_{12}	-0.00924	-0.01033	-0.07494
β_{13}	-0.02090	-0.03170	-0.19523
β_{22}	0.03737	0.05477	0.40598
β_{23}	-0.00396	-0.00694	-0.09805
β_{33}	0.01301	0.02617	0.24970
γ_{111}	0.00194	0.00490	0.11551
γ_{112}	0.00015	0.00033	0.00590
γ_{113}	-0.00009	-0.00011	-0.00135
γ_{122}	0.00162	0.00310	0.06170
γ_{123}	-0.00010	-0.00017	-0.00294
γ_{133}	0.00078	0.00221	0.05816
γ_{222}	-0.00012	-0.00012	-0.00177
γ_{223}	0.00012	0.00011	-0.00553
γ_{233}	-0.00023	-0.00044	-0.01458
γ_{333}	-0.00043	-0.00096	-0.01825

The expansion parameters listed in Tables 5.6 and 5.7 and the harmonic frequencies listed in Table 5.5 enable the coefficients G, A and B of the quantum-number expansion of the property to be determined. The quantum-number expansion for the energy or spin density is given by

$$P_v = G + \sum_{i=1}^{N} A_i(v_i + 1/2) + \sum_{i \leq j}^{N} B_{ij}(v_i + 1/2)(v_j + 1/2) \qquad (5.4)$$

where v is the vibrational quantum number. This expression enables the vibrationally averaged energy and spin density to be computed for the isotopic variants of the ethyl radical under consideration. The computed coefficients of expression (5.4) for the energy and the spin density at nucleus X are tabulated in Tables 5.8 and 5.9.

Table 5.8 Vibrational quantum-number expansion constants for the energy expression of selected isotopomers of the ethyl radical / cm^{-1}

	E / cm^{-1}		
Constant	C-D	C-H	C-Mu
G	-6.077	-7.476	-67.376
A_1	2344.085	3187.323	9136.310
A_2	1699.356	1895.180	3819.564
A_3	1036.828	1359.225	3725.591
B_{11}	-33.492	-62.266	-511.888
B_{22}	-7.924	-3.991	-18.171
B_{33}	-4.099	-6.914	-52.485
B_{12}	-29.969	-51.033	-282.686
B_{13}	-11.116	-22.135	-187.192
B_{23}	3.988	5.612	47.420

Table 5.9 Vibrational quantum-number expansion constants for the spin density (ρ^s) function of nucleus X in selected isotopic variants of the ethyl radical

	ρ^s (x 10^2) / a.u.		
Constant	C-D	C-H	C-Mu
G	0.00008	0.00138	-0.00016
A_1	0.23243	0.31929	0.92188
A_2	0.05418	0.06252	0.13696
A_3	0.00597	0.00934	0.37527
B_{11}	0.01557	0.02854	0.23397
B_{22}	-0.00013	0.00085	-0.01306
B_{33}	-0.00046	-0.00722	-0.40811
B_{12}	0.02514	0.02441	0.20463
B_{13}	0.02909	0.04097	0.26179
B_{23}	-0.01454	-0.01301	-0.06299

The first-order wavefunctions that are used to derive the quantum number expansions listed in Tables 5.8 and 5.9 are also used to compute the vibrational expectation values of the root-mean-square amplitudes and the bond and angle displacements. From the results listed in Table 5.5 it can be seen that the zero-point energy of the muonium substituted ethyl radical is considerably larger than the analogous protium or deuterium substituted radicals. The vibrational corrections to the internal coordinates are expected therefore to follow similar trends to those observed in chapter 4 for isotopic variants of the water molecule. The vibrational corrections to the internal displacement coordinates of the ethyl radical are listed in Table 5.10.

Table 5.10 Expectation values of internal displacement coordinates $\langle \Delta R \rangle$ / pm and $\langle \Delta \vartheta \rangle$ / ^{o} of the ethyl radical

Bond	$\langle \Delta R \rangle$	$\langle \Delta \vartheta_1 \rangle$	$\langle \Delta \vartheta_2 \rangle$	$\langle \Delta R \rangle^{1/2}$	$\langle \Delta \vartheta_1 \rangle^{1/2}$	$\langle \Delta \vartheta_2 \rangle^{1/2}$
C–H	1.45	0.077	-0.072	7.54	6.40	8.50
C-Mu	4.70	0.251	-0.030	12.78	10.58	12.08
C-D	0.73	0.056	-0.092	6.46	5.60	8.05

The largest vibrational corrections in Table 5.10 correspond to isotope shifts in the C-X bond length. For the isotopic variants X = D, H and Mu, the average bond lengths are 109.8, 110.52 and 113.77 pm, respectively. Muonium substitution therefore results in about a 4 % increase in the C-X bond length over the protium value. The vibrational corrections to the bond and dihedral angles are considerably smaller than those to the bond length. The direction of the isotope shifts in the bond angle displacements is equivalent to that observed in the bond lengths. However the isotope shifts in the dihedral angle corrections are in the opposite direction to those observed in the bond length and bond angle. For all isotopic variants considered the computed vibrational corrections to the dihedral angle result in a small decrease in the dihedral angle. For this parameter deuterium substitution results in the largest isotope shift, a 0.1 % decrease in the dihedral angle. These corrections to the dihedral angle indicate that on isotopic substitution at position X, the angle between the axis of the C-X bond and the axis of the notional $2p_z$ orbital centred on the methylenic carbon (see Figure 1.5) deviates slightly from zero. The deuterium experiences the largest deviation which is in agreement with experimental results [47] and previous theoretical studies of isotopomers of the ethyl radical [131, 136]. The size of the deviation is small for all isotopomers considered. The results however indicate that

the preferred conformation of the deuterium isotopomer does not have the C-D bond eclipsing the $2p_z$ orbital centred on the methylenic carbon.

The vibrational corrections to the internal coordinates of the ethyl radical and its isotopomers listed in Table 5.10 are the result of including third order terms in the normal-coordinate expansion (5.3). The computed isotope shifts in the internal coordinates indicate that each isotopic variant of the ethyl radical experiences a different region of the energy surface. This is confirmed by the difference in the normal-coordinate expansion constants listed in Table 5.6. Neglection of third order terms in expression (5.3) results in the isotope shifts in the internal-coordinates being zero. The results would therefore provide no information on the conformational changes that occur on isotopic substitution. The values of the root-mean-square amplitudes listed in Table 5.10 give a measure of the harmonic motion of each isotopomer. Due to the large zero-point energy of the muonium substituted ethyl radical it has the largest root-mean-square amplitudes and therefore samples the largest area of the energy surface about its equilibrium geometry. The heavy deuterium isotope has the lowest zero-point energy and therefore samples the smallest area of the energy surface.

The vibrational corrections to the energy and to the spin density (ρ^s) at nucleus X are given in Table 5.11. The corrections to both properties show that isotopic substitution by muonium produces the largest isotope shifts. The corrections to the β-hyperfine coupling constant of nucleus X for each isotopomer has been calculated using the relationship

$$A_x = \frac{8\pi}{3h} g_e g_N \mu_e \mu_N |\rho^s| \qquad (5.5)$$

as described in chapter 3. Since spin density is often calculated in atomic units A_x can be expressed in atomic units by

$$A_x = \frac{\alpha^2}{3m_x} g_e g_N |\rho^s| \qquad (5.6)$$

where α is the fine structure constant and m_x is the nuclear mass. The velocity of light in atomic units is specified as α^{-1} and has a value of 137 a.u. Therefore if the spin density alone is reported in a.u. then A_μ / MHz = $14229.0|\rho^s|$, similarly the conversion factors for deuterium and protium are 1372.26 and 4469.879, respectively.

Table 5.11 Zero-point vibrational corrections to the energy (E) and spin density (ρ^s) / a.u.

Property	P_o[a]	C-H	C-Mu	C-D
E	-78.59715	-0.01448(3)	-0.0368(2)	-0.01145(2)
ρ^s	0.03022	0.002(5)	0.007(5)	0.0015(4)

[a] P_o denotes the value of the property at the stationary point of the analytic function.

The error limits given in parentheses are three times the standard deviations [99].

The corrections to the β-hyperfine coupling constants calculated from the computed spin densities for each isotopomer are given in Table 5.12. These vibrational corrections are decomposed into harmonic and anharmonic contributions and the coupling of Mu and D are reported in their reduced form to facilitate comparisons.

In Table 5.12 the quantity C, is a constant independent of the

vibrational state, which corresponds to the parameter G in Table 5.9, arising from the inclusion of anharmonicity in the vibrational analysis. For all cases the anharmonic corrections reinforce the dominant harmonic corrections and result in an increased value of the coupling. The coupling increases from 142.172 MHz for the C-D species to 166.097 MHz for the C-Mu species. Table 5.12 shows that the harmonic and anharmonic terms

Table 5.12 Harmonic and anharmonic corrections to the β—hyperfine coupling constant (A) / MHz

	A_P	A_μ	A_D
P_o	135.079	135.079	135.079
C	0.0616	-0.0073	0.0039
Harmonic	8.743	24.504	6.539
Anharmonic	0.831	6.527	0.550
Total	144.715	166.097	142.172

are isotope dependent as found in the vibrational corrections to the quadrupole coupling constant of isotopic variants of the water molecule. The calculated isotope effects must arise from the different nuclei sampling different regions of the spin density surface. The isotope dependence of the normal-coordinate coefficients listed in Table 5.7 are clearly isotope dependent and can therefore be seen to account for the difference in the spin density of the three isotopomers considered. The results also show that the dominant terms in describing the spin density at nucleus X are the coefficients of the normal-coordinate describing the C-X bond stretching motion. For example the value for the expansion constant α_1 is 0.000479, 0.000661 and 0.001916 for C-D, C-H and C-Mu,

respectively.

Figures 5.3 and 5.4 show the variation of the energy and the spin density of the ethyl radical with internal coordinates R and ϑ_1. The Figures clearly show that for displacements equivalent to those reported in Table 5.10 the region of the surface sampled by each isotope will be markedly different. Figure 5.4 shows that due to the muon's large root-mean-square amplitude the spin density is sampled over a region of the surface where there is a large variation of this property. The large harmonic correction to the coupling constant of the muon can be attributed to this variation of the spin density within the limits of the muon's zero-point motion. The other isotopes experience less of an effect due to their smaller zero-point energies. Table 5.12 indicates that the anharmonic contribution to the vibrational correction is only significant for the light isotope muonium. For the protium and deuterium substituted species the anharmonic correction is almost negligible. In contrast the vibrational corrections to the β-hyperfine coupling constant leads to a residual isotope effect of ca. 15 % for the muon over the proton.

The computed theoretical results enable an estimate of the high-temperature limit ($\overline{A}$) of the β-hyperfine couplings of the ethyl radical to be calculated. At the high temperature limit there is essentially free rotation about the central C-C bond of the radical. The β–hyperfine coupling constant is normally reported as the average of the β-hyperfine couplings, $\overline{A}_\beta = 1/3(A_x + 2A_p)$, since free rotation is assumed. Where A_p is the hyperfine coupling constant of the β-protons not contained in the plane of the notional $2p_z$ orbital containing the unpaired electron. If it is assumed that the value of A_p is that obtained at the SCF level, $\overline{A}_p$ = 37.87 MHz. Then the high-temperature limits are $\overline{A}(CH_2Mu)$ = 80.65 MHz and $\overline{A}(CH_3)$ = 73.48 MHz. These results are in surprisingly good

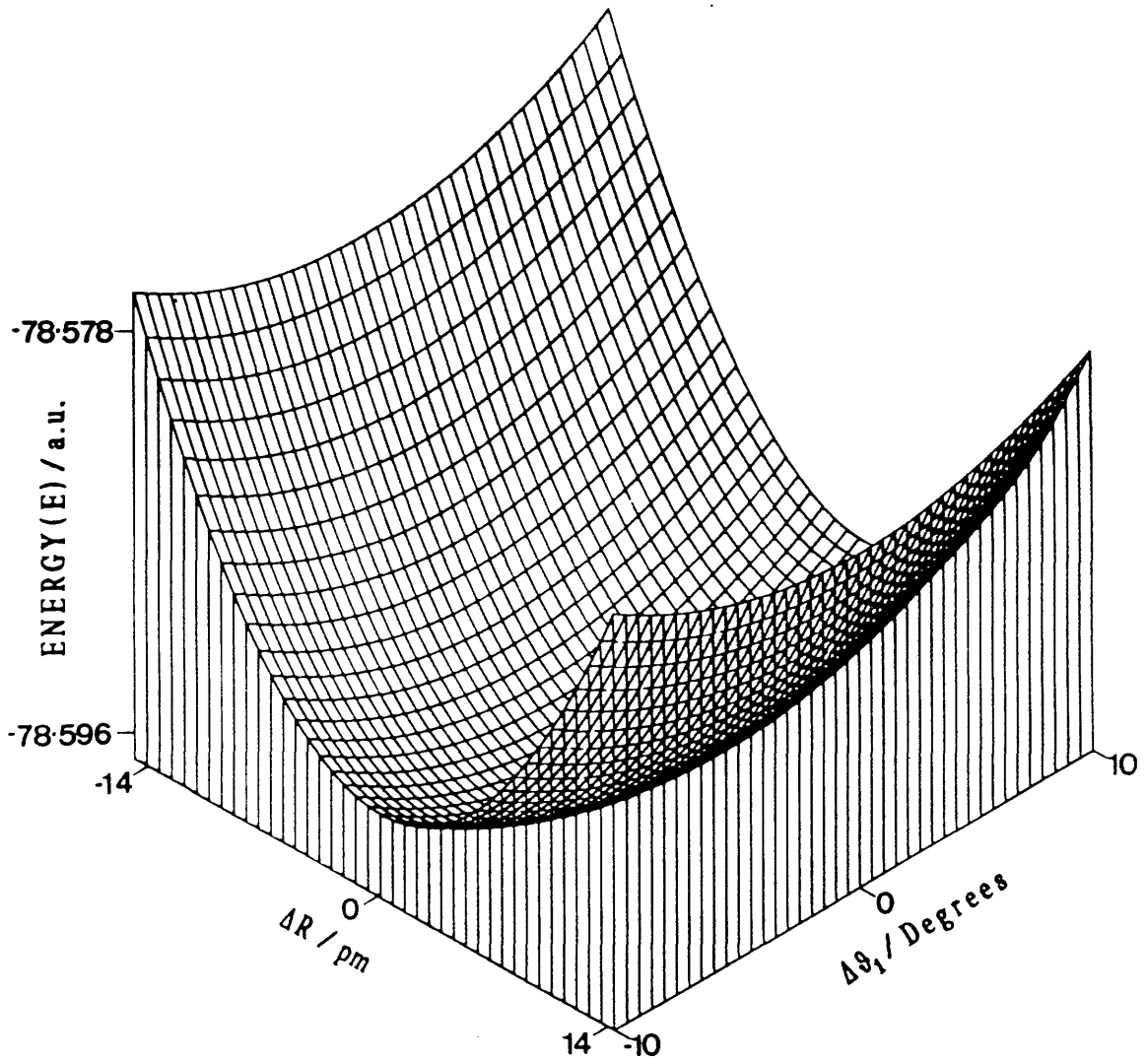

Figure 5.3 Variation of the energy of the ethyl radical with internal displacement coordinates ΔR and $\Delta \vartheta_1$.

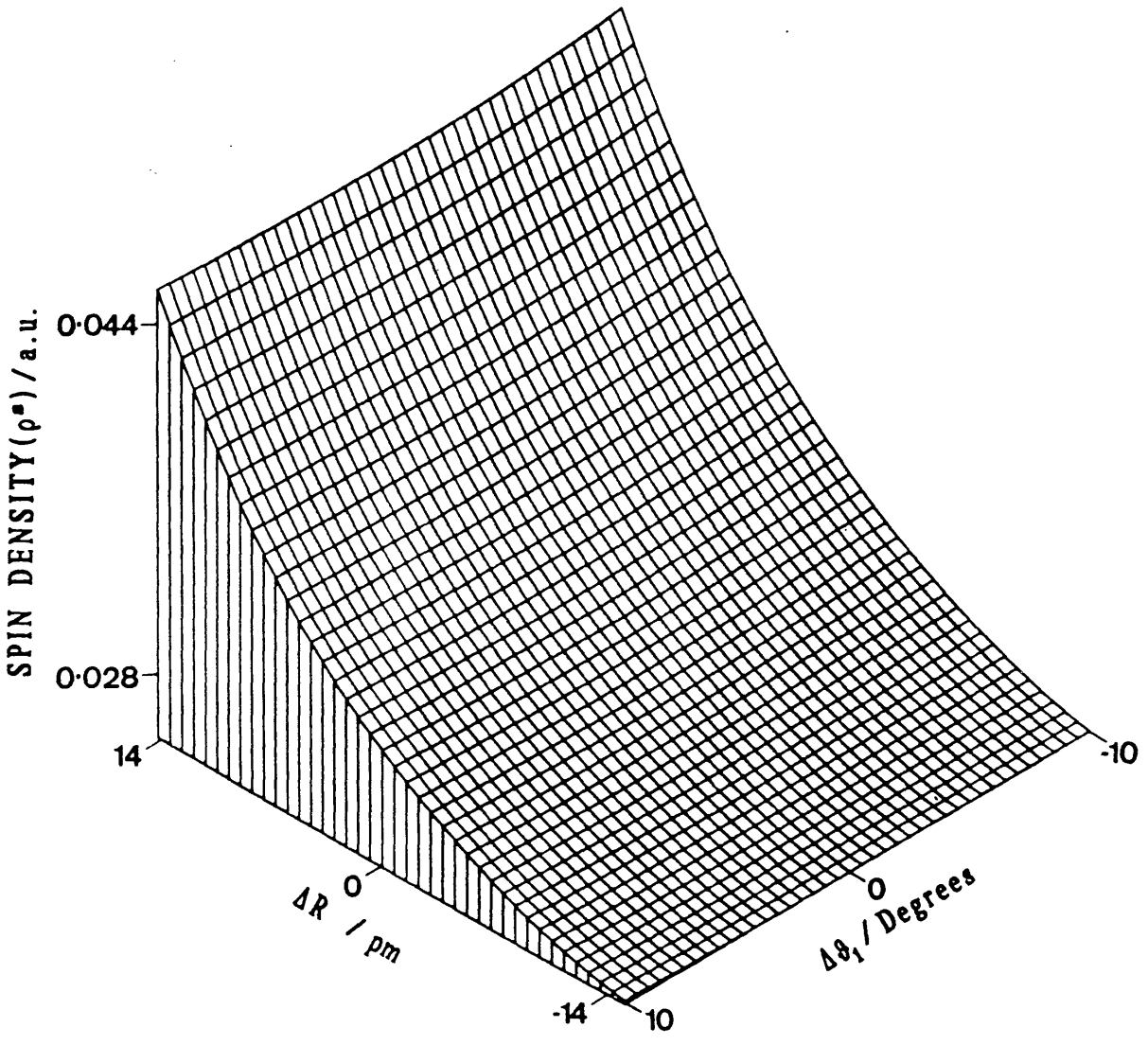

Figure 5.4 Variation of the spin density at nucleus X of the ethyl radical with internal displacement coordiantes ΔR and $\Delta\vartheta_1$.

agreement with the experimentally measured high temperature limits of $\bar{A}(CH_2Mu)$= 79 MHz [67] and $\bar{A}(CH_3)$ = 75.3 MHZ [45]. The computed proton high-temperature limit is probably less accurate because of the neglect of the vibrational coupling between the C-X group and the rest of the radical. These estimates could of course be improved by a more complete treatment of the vibrational averaging. The good agreement of the muon result, however, confirms that the major contributions to the vibrational corrections of the muon arise from the three normal modes considered and their coupling.

The vibrational analysis presented in this chapter and the work of Claxton et al. [75], show that the residual isotope effect observed for the muon β-hyperfine couplings can be explained through consideration of vibrational averaging. The vibrational corrections are found to be composed of a dominant harmonic term and a small anharmonic term. The harmonic term arises from the fact that for each isotopomer the spin density is averaged over a different region of the surface about the stationary point. The large root-mean-square amplitude of the muon results in the muonic species having the largest anharmonic correction. The corresponding anharmonic corrections for the protium and deuterium species are negligible in comparison. These effects can also be used to explain the difference in the barriers to internal rotation of different isotopically substituted ethyl radicals.

It should be noted that all computed results have neglected vibrational-rotational coupling and assumed the radical to be in its ground vibrational state. Corrections over excited vibrational and rotational states would have to be included for a complete study. These corrections would be expected to result in larger vibrational corrections and therefore an increase in the residual isotope effect.

5.4 The Residual Isotope Effect

In the previous section it has been shown that it is possible to account for the observed residual isotope effect in the hyperfine coupling of the ethyl radical by considering the effects of zero-point vibrational corrections to the spin density at the β-nuclei. This implies that the residual isotope effect is primarily dynamic in origin. This is supported by a theoretical study of the difference in the barriers to internal rotation of isotopomers of the ethyl radical performed by Claxton and Graham [131]. In this work it was found that the differences in the barriers could be attributed largely to contributions from the zero-point energy of the different isotopomers. Previous studies of muonium substituted radicals have proposed that the residual isotope effect is governed by a hyperconjugative mechanism [33, 54, 63, 64].

The term hyperconjugation was first introduced by Mulliken in 1939 [137] and was later used to explain the different electron releasing strengths of alkyl groups and the effect of such alkyl groups on reaction rates [138]. For the case of organic free-radicals hyperconjugation is normally used to explain the appearance of unpaired spin density at different nuclear sites. The mechanism of hyperconjugation can, in a restricted sense, be associated with a through space delocalisation of electron spin between non-bonded atoms [139]. This delocalisation of the spin density is governed by the conformation of the system and therefore the relative overlap of the orbitals located on the non-bonded atoms. In a more general sense hyperconjugation can also be taken to include the effects of spin polarization mechanisms. These mechanisms result from conformations which induce the transfer of spin density to a particular nucleus without the transfer of electron density. The transfer of spin

density by this mechanism can occur in molecular systems where there is more than one intervening bond between the unpaired electron and the nucleus of interest. Both spin polarization and delocalization can occur through direct or indirect processes. A direct process implies the transfer of spin density through space and an indirect process implies spin density transfer through the classical bonding pathway. The mechanisms of hyperconjugation enable an understanding, in relatively straight forward terms, of the factors governing the appearance of unpaired spin density at different sites throughout the molecule.

However, application of the concept of hyperconjugation to the residual isotope effect observed in the hyperfine coupling of the ethyl radical infers that isotopic substitution results in a change in the electronic wavefunction of the system. This is contrary to the Born-Oppenheimer approximation which proposes that the electronic wavefunction and potential energy surface of all isotopomers of the ethyl radical are the same. The residual isotope effect, within the limits of the Born-Oppenheimer approximation, can be attributed to the isotopomers sampling different regions of the same potential energy surface due to their different zero-point vibrational energies, as shown in the previous section. This dynamic effect can also be extended to explain the difference in the rotational barriers of the isotopomers. The hyperconjugation argument, which becomes increasingly difficult to interpret in terms of the electronic wavefunctions obtained from sophisticated *ab initio* calculations, is therefore only applicable if it considers spin transfer mechanisms that do not involve the transfer of electron density and which can be related to the dynamic effect governing the residual isotope effect.

CHAPTER 6

6 Summary and Suggestions for Further Work

The experimental and theoretical investigations of muonic species reported in this thesis, show that substitution of hydrogen by its light, isotope, muonium results in significant isotope effects on molecular properties. This effect is observed very clearly in the experimentally observed muon-electron β-hyperfine coupling constant of the 2-muoxyprop-2-yl radical reported in chapter two. This radical was formed by muon implantation in several propan-2-one:water mixtures and a mixture of propan-2-one:n-hexane; and was studied using the technique of transverse field μSR spectroscopy. For all mixtures studied, the hyperfine coupling constant of the muoxy radical formed is found to be small and to show a positive temperature dependence. The temperature dependence, over the liquid range of the samples, of the hyperfine coupling is observed to be almost linear with only a slight deviation form linearity at low temperatures. The hyperfine coupling constant of the 2-muoxyprop-2-yl radical, in each of the mixtures studied, is found to be larger, at all temperatures, than the corresponding hydroxy hyperfine coupling constant of the analogous 2-hydroxyprop-2-yl radical. This increase in the magnitude of the hyperfine coupling on substitution of hydrogen by muonium is attributed to the difference in the zero-point vibrational energies of the different isotopomers. The larger zero-point energy of the muon results in the OMu group of the radical undergoing greater librational motion about the central C-O bond than the analogous OH group of the hydroxy radical. Consequently the increase in the average torsional motion, on muonium substitution, results in an increased value of the hyperfine coupling constant, as observed.

It is also shown in chapter two that the addition of small quantities of water to a sample of pure propan-2-one results in a slight lowering, over the full liquid range of the mixture, in the value of the muon-electron hyperfine coupling constant with respect to the coupling in pure propan-2-one. The lowering in the value of the hyperfine coupling constant, on the addition of water, is thought to arise from the OMu group of the radical experiencing a greater degree of hydrogen bonding due to the presence of the water. The increase in the hydrogen bonding in the aqueous mixtures hinders the torsional motion of the OMu group, which results in a lowering in the magnitude of the observed hyperfine coupling constant.

Associated with the increased hydrogen bonding in the aqueous mixtures is an increase in the barrier to internal rotation of the OMu group against the rest of the radical. Using the rotational averaging technique outlined in chapter one the barrier to internal rotation of the 2-muoxyprop-2-yl radical, in pure propan-2-one, is found to equal 3828.0 J mol^{-1} and in a 15:1, by volume, propan-2-one:water mixture is 8816.8 J mol^{-1}. The barrier to internal rotation derived from the experimentally measured hyperfine coupling constants is for all aqueous mixtures studied, higher than the barrier height reported for the 2-muoxyprop-2-yl radical formed in pure propan-2-one. This result supports the concept that the addition of water to a solution of propan-2-one increases the degree of hydrogen bonding in the solution and results in a hindering of the torsional motion of the OMu group about the central C-O bond.

The barrier to internal rotation of the analogous 2-hydroxyprop-2-yl radical is known from an EPR study of the temperature dependence of the hydroxy hyperfine coupling constant in different solvents. The

calculated barrier to internal rotation for this radical is 10467 J mol^{-1} and is considerably higher than the barrier to internal rotation of the 2-muoxyprop-2-yl radical. This result indicates that the OH group of the hydroxy radical experiences a greater degree of intermolecular hydrogen bonding than the analogous muoxy radical. The difference in the degree of hydrogen bonding experienced by the isotopomers could arise from the difference in their zero-point vibrational energies.

The addition of a quantity of n-hexane to liquid propan-2-one is expected to result in a decrease in the hydrogen bonding present in the solution and consequently an increase in the magnitude of the observed muon-electron β-hyperfine coupling constant. However, at the temperatures 183 and 232 k at which the coupling constant was measured, there is no apparent increase in the value of the hyperfine coupling. In fact, at the lower temperature the hyperfine coupling was found to be slightly smaller than that measured in pure propan-2-one. This result is contrary to the results obtained from a room temperature ALC study of a propan-2-one:hexane mixture. At room temperature the value of the hyperfine coupling constant of the muoxy radical formed in the hexane mixture shows the expected increase in magnitude. This variation in the temperature dependence of the coupling constant could arise from the difference in the sign and magnitude of the average hyperfine coupling constants corresponding to the low lying torsional states of the radical. The difference in the contribution to the average hyperfine coupling constant of the low lying torsional states could also explain the small deviation from linearity observed in the temperature dependence of the hyperfine coupling constant of the 2-muoxyprop-2-yl radical formed in propan-2-one:water mixtures. Further, from similar considerations it is

predicted that at low temperatures, the temperature dependence of the hyperfine coupling of the muoxy and hydroxy prop-2-yl radicals is markedly different.

To further investigate the influence of the low lying torsional states upon the muon-electron hyperfine coupling constant of the 2-muoxyprop-2-yl radical a low temperature TF-μSR study of propan-2-one should be performed. This experiment requires the introduction of a small quantity of solvent, such as 2-methylbutane, to depress the freezing point of the resulting solution. A complete study of the temperature dependence of the hyperfine coupling constant of a sample of propan-2-one:n-hexane could provide useful information on this effect and also the influence of hydrogen bonding on the hyperfine coupling constant.

The regioselectivity of muonium addition to the αβ-unsaturated ketone, 3-methyl-2-butenal has also been studied. The results reported in chapter two show that on muon implantation in this substrate two different muonium substituted radicals are formed. The reduced muon-electron hyperfine coupling constants of the radicals formed at 273 K are 59.96 and 2.89 MHz. A study of the temperature dependence of these couplings enables assignments of the radicals' structures to be made. The higher coupling constant results from muonium addition to the C=C group of the substrate to form a delocalized allyl type radical and the lower coupling constant is the consequence of muonium addition to the carbonyl group to form a muoxy type radical. These results are the first clear observation of competitive muonium addition to an αβ-unsaturated ketone. A complete understanding of the effects influencing the regioselectivity of muonium addition can only be achieved from further

experimental studies of αβ-unsaturated ketones and complementary theoretical calculations of the electronic structure of the radicals formed on muonium addition.

Chapters four and five report the results obtained from comprehensive theoretical studies of the effect of isotopic substitution on molecular properties of the water molecule and the ethyl radical, respectively. These studies are based upon *ab initio* molecular orbital theory and involve the computation of vibrationally averaged molecular properties using a variation-perturbation technique. The vibrationally averaged properties are computed by calculating the expectation value of the electronic property, described by an analytical function, using vibrational wavefunctions corrected through first-order. The vibrational wavefunctions used in these calculations are dependent on the isotopic variant being considered and therefore enable isotope effects on molecular properties to be studied. Since the vibrational wavefunctions are corrected through first-order the computed vibrational corrections to *ab initio* molecular properties include the effects of harmonic and anharmonic motions.

The investigations show that the electric field gradient of the ^{17}O nucleus of the water molecule and the nuclear spin density of the ethyl radical are significantly affected by substitution of hydrogen by muonium. For example the zz-component of the electric field gradient of the oxygen nucleus of the muonic isotopic variant, MuOH, of the water molecule is 2 % larger than the corresponding protium value. Similarly the muon-electron hyperfine coupling constant of the ethyl radical is computed to be 15 % greater than the analogous proton-electron coupling constant. These results show that the isotope effect observed in molecular properties, on substitution of hydrogen by muonium, is the

result of the difference in the vibrational energies of the different isotopomers. The isotope effect arises because each isotopomer samples a different region of the property surface of interest. Due to its high zero-point vibrational energy the muon samples the largest region of the property surface and therefore muonic species show the largest isotope effects. The actual magnitude of the isotope effect is dependent on the nature of the property surface about its stationary point. These calculations also show that for the properties considered in this thesis, the vibrational corrections and therefore the isotope effects are dominated by a harmonic contribution. The contribution of anharmonic vibrational motion to the isotope effect is found to be significant only for the muonic isotopic variants.

As discussed in chapters four and five the theoretically computed, vibrationally averaged, molecular properties are in surprisingly good agreement with experimentally reported results considering the inherent approximations in the theoretical treatment. This investigation has clearly shown that the residual isotope effect observed in selected molecular properties can be attributed to the difference in the vibrational motions of the isotopomers of interest. Additionally, the theoretical study of vibrational corrections reported in the later chapters of this thesis provide some support for the interpretation of the experimental results reported in chapter two.

Theoretical investigations of vibrational effects on molecular properties, as shown here, are clearly important in understanding the effects of muonium substitution on molecular properties. Cox and co-workers [140] have proposed the use of several different quadrupolar nuclei for ALC studies of diamagnetic states. Theoretical calculations comparable to

those reported for the water molecule could assist in determining the most appropriate nuclei for use in these studies and aid in the interpretation of any experimental results. The vibrational averaging technique could also be used to investigate small radicals and ions, such as $HCO^{\cdot}$ and HCO^{+} and their isotopic variants, that have been observed in interstellar clouds. Highly accurate calculations could be performed on these species and the results compared with previous experimental and theoretical studies [141, 142, 143, 144].

REFERENCES

[1]. S. H. Neddermeyer, C. D. Anderson, *Phys. Rev.*, **54**, (1938), 88.

[2]. M. Goldhaber, L. Grodzins, A. W. Sunyar, *Phys. Rev.*, **109**, (1958), 1015.

[3]. E. R. Cohen, B. N. Taylor, *J. Phys. Chem., Ref. Data,* **2**, (1973), 663.

[4]. A. Abragam, *C. R. Acad. Sci. Paris*, C299 Serie II, no. **3**, (1984), 95.

[5]. M. Heming, E. Roduner, B. D. Patterson, W. Odermatt, J. Schneider, H. Baumeler, H. Keller, I. M. Savic, *Chem. Phys. Lett.*, **128**, (1986), 100.

[6]. R. F. Kiefl, S. Kreitzman, M. Celio, R. Keitel, G. M. Luke, J. H. Brewer D. R. Noakes, P. W. Percival, T. Matsuzaki, K. Nishiyama, *Physical Rev. A*, **34**, (1986), 681.

[7]. S. F. J. Cox, G. H. Eaton, J. E. Magraw, C. A. Scott, *Chem. Phys. Lett.*, **160**, (1989), 85.

[8]. D. C. Walker, Y. C. Jean, D. G. Fleming, *J. Chem. Phys.*, **70**, (1979), 4534.

[9]. P. W. Percival, E. Roduner, H. Fischer, *Chem. Phys.*, **32**, (1978), 353.

[10]. E. Roduner, *The Positive Muon as a Probe in Free Radical Chemistry,* Springer, Heidelberg, 1988.

[11]. S. F. J. Cox, J. A. S. Smith, M. C. R. Symons, *Hyperfine Interact.*, **65**, (1990), 993.

[12]. E. Roduner, P. W. Percival, D. G. Fleming, J. Hochmann, H. Fischer, *Chem. Phys. Lett.*, **57**, (1978), 37.

[13]. C. Bucci, G. Guidi, G. M. De'Munari, M. Manfredi, P. Podini, . R. Tedeschi, P. R. Crippa, A. Vecli, *Chem. Phys. Lett.*, **57**, (1978), 41.

[14]. E. Roduner, W. Strub, P. Burkhard, J. Hochmann, P. W. Percival, H. Fischer, M. Ramos, B. C. Webster, *Chem. Phys.*, **67**, (1982), 275.

[15]. E. Roduner, G. A. Brinkman, P. W. F. Louwrier, *Chem. Phys.*, **73**, (1982), 117.

[16]. E. Roduner, B. C. Webster, *J. Chem. Soc., Faraday Trans. 1*, **79**, (1983), 1939.

[17]. E. Roduner, G. A. Brinkman, P. W. F. Louwrier, *Chem. Phys.*, **88**, (1984), 143.

[18]. B. C. Webster, *Ann. Rept. C, Royal Soc. Chem.*, **81**, (1984), 3.

[19]. E. Roduner, *Prog. Reaction Kinetics*, **14**, (1986), 1.

[20]. S. F. J. Cox, *J. Phys. C, Solid State Phys.*, **20**, (1987), 3187.

[21]. S. F. J. Cox, M. C. R. Symons, *Radiat. Phys. Chem.*, **27**, (1986), 53.

[22]. E. Roduner, *Radiat. Phys. Chem.*, **28**, (1986), 75.

[23]. C. J. Rhodes, M. C. R. Symons, E. Roduner, *J. Chem. Soc., Chem. Commun.*, **1**, (1988), 3.

[24]. V. W. Hughes, C. S. Wu, eds., *Muon Physics*, vols. 1-3, Academic Press, New York, 1975.

[25]. P. W. Percival, *Radiochim. Acta*, **26**, (1979), 1.

[26]. J. H. Brewer, D. G. Fleming, P. W. Percival, in Marshall (ed.), *Fourier, Hadamard, and Hilbert Transforms in Chemistry*, Plenum Press, New York, 1982.

[27]. F. James, M. Roos, *Comp. Phys. Commun.*, **10**, (1975), 343.

[28]. A. Schenck, *Muon Spin Rotation Spectroscopy: Principles and Applications in Solid State Physics,* Adam Hilger, Bristol, 1985.

[29]. D. C. Walker, *Muon and Muonium Chemistry,* Cambridge University Press, 1983.

[30]. J. Chappert, R. I. Grynszpan (eds.), *Muons and Pions in Materials Research,* North-Holland, Amsterdam, 1984.

[31]. E. Roduner, H. Fischer, *Chem. Phys. Lett.,* **65**, (1979), 582.

[32]. E. Roduner, H. Fischer, *Chem. Phys.,* **54**, (1981), 261.

[33]. A. Hill, G. Allen, G. Stirling, M. C. R. Symons, *J. Chem. Soc., Faraday Trans. 1,* **78**, (1982), 2959.

[34]. J. H. Brewer, F. N. Gygax, D. G. Fleming, *Phys. Rev.,* **A8**, (1973), 77.

[35]. A. Schenck, in Warren (ed.), *Nuclear and Particle Physics at Intermediate Energies,* Plenum Press, New York, 1975, 159.

[36]. P. W. Percival, H. Fischer, *Chem. Phys.,* **16**, (1976), 89.

[37]. L. D. Landau, E. M. Lifshitz, *Quantum Mechanics,* Pergamon Press, Oxford, 1965.

[38]. J. J. Sakurai, *Modern Quantum Mechanics,* Addison-Wesley Publishing Co., Inc., California, 1985.

[39]. Y. Ito, B. W. Ng, Y. Jean, D. C. Walker, *Can. J. Chem.,* **58**, (1980), 2395.

[40]. K. Venkateswaran, M. V. Barnabas, Z. Wu, J. M. Stadlbauer, B. W. Ng, D. C. Walker, *Chem. Phys.,* **137**, (1989), 239.

[41]. G. Breit, I. I. Rabi, *Phys. Rev.,* **38**, (1931), 2082.

[42]. E. Roduner, Doctoral Thesis, Zürich, 1979.

[43]. M. J. Ramos, D. McKenna, B. C. Webster, E. Roduner, *J. Chem. Soc., Faraday Trans. 1,* **80**, (1984), 255.

[44]. R. M. Macrae, B. C. Webster, E. Roduner, *Muon Studies in Solid State Physics,* IOP Short Meetings Series No.**22**, 95.

[45]. R. W. Fessenden, R. H. Schuler, *J. Chem. Phys.,* **39**, (1963), 2147.

[46]. C. Heller, H. M. McConnel, *J. Chem. Phys.,* **32**, (1960), 1535.

[47]. R. W. Fessenden, *J. Chim. Phys.,* **61**, (1964), 1570.

[48]. P. J. Krusic, P. Meakin, J. P. Jesson, *J. Phys. Chem,* **75**, (1971), 3438.

[49]. J. K. Kochi, *Advances in Free Radical Chemistry,* **5**, (1975), 189.

[50]. D. G. Lister, J. N. MacDonald, N. L. Owen, *Internal Rotation and Inversion-An Introduction to Large Amplitude Motions in Molecules,* Academic Press, London, 1978.

[51]. P. W. Percival, E. Roduner, H. Fischer, *Advances in Chemistry Series,* **175**, (1979), 335.

[52]. A. Hill, S. F. J. Cox, R. DeRenzi, C. Bucci, A. Vecli, M. C. R. Symons, *Hyperfine Interact.,* **17-19**, (1984), 815.

[53]. A. Hill, M. C. R. Symons, S. F. J. Cox, R. DeRenzi, C. A. Scott, C. Bucci, A. Vecli, *J. Chem. Soc., Faraday Trans. 1,* **81**, (1985), 433.

[54]. S. F. J. Cox, D. A. Geeson, C. J. Rhodes, E. Roduner, C. A. Scott, M. C. R. Symons, *Hyperfine Interact.,* **32**, (1986), 763.

[55]. R. M. Macrae, Doctoral Thesis, University of Glasgow, 1990.

[56]. K. Venkateswaran, R. F. Kiefl, M. V. Barnabas, J. M. Stadlbauer, B. W. Ng, Z. Wu, D. C. Walker, *Chem. Phys. Lett.,* **145**, (1988), 289.

[57]. R. Livingston, H. Zeldes, *J. Chem. Phys.,* **44**, (1966), 1245.

[58]. H. Zeldes, R. Livingston, *J. Chem. Phys.,* **45**, (1966), 1946.

[59]. M. Lehni, Doctoral Thesis, University of Zürich, 1983.

[60]. J. F. Gibson, D. J. E. Ingram, M. C. R. Symons, M. G. Townsend, *Trans. Faraday Soc.*, **53**, (1957), 914.

[61]. M. H. Lien, A. C. Hopkinson, *J. Comput. Chem*, **6**, (1985), 274.

[62]. W. Strub, E. Roduner, H. Fischer, *J. Phys. Chem.*, **91**, (1987), 4379.

[63]. S. F. J. Cox, T. A. Claxton, M. C. R. Symons, *Radiat. Phys. Chem.*, **28**, (1986), 107.

[64]. C. J. Rhodes, M. C R. Symons, *J. Chem. Soc., Faraday Trans. 1*, **84**, (1988), 1187.

[65]. M. J. Ramos, D. McKenna, B. C. Webster, E. Roduner, *J. Chem. Soc., Faraday Trans. 1*, **80**, (1984), 267.

[66]. D. A. Geeson, M. C. R. Symons, E. Roduner, H. Fischer, S. F. J. Cox, *Chem. Phys. Lett.*, **116**, (1985), 186.

[67]. P. W. Percival, J. C. Brodovitch, S. K. Leung, D. Yu, R. F. Kiefl, D. M. Garner, D. J. Arseneau, D. G. Fleming, A. Gonzalez, J. R. Kempton, M. Senba, K. Venkateswaran, S. F. J. Cox, *Chem. Phys. Lett.*, **163**, (1989), 241.

[68]. I. Carmichael, *J. Phys. Chem.*, **95**, (1991), 6198.

[69]. W. T. Raynes, P. Lazzeretti, R. Zanasi, A. J. Sadlej, P. W. Fowler, *Mol. Phys.*, **60**, (1987), 509.

[70]. W. T. Raynes, P. Lazzeretti, R. Zanasi, *Mol. Phys.*, **61**, (1987), 1415.

[71]. W. T. Raynes, *Mol. Phys.*, **63**, (1988), 719.

[72]. W. T. Raynes, P. W. Fowler, P. Lazzeretti, R. Zanasi, M. Grayson, *Mol. Phys.*, **64**, (1989), 143.

[73]. E. Roduner, I. D. Reid, *Is. J. Chem.*, **29**, (1989), 3.

[74]. A. Lopes de Magalhães, M. J. Ramos, *Chem. Phys. Lett.*, **165**, (1990), 528.

[75]. T. A. Claxton, A. M. Graham, S. F. J. Cox, D. M. Maric, P. F. Meier, S. Vogel, *Hyperfine Interact.*, **65**, (1990), 913.

[76]. D. Chipman, *J. Chem. Phys.*, **94**, (1991), 6632.

[77]. E. Schrödinger, *Ann. Physik*, **79**, (1926), 361 and 489.

[78]. M. Born, J. R. Oppenheimer, *Ann. Phys.*, **84**, (1927), 457.

[79]. P. O. Löwdin, *Phys. Rev.*, **97**, (1955), 1490.

[80]. P. O. Löwdin, *Phys. Rev.*, **97**, (1955), 1509.

[81]. J. C. Slater, *Phys. Rev.*, **34**, (1929), 1293.

[82]. C. C. J. Roothaan, *Rev. Mod. Phys.*, **32**, (1960), 179.

[83]. J. A. Pople, R. K. Nesbet, *J. Chem. Phys.*, **22**, (1954), 571.

[84]. G. G. Hall, *Proc. Royal Soc., London*, **A205**, (1951), 541.

[85]. C. C. J. Roothaan, *Rev. Mod. Phys.*, **23**, (1951), 69.

[86]. J. Simons, *J. Phys. Chem.*, **95**, (1991), 1017.

[87]. A. Szabo, N. S. Ostlund, *Modern Quantum Chemistry, Introduction to Advanced Electronic Structure Theory*, McGraw-Hill, New York, 1982.

[88]. W. J. Hehre, L. Radom, P. V. R. Schleyer, J. A. Pople, *Ab Initio Molecular Orbital Theory*, John Wiley & Sons, New York, 1986.

[89]. C. E. Dykstra, *Ab Initio Calculation of Structure and Properties of Molecules*, Elsevier, Amsterdam, 1988.

[90]. J. C. Slater, *Phys. Rev.*, **36**, (1930), 57.

[91]. S. F. Boys, *Proc. Royal Soc., London Ser.*, **A200**, (1950), 542.

[92]. E. R. Davidson, D. Feller, *Chem. Rev.*, **86**, (1986), 681.

[93]. J. Almlöf, T. Helgaher, P. R. Taylor, *J. Phys. Chem.*, **92**, (1988), 3029.

[94]. D. Feller, E. R. Davidson, *Theor. Chim. Acta*, **68**, (1985), 57.

[95]. D. M. Chipman, I. Carmichael, D. Feller, *J. Phys. Chem.*, **95**, (1991), 4702.

[96]. V. Keshari, S. P. Karna, P. Chandra, *J. Mol. Struct.*, **192**, (1989), 271.

[97]. S. P. Gejji, S. Lunell, *J. Phys. Chem.*, **94**, (1990), 4447.

[98]. C. W. Kern, R. L. Matcha, *J. Chem. Phys.*, **49**, (1968), 2081.

[99]. W. C. Ermler, C. W. Kern, *J. Chem. Phys.*, **55**, (1971), 4851.

[100]. B. J. Krohn, W. C. Ermler, C. W. Kern, *J. Chem. Phys.*, **60**, (1974), 22.

[101]. W. C. Ermler, B. J. Krohn, *J. Chem. Phys*, **67**, (1977), 1360.

[102]. E. B. Wilson Jr., J. C. Decius, P. C. Cross, McGraw-Hill, New York, *Molecular Vibrations*, 1955.

[103]. S. Califano, *Vibrational States*, John-Wiley & Sons, London, 1976.

[104]. L. B. Harding, W. C. Ermler, *J. Comput. Chem.*, **6**, (1985), 13.

[105]. J. O. Hirschfelder, W. B. Brown, S. T. Epstein, *Advan. Quantum Chem.*, **1**, (1964), 255.

[106]. D. A. Clabo Jr., W. D. Allen, R. B. Remington, Y. Yamaguchi, H. F. Schaefer III, *Chem. Phys.*, **123**, (1988), 187.

[107]. L. B. Harding, *J. Phys. Chem.*, **93**, (1989), 8004.

[108]. K. Kuchitsu, L. S. Bartell, *J. Chem. Phys.*, **36**, (1961), 2460.

[109]. B. J. Rosenberg, W. C. Ermler, I. Shavitt, *J. Chem. Phys.*, **65**, (1976), 4072.

[110]. P. Henning, W. P. Kraemer, G. H. F. Diercksen, G. Strey, *Theoret. Chim. Acta.*, **47**, (1978), 233.

[111]. J. F. Gaw, N. C. Handy, *Chem. Phys. Lett.*, **121**, (1985), 321.

[112]. M. A. Aguilar, F. J. Olivares del Valle, J. Tomasi, *Chem. Phys.*, **150**, (1991), 151.

[113]. M. W. Schmidt, J. A. Boatz, K. K. Baldridge, S. Koseki, M. S. Gordon, S. T. Elbert, B. Lam, QCPE Bulletin, Vol. 7, (1987), 115.

[114]. J. Baker, *J. Comput. Chem.*, **7**, (1986), 385.

[115]. P. C. Hariharan, J. A. Pople, *Theoret. Chim. Acta.*, **28**, (1973), 213.

[116]. M. M. Franci, W. J. Pietro, W. J. Hehre, J. S. Binkley, M. S. Gordon, D. J. DeFrees, J. A. Pople, *J. Chem. Phys.*, **77**, (1982), 3654.

[117]. G. Simons, R. G. Parr, J. Finlan, *J. Chem. Phys.*, **59**, (1973), 3229.

[118]. K. Kuchitsu, Y. Morino, *Bull. Chem. Soc. Jpn.*, **38**, (1965), 814.

[119]. D. F. Smith Jr., J. Overend, *Spectrochim Acta, Part A*, **28**, (1972), 471

[120]. J. Pliva, V. Špirko, D. Papoušek, *J. Mol. Spec.*, **23**, (1967), 331.

[121]. W. S. Benedict, N. Gailar, E. K. Plyer, *J. Chem. Phys.*, **24**, (1956), 1139.

[122]. J. S. M. Harvey, *Proc. Royal Soc.*, **285A**, (1965), 581.

[123]. S. G. P. Brosnan, D. T. Edmonds, *J. Mol. Struct.*, **58**, (1980), 23.

[124]. H. W. Spiess, B. B. Garrett, R. K. Sheline, S. W. Rabideau, *J. Chem. Phys.*, **51**, (1969), 1201.

[125]. J. Verhoeven, A. Dymanus, H. Bluyssen, *J. Chem. Phys.*, **50**, (1969), 3330.

[126]. D. T. Edmonds, S. D. Goren, A. A. L. White, W. F. Sherman, *J. Magn. Reson.*, **27**, (1977), 35.

[127]. D. T. Edmonds, S. D. Goren, A. L. MacKay, A. A. L. White, W. F. Sherman, *J. Magn. Reson.*, **23**, (1976), 505.

[128]. Y. Margalit, M. Shporer, *J. Magn. Reson.*, **43**, (1981), 112.

[129]. I. J. F. Poplett, *J. Magn. Reson.*, **50**, (1982), 397.

[130]. P. L. Cummins, G. B. Bacskay, N. S. Hush, B. Halle, S. Engström, *J. Chem. Phys.*, **82**, (1985), 2002.

[131]. T. A. Claxton, A. M. Graham, *J. Chem. Soc., Faraday Trans. 2*, **83**, (1987), 2307.

[132]. J. Pacansky, M. Dupuis, *J. Chem. Phys.*, **68**, (1978), 4276.

[133]. B. Webster, R. Macrae, *Chem. Phys. Lett.*, **150**, (1988), 18.

[134]. R. W. Fessenden, *J. Phys. Chem.*, **71**, (1967), 74.

[135]. J. Pacansky, M. Dupuis, *J. Am. Chem. Soc.*, **104**, (1982), 415.

[136]. T. A. Claxton, A. M. Graham, *J. Chem. Soc. Chem. Commun.*, **2**, (1987), 1167.

[137]. R. S. Mulliken, *J. Chem. Phys.*, **7**, (1939), 339.

[138]. R. S. Mulliken, C. A. Rieke, W. G. Brown, *J. Am. Chem. Soc.*, **63**, (1941), 41.

[139]. F. W. King, *Chem.* Rev., **76**, (1976), 157.

[140]. S. F. J. Cox, D. Buttar, J. A. S. Smith, *Hyperfine Interact.*, **65**, (1990), 987.

[141]. E. Herbst, W. Klemperer, *Astrophys. J.*, **185**, (1973), 505.

[142]. E. Herbst, W. Klemperer, *Astrophys. J.*, **207**, (1976), 110.

[143]. L. E. Snyder, J. M. Hollis, F. J. Lovas, B. L. Ulich, *Astrophys. J.*, **209**, (1976), 67.

[144]. B. Webster, M. Hilazer, M. J. Ramos, I. Carmichael, *J. Chem. Soc., Faraday Trans. 2*, **81**, (1985), 1761.

PUBLICATIONS

1. Competitive Muonium Addition to 3-Methyl-2-butenal.
   D. Buttar, R. M. Macrae, B. C. Webster, E. Roduner,
   J. Chem. Soc., Faraday Trans., **86**, (1990), 220.

2. Solvent Effects on the Hyperfine Coupling Constant and Barrier to Internal Rotation of the 2-Muoxyprop-2-yl Radical.
   D. Buttar, R. M. Macrae, B. C. Webster, E. Roduner,
   Hyperfine Interact., **65**, (1990), 927.

3. Muon Addition to Nitrogen, Oxygen and other Atoms; Considerations for Level Crossing Resonance Studies.
   S. F. J. Cox, D. Buttar, J. A. S. Smith,
   Hypefine Interact., **65**, (1990), 987.

4. Vibrationally Averaged β-Hyperfine Coupling Constants for the Muonium Substituted Ethyl Radical.
   D. Buttar, B. C. Webster,
   J. Chem. Soc., Faraday Trans., **87**, (1991), 2901.

SOLVENT EFFECTS ON THE HYPERFINE COUPLING CONSTANT AND BARRIER TO INTERNAL ROTATION FOR THE 2-MUOXYPROP-2-YL RADICAL

D. BUTTAR, R.M. MACRAE, B.C. WEBSTER

Chemistry Department, The University, Glasgow G12 8QQ, Scotland

and

E. RODUNER

Physikalisch-Chemisches Institut der Universität, CH-8057, Zürich, Switzerland

The muon-electron β-hyperfine coupling constant is reported for the 2-muoxyprop-2-yl radical formed by positive muon (μ^+) implantation in propan-2-one and aqueous solutions of propan-2-one. Using the technique of muon spin rotation (μSR) spectroscopy the coupling constant was measured over a full temperature range in which the samples were in the liquid state. In all cases, the coupling constants were found to be small, and to show a positive temperature dependence. In the aqueous mixtures the presence of the water produces a slight lowering, at all temperatures, in the coupling constant with respect to the coupling in pure propan-2-one. An interpretation is given which relates the radical structure, to the barrier hindering internal rotation and to solvent interactions.

1. Introduction and experimental

Comprehensive studies of the muonated radical formed in propan-2-one have been conducted already using the techniques of avoided level crossing and muon spin rotation spectroscopy [1–5]. However in these studies the experimental measurement of the muon-electron β-hyperfine coupling constants was limited to a small temperature range. Previously we have outlined the result obtained from measurements of the hyperfine couplings over the liquid range of propan-2-one and a sample consisting of propan-2-one and water in the volume ratio, 20 : 1. [6]. Here we report, in full, the results of these experiments, together with those for propan-2-one : water mixtures in the ratios of 100 : 1, 40 : 1, 15 : 1 and 10 : 1.

All experiments were performed at the Paul Scherrer Institute, Villigen, Switzerland using the μE1 and μE4 beamlines. The reagents were degassed using the normal freeze-pump-thaw procedure and sealed under vacuum in thin-walled spherical glass vessels. In each experiment a field of 0.2 T was applied transverse to the muon spin direction in the polarised beam. Consequently, the radical formed is characterised by a pair of lines in the Fourier transform spectrum.

After subtraction of the diamagnetic signal the value of, $|A_\mu|$, the isotropic muon-electron hyperfine coupling constant was obtained for the radical. The theory for the analysis of μSR spectra of muonium-substituted organic free radicals is well documented elsewhere [7].

The experimentally measured coupling constants have been analysed, using a rotational averaging technique to give the barrier height to internal rotation, V_2, of the 2-muoxy-prop-2-yl radical in each mixture. The barriers are the rotational barriers, averaged over the librational motion of the muon. As a result of the large mass difference of the muon and the proton it is possible to observe the difference in the rotational barrier of the 2-hydroxy and 2-muoxy prop-2-yl radicals.

2. Results

The reduced muon hyperfine coupling constants, A'_μ, defined as the coupling constant scaled by the ratio of the proton's magnetic moment to the muon's magnetic moment are listed in table 1 for the 2-muoxyprop-2-yl radical in the temperature range from 319 K to 180 K. The results show an expected decrease in the couplings, from 9.38 MHz at 319 K to 3.64 MHz at 180 K. The temperature dependence of the coupling constants is nearly linear with only a slight deviation from linearity at low temperatures. Listed in table 1 are the reduced hyperfine coupling constants for propan-2-one : water mixtures. The couplings for the 20 : 1 mixture are found to be slightly lower than those of pure propan-2-one, decreasing from 8.86 MHz at 323 K to 2.91 MHz at 183 K. For the 20 : 1 mixture the hyperfine couplings are dependent on the water concentration in the solution as found by Hill et al. [1,2]. To elucidate the solvent dependence of

Table 1
The temperature, T/K, and solvent dependence of the reduced muon-electron hyperfine coupling constant, A'_μ/MHz of the 2-muoxyprop-2-yl radical in various H_2O mixtures

Propan-2-one solutions											
Pure		100 : 1		40 : 1		20 : 1		15 : 1		10 : 1	
T	A'_μ	T	A'_μ	T	A'_μ	T	A'_μ	T	A'_μ	T	A'_μ
180	3.64	181	3.30	170	2.97	183	2.91	193	3.25	182	3.07
203	4.49	211	4.42	201	3.72	203	3.47	207	3.73	200	3.57
228	5.48	228	5.13	225	4.62	223	4.20	233	4.70	226	4.45
251	6.44	251	6.08	248	5.64	243	5.06	250	5.39	239	4.93
277	7.59	277	7.28	290	7.62	263	5.97	269	6.26	258	5.77
300	8.56	289	7.88	314	8.74	283	6.98	277	6.51	280	6.70
319	9.38	316	9.11			303	7.85	291	7.24	317	8.47
						323	8.86	313	8.32		

$T \pm 0.1$ K.

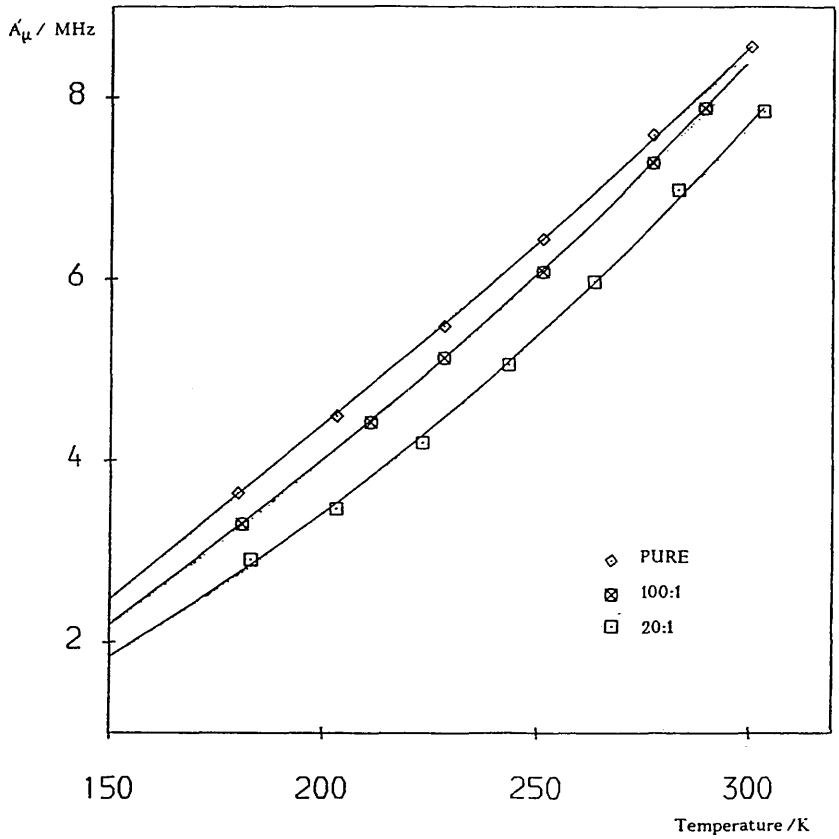

Fig. 1. Temperature and solvent dependence of the reduced hyperfine coupling constant, A'_μ, of the 2-muoxyprop-2-yl radical.

the coupling constants other mixtures were studied with propan-2-one and water in the volume ratios, 10 : 1, 15 : 1, 40 : 1 and 100 : 1. The reduced hyperfine couplings of each of these mixtures are given in table 1. In each case the couplings followed the same temperature dependence, deviating only slightly from linearity at low temperatures. At all temperatures the observed couplings of the binary aqueous mixtures are smaller than those obtained in pure propan-2-one. However, closer inspection of the results shows that whereas near room temperature the value of the coupling constant decreases with increasing water concentration, at around 220 K there appears to be a crossing of the results obtained from the 15 : 1 and the 20 : 1 solutions. This behaviour is observed to a greater extent in the 10 : 1 solution. Fig. 1 shows the temperature and solvent dependence of the hyperfine coupling of the 2-muoxyprop-2-yl radical in the pure, 100 : 1 and 20 : 1 solutions.

3. Discussion

An EPR study of the hydroxyprop-2-yl radical [8] provides a comparison between the proton β-hyperfine coupling constants and the muon coupling constants. The coupling constants of the hydroxy radical appear to follow the same trends as those of the muoxy prop-2-yl radical. The values of the proton coupling constants decrease as the temperature is lowered and the addition of a polar solvent produces a lowering in the observed coupling constants. The couplings measured by the EPR study are considerably smaller than those of the muoxy radical this is probably due to the large moment of inertia of the O-H group relative to the O-Mu group. This results in a greater amplitude of libration for the muon.

The solvent interactions which affect the measured β-hyperfine coupling constants of the 2-hydroxy and 2-muoxy prop-2-yl radicals are probably of a similar nature. In each case the coupling constants will be influenced by spin delocalisation which follows from the resonance structure shown below. It is thought that the optimum *ab initio* geometry of the 2-hydroxyprop-2-yl radical, in which the radical centre is somewhat pyramidal [6], is similar to that of the 2-muoxyprop-2-yl radical. The resonance structures show two of the possible structures that occur as a result of the librational motion of the muon. In polar

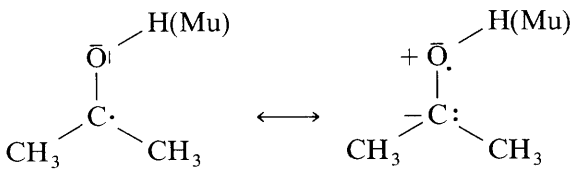

(I) (II)

solvents, like water, resonance structure (II) could have a greater significance than in non-polar solvents. In this structure spin polarisation of the unpaired electron at the oxygen leads to a negative contribution of the spin density at the hydroxy proton(muon) site. The lowering of the muon coupling constant on addition of water is thought to result from the increasing role of structure (II) through an increase in hydrogen bonding, over that of pure propan-2-one, in the solutions.

The further lowering of the coupling constants on increasing the concentration of water present in the solution is thought to reflect a further increase in hydrogen bonding within the mixtures. In studies of a binary mixture of propan-2-one : D_2O in the volume ratio of 20 : 1 we find the reduced hyperfine coupling constant to be 7.5 MHz at 298 K. This value shows no significant difference from that of the coupling constant measured for the 20 : 1 propan-2-one : water mixture

at a similar temperature. The correspondence between the coupling constants indicates that the increased contribution to the hydrogen bonding in the aqueous muoxy radical systems is through bonding by muonium to the oxygen of the water molecule.

3.1. INTERNAL ROTATION STUDIES

The hydrogen bonding present in the solution is expected to hinder the internal rotation of the O-Mu group against the rest of the molecule [12]. We develop this argument quantitatively by considering the barrier height, V_2, to internal rotation, of the radical. V_2 can be extracted from the temperature dependence of the β-hyperfine coupling constants, as described elsewhere. The procedure used involves the fitting of the experimentally measured coupling constants to theoretical values using a quantum mechanical averaging technique and has already been applied in a study of the internal rotation of muonium substituted ethyl isotopomers [9]. It is assumed that in this method the major contribution to the temperature dependence of the coupling constants is the difference in the average torsional angle (γ) about the $\dot{C}$-O internuclear axis. In general the dependence of the coupling constant upon the torsional angle can be expressed as.

$$\langle A_\beta(\gamma)\rangle = L + M\langle\cos^2\gamma\rangle, \qquad \gamma = \vartheta + \vartheta_0 \tag{1}$$

where L and M are constants ($M \gg L$) and ϑ is the dihedral angle between the axis of the half-filled $2p_z$ orbital centred on C_2 and the C_β – Mu axis. ϑ_0 is the value of ϑ at the minimum of the potential barrier to internal rotation and therefore specifies the equilibrium conformation of the radical.

For the radicals discussed here it is assumed that the potential barrier hindering internal rotation is principally of a two fold nature and can be represented by the truncated Fourier series,

$$V(\vartheta) = \tfrac{1}{2}V_2(1 - \cos 2\vartheta). \tag{2}$$

In addition it is assumed that the transitions between different torsional states is rapid on the time scale of the μSR experiment. The observed splitting is therefore the average of the quantum mechanical expectation values, $\langle A_\beta(\gamma)\rangle_i$, for all the torsional states, i, weighted by their populations. If there is a Boltzmann population of the torsional energy levels, E_i, then the temperature dependence of the β-hyperfine coupling constant obeys the relationship.

$$A_\beta(T) = \frac{\sum_i \langle A_\beta(\gamma)\rangle_i \exp(-E_i/kT)}{\sum_i \exp(-E_i/kT)}. \tag{3}$$

With a basis comprising 21 functions, as

$$\Psi_j = 1/(2\pi)^{1/2}\sum_m c_m \exp(\mathrm{i}m\vartheta), \qquad \begin{matrix} m = -10, 10 \\ j = 1, 2m_{\max}+1 \end{matrix}. \tag{4}$$

Table 2
Values for the parameters L/MHz and M/MHz, and V_2/J mol^{-1} for the 2-muoxyprop-2-yl radical in various H_2O mixtures

Solutions	L	M	V_2
Pure	−117.0	315.3	3828.0
100:1	−105.0	298.1	4572.1
40:1	−94.9	283.7	5307.0
20:1	−76.7	259.3	7037.0
15:1	−69.6	262.9	8816.8
10:1	−70.4	246.7	7554.9

The barrier height for the 2-muoxyprop-2-yl radical is ascertained by fitting the theoretically calculated coupling constants obtained from eq (3) to the observed couplings through simultaneous variation of the three parameters L, M and V_2 in eqs. (1) and (2). The parameters L, M and V_2 for each mixture are collated in table 2. Fig. 2 displays the values of, $\langle A_\beta(\gamma)\rangle_i$, for the six lowest torsional levels

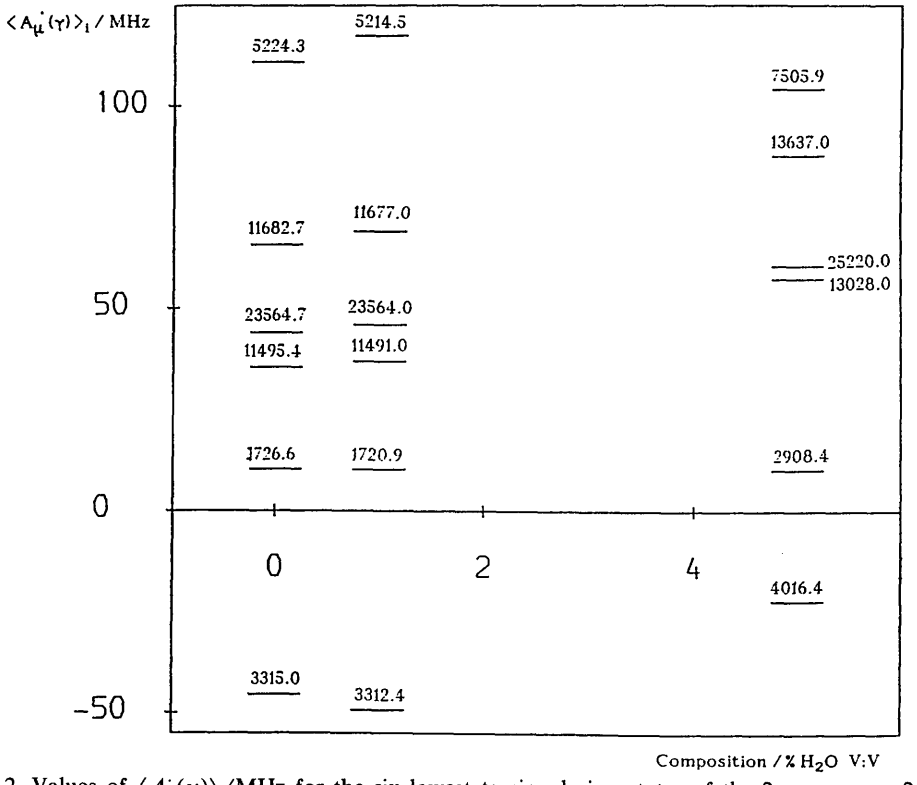

Fig. 2. Values of $\langle A_\mu^{\cdot}(\gamma)\rangle$/MHz for the six lowest torsional eigenstates of the 2-muoxyprop-2-yl radical in pure propan-2-one and the 20:1 and 100:1 mixtures. The corresponding torsional eigenvalues, E_i/J mol^{-1}, for each state are also shown.

of pure propan-2-one and the 100 : 1 and 20 : 1 mixtures. It is found that for all mixtures studied only one level, that of $i = 2$, yields a negative coupling constant. In the temperature range of the experiment only the lowest five torsional levels are significantly populated, as a consequence the contribution of the level, $i = 2$, to the theoretical temperature-dependence curve for all mixtures, shows a minimum at around 150 K. The difference in the value of the coupling constant yielded by the torsional level, $i = 2$, for each mixture could explain the small deviation from linearity observed in the experimentally measured couplings at temperatures about 220 K. We see that the barrier increases from 4572 J mol^{-1} in the 100 : 1 propan-2-one: water mixture up to 8816 J mol^{-1} in the 15 : 1 mixture. In all cases, the value of the barrier exceeds that of 3828 J mol^{-1} for the 2-muoxyprop-2-yl radical in pure propan-2-one.

The dependence of the barrier to internal rotation of the radical on the water concentration in the mixture is shown in fig. 3. Two results appear anomalous;

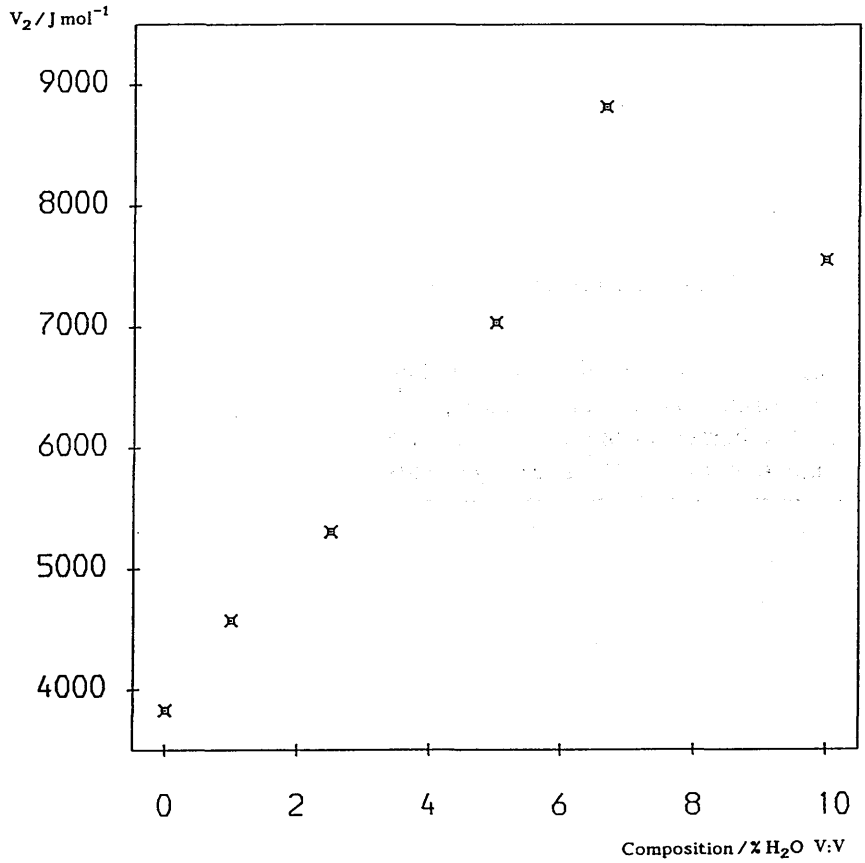

Fig. 3. Dependence of the barrier height, V_2, to internal rotation of the 2-muoxyprop-2-yl radical on the composition of the mixture.

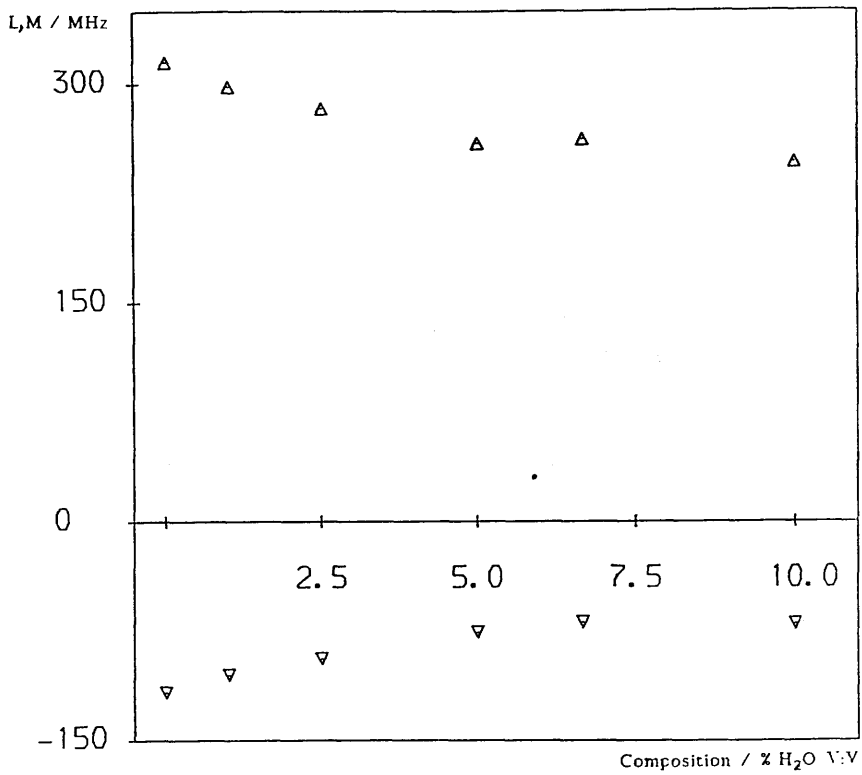

Fig. 4. Solvent dependence of the parameters L: ▽ and M: △.

the expected trend is that the torsional barrier should increase in value as the water concentration is raised as a consequence of greater hydrogen bonding in the solutions. The barrier of the of the 15 : 1 mixture is actually about 1000 J mol^{-1} higher than that of the 10 : 1 mixture. This anomaly is not apparent in fig. 4 which shows the dependence of the parameters L and M on the water concentration. At present we are unable to provide any explanation as to the nature of this anomaly, although it could result from the experimental data reported for the pure, 20 : 1 and 15 : 1 solutions being collected during a different beam period to that of the 100 : 1, 40 : 1 and 10 : 1 mixtures.

The EPR study of the 2-hydroxyprop-2-yl radical by Lehni [8] allows a barrier height to be determined for this radical. Using the β-proton hyperfine couplings the barrier to internal rotation of the hydroxy radical in a dilute solution of butan-2-ol was calculated as 10467 J mol^{-1}, with $L = -7.89$ MHz and $M = 56.40$ respectively. The study reports splitting parameters for the radical in several different solvents and in each case the barrier from the couplings is higher than that of the 2-muoxyprop-2-yl radical and the values of the fitting parameters L and M are similar to those reported. The errors on the parameters L and M are

at present unknown. The difference in the torsional barriers of of the 2-muoxy and 2-hydroxy prop-2-yl radicals can be explained from consideration of ancilliary motions in the radical.

The high temperature limit of the β-hyperfine coupling constant, given by $L + M/2$, is 40.65 MHz for the 2-muoxyprop-2-yl radical in pure propan-2-one and 20.31 MHz for the 2-hydroxyprop-2-yl radical. The ethyl radical and its muonic isotopomers have similar high temperature limits, of about 75 MHz [10]. For the prop-2-yl radical the large difference in the high temperature limits could be a result of a greater difference in the reduced moment of inertia to that of the ethyl isotopomers. The result may also indicate that it is insufficient to consider only torsional motion for these radicals.

The barrier height to internal rotation of the 2-muoxy and 2-hydroxy prop-2-yl radicals have been distinguished by the assumption of a simple model to represent the solvent system. This model neglects the possibility that the bonding that occurs in the system could affect the moment of inertia of the rotating group, and that the addition of a small volume of water to a solution of propan-2-one produces a homogeneous mixture. A more complete study will have also to consider the effect of the internal rotation on the hydrogen and intermolecular bonds formed during the timescale of the experiment.

Nevertheless, we believe that given the complex nature of the solvent system, the model used provides a first step in the study of solvent effects on the barriers to internal rotation in muonic radicals.

Acknowledgements

This work was supported by the Carnegie Trust for the Universities of Scotland, the Swiss National Foundation for Scientific Research, and the Paul Scherrer Institute. We gratefully acknowledge the award of a research studentship to DB by the SERC and an award to RMM by the James Clerk Maxwell Foundation. We should like also to thank Drs. T. Azuma, I.D. Reid and C.J. Rhodes for their assistance with the μSR experiments.

References

[1] A. Hill, S.F.J. Cox, R. de Renzi, C. Bucci, A. Vecli and M.C.R. Symons, Hyp. Int. 17–19 (1984) 815.

[2] A. Hill, M.C.R. Symons, S.F.J. Cox, R. de Renzi, C.A. Scott, C. Bucci and A. Vecli. J. Chem. Soc., Faraday Trans. 81 (1985) 433.

[3] S.F.J. Cox, D.A. Geeson, C.J. Rhodes, E. Roduner, C.A. Scott and M. C.R. Symons, Hyp. Int. 32 (1986) 763.

[4] K. Venkateswaran, R.F. Kiefl, M.V. Barnabas, J.M. Stadlbauer, B.W. Ng, Z. Wu and D.C. Walker. Chem. Phys. Lett. 145 (1988) 289.

[5] M. Heming, E. Roduner, B.D. Patterson, W. Odermatt, J. Schneider, H. Baumeler, H. Keller and I.M. Savic, Chem. Phys. Lett. 128 (1986) 100.
[6] R.M. Macrae, B.C. Webster and E. Roduner, *Muon Studies in Solid State Physics*, IOP Short Meetings, No. 22 (1988) 95.
[7] E. Roduner, in: *Muons and Pions in Materials Research*, eds. J. Chappert and R.I. Grynszpan (North-Holland, Amsterdam, 1984) Ch. 12.
[8] M. Lehni, Doctoral Thesis University of Zurich, 1983.
[9] M.J. Ramos, D. McKenna and B.C. Webster, J. Chem. Soc., Faraday Trans. 1, 80 (1984) 255.
[10] R.M. Macrae, Doctoral Thesis University of Glasgow, 1990.

REPRINTED FROM:

HYPERFINE INTERACTIONS

Hyperfine Interactions 65 (1990) 987–992

MUON ADDITION TO NITROGEN, OXYGEN AND OTHER ATOMS: CONSIDERATIONS FOR LEVEL CROSSING RESONANCE STUDIES

S.F.J. COX, D. BUTTAR *

Rutherford Appleton Laboratory, Chilton, Oxon OX11 0QX, U.K.

and J.A.S. SMITH

Department of Chemistry, King's College, Strand, London WC2R 2LS, U.K.

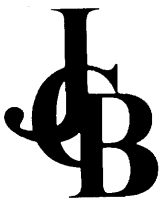

J.C. BALTZER AG, SCIENTIFIC PUBLISHING COMPANY, BASEL, SWITZERLAND

Hyperfine Interactions 65 (1990) 987–992

MUON ADDITION TO NITROGEN, OXYGEN AND OTHER ATOMS: CONSIDERATIONS FOR LEVEL CROSSING RESONANCE STUDIES

S.F.J. COX, D. BUTTAR *

Rutherford Appleton Laboratory, Chilton, Oxon OX11 0QX, U.K.

and J.A.S. SMITH

Department of Chemistry, King's College, Strand, London WC2R 2LS, U.K.

The purpose of this note is to examine the conditions under which muon level crossing resonance with quadrupolar nuclei may be used to characterise the elusive diamagnetic fraction which is formed when positive muons are stopped in various media and associate chemically with the host molecules. A potential difficulty is identified for nuclei having integral spin, which may explain why cross polarisation to ^{14}N has not yet been detected. The general suitability of nuclei with half-integral spin ($I \geqslant 3/2$) is illustrated with the case of ^{17}O, and suggestions are made for future studies with other nuclei, including species such as molecular ions and defect complexes (muon-impurity pairs).

Although some proportion of muons invariably adopts diamagnetic states when implanted in molecular materials, there is rarely any signature in the muon spin rotation spectrum which identifies the chemical species formed. Precession signals are obtained at frequencies which are generally indistinguishable from the Larmor frequency corresponding to the applied field; chemical shifts (used routinely in proton NMR as a signature of the proton's chemical environment) are expected to be resolved only in very high magnetic fields and have only been measured in a few instances. This situation contrasts markedly with that pertaining to paramagnetic species, e.g. muonic radicals and defect centres, where the hyperfine frequencies in the μSR spectra serve to identify the species formed.

The purpose of this note is to examine under what circumstances Level Crossing Resonance [1] may be observed in molecular materials and used to identify the elusive diamagnetic fraction. The first requirement is that the muon should adopt a position in the product molecule or molecular species which is in close proximity to a quadrupolar nucleus. It is the quadrupolar splitting which provides an energy level scheme permitting cross polarization to the muon in non-zero fields, and the magnetic dipole interaction between the muon and the nucleus in question which effects the cross polarization rate, just as in the first demonstration of LCR in metallic copper [2]. Unlike the situation in para-

* Present address: Department of Chemistry, The University, Glasgow, G12 8QQ, U.K.

magnetic species, where the unpaired electron spin can mediate the polarization transfer from the muon to quite distant nuclei, the r^{-3} dependence of the magnetic dipole interaction implies that cross relaxation can only be detected, on the timescale of the muon lifetime, between the muon and its nearest neighbour nuclei; this will usually mean that the muonium is chemically bound or hydrogen bonded to the atom concerned.

The question is illustrated by muon addition or muonium substitution in molecules containing nitrogen and oxygen; this is expected to occur as in eqs. (1) and (2), the muon behaving in its capacity as a lightweight proton. The examples of nitrogen in amines and oxygen in water are used; proton exchange between the ionic species formed initially and the surrounding host molecule is expected to be rapid, providing a route to the substitution of hydrogen by muonium. Process (2) is discussed in a companion paper [3].

$$NHR_2 \rightarrow NHR_2Mu^+ \rightarrow NMuR_2 \tag{1}$$

$$H_2O \rightarrow H_2OMu^+ \rightarrow HMuO. \tag{2}$$

Process (1) involves the 99.6% abundant isotope ^{14}N, so that compounds containing nitrogen appear to be obvious candidates for a demonstration experiment. Its spin of $I = 1$ provides a potential problem, however, which is illustrated in fig. 1. Here the ^{14}N frequencies are drawn as a function of the magnetic field $\boldsymbol{B}$, with the zero-field case on the left and the high-field case on the right of the diagram; the asymmetry parameter η has been arbitrarily fixed as 0.1 and $\boldsymbol{B}$ is taken parallel to the x principal axis of the electric field gradient [4]. All degeneracy is lifted, even in zero field. In consequence, all three frequencies and the corresponding energy levels have horizontal tangents at the origin, that is, the magnetic moment of the ^{14}N nucleus is effectively quenched. Calculation shows [5] that the magnetic moment, and therefore the cross-polarization rate, are reduced in first order by a factor $Z/(1+Z^2)^{1/2}$, in which $Z = \gamma_\mu \hbar B/K\eta$, γ_μ

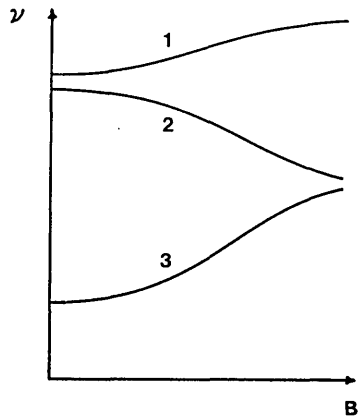

Fig. 1. Variation of spin-1 quadrupole resonance frequencies ν with the magnitude of the magnetic field $\boldsymbol{B}$ applied parallel to the x principal axis of the electric field gradient at the nucleus.

being the muon gyromagnetic ratio and $K = \frac{1}{4}(e^2qQ), (e^2qQ/h)$ being the quadrupole coupling constant. This effect reduces the resonance intensity considerably, especially in the low fields at which signals are expected to occur. In principle, the problem should be overcome by choosing a species with axial symmetry at the nitrogen atom (i.e. with asymmetry parameter $\eta = 0$), such as tertiary amines R_3N, for which proton exchange is unlikely, so that the ionic species is stabilized, as in eq. (3).

$$R_3N \rightarrow R_3NMu^+. \tag{3}$$

However, no resonance has been detected in preliminary experiments on frozen triethylamine [6]. Either the constraints of the solid phase distort the expected trigonal symmetry of the muonic ion or the muon has produced near tetrahedral symmetry in the charge distribution at the nitrogen atom, so that the resonance is at very low field and is buried in the initial steep section of the repolarization curve. In order to investigate this problem, as well as to model the expected isotope effect between the muonated and protonated forms, a systematic *ab initio* SCF MO study of the dependence upon the N-H bond length and the asymmetry parameter, η, of the nuclear quadrupole coupling constant (QCC) in amines has been performed. The species studied was the positively charged ammonium ion. All calculations were performed on the University of Glasgow MicroVAX 3600, using the GAMESS molecular orbital program [7]. The basis set used was Dunning's sp set [8] for nitrogen, using the contraction (11, 6) → [5,3] and for hydrogen a (5) → [3] contraction [9]. These functions were found to be adequate for the calculation of the electric field gradients (EFG) and the QCC of ammonia.

The effect of muon addition in frozen ammonia was studied by lengthening one of the N-H bonds with respect to the optimised ammonium ion geometry, the bond length being isotope dependent as a result of the difference in zero-point energies of the N-H and N-Mu bonds. The first series of calculations was performed under the constraint that the species formed retained axial symmetry. A systematic increase in the N-H bond length was found to result in an increase in the z-component of the electric field gradient. The quadrupole coupling constant was found to increase in consequence from 0.05 MHz for a 0.02 Å increase in bond length up to 0.313 MHz for a 0.14 Å increase in the N-H bond length. These results indicate that the species formed on muon addition would have a significantly non-zero QCC (compared with the analogous proton species for which the QCC vanishes by symmetry). The exact value of the N-Mu bond length is unknown. From these results the level crossing resonance for an axially symmetric species would be expected to occur in the 0.4 to 2.5 mT region. An increase in bond length between C-H and C-Mu is likewise in part responsible for the hyperfine isotope effect in organic radicals [10,11]. In this case an extension of about 5% (0.06 Å) is estimated [12]. By variation of a single HNH bond angle, the calculations were repeated for a non axially symmetric ion. It was found that small deviations from the equilibrium bond angle have no significant effect on

the EFG or QCC, the values being similar to those reported above. However, as mentioned above, the introduction of an asymmetry parameter lifts all degeneracy of the quadrupole energy levels and makes observation of the level crossing resonance unlikely.

The problem is overcome if the muon is adjacent to a quadrupolar nucleus with half-integral spin. The energy levels are then Kramers doublets in zero-field, so that the full magnetic dipole moment is available to drive the resonance. This consideration led to the choice of ^{17}O ($I = 5/2$) for the first successful demonstration in ice-I_h at 200 K [13], in which the muonium is directly bonded or "hydrogen"-bonded to a quadrupolar nucleus; a disadvantage is that a considerable degree of ^{17}O enrichment is required.

The information that can be obtained from ^{17}O μLC studies is likely to be considerable; for example, in ice [3], a species tentatively identified as $\{H_2O...Mu...OH_2\}^+$ is formed at 50 K, with an ^{17}O quadrupole coupling constant of 8.24 MHz and asymmetry parameter of 0.55, the first time these quantities have been measured in this ion. At higher temperatures, the ionic precursor loses a proton to give the HMuO molecule, with a quadrupole coupling constant of 6.1 MHz assuming an asymmetry parameter of unity (at 200 K). This is the first example of a muonium isotope effect on a quadrupole coupling constant; in normal ice I_h at 77 K, the ^{17}O quadrupole parameters are +6.410 MHz ($\eta = 0.93$), in ice-d_2 at 260 K 6.66 MHz ($\eta = 0.94$), so the shift in the ^{17}O quadrupole coupling constant is in the opposite direction to that of deuteration, as expected. Following detection of a μLC resonance with ^{17}O [13], the technique has been employed to investigate the site adopted by the muon probe in $YBa_2Cu_3O_x$, enriched in ^{17}O for the purpose [14]; the signals detected indicate a quadrupole coupling constant of 6.6 MHz and near zero asymmetry parameter and almost certainly represent the ^{17}O-Mu^- ion - compare the ^{17}O quadrupole parameters in $LiOH \cdot H_2O$ of 6.69 MHz, $\eta = 0.03$.

There are, however, a considerable number of other quadrupolar nuclei of half-integral spin which form hydrides or hydrido complexes in which cross-polarization may be fast enough to make level-crossing experiments feasible; among these, we mention the Group III nuclei ^{11}B (3/2, 81.2%), ^{27}Al (5/2), the halogen nuclei ^{35}Cl (3/2, 75.8%), ^{79}Br (3/2, 50.7%), ^{127}I (5/2), and transition metal nuclei such as ^{55}Mn (5/2), ^{57}Co (7/2), ^{181}Ta (7/2), ^{193}Ir (3/2, 61.5%). A possible disadvantage is the size of their quadrupole interactions which in some cases will require the use of higher magnetic fields and lead to broad absorptions [15]. The problem is alleviated by the large gyromagnetic ratio of the muon, three times that of the proton; on past experience, it should be possible to detect level-crossing from quadrupole frequencies as high as 30 MHz, in which case it will almost certainly be necessary to fit calculated lineshapes in order to derive the quadrupole parameters.

Applications in metals are already well advanced [16] although the possibility of studying muon-impurity pairs does not yet seem to have been exploited. In

semiconductors, attention has focussed on the paramagnetic defect centres [17] but μLCR may also be able to report on the elusive diamagnetic fraction. The Group III elements are particularly interesting in their capacity as substitutional defects (acceptors) in silicon or germanium. It is believed that these electrically active impurities may be passivated by interstitial hydrogen, via formation of a diamagnetic complex in which the proton adopts a bond-centre location immediately adjacent to the acceptor ion. LCR experiments on the analogous complexes with a muon playing this role offer the prospect of confirming the model and studying this important process further [18].

In molecular crystals, there is the possibility of generating chemically interesting species which are inaccessible to other spectroscopic techniques because of their transient existence. Solid halogens may give rise to the ion X_2Mu^+, for examples ($X = {}^{35}Cl$, ^{79}Br, or ^{127}I); the species N_2Mu^+ has already been identified in solid nitrogen [19] and has the axial symmetry necessary to make it a good candidate for study by LCR. The halogen hydrides may give rise to $XHMu^+$, which so far has only been detected in the gas phase [20].

Unlike double resonance or ENDOR methods, muon implantation should produce LCR signals only from those nuclei immediately adjacent to the muon site, but the method is still of wide potential, and more promising in identifying trapping sites than measurements of the dipolar interaction from the muon relaxation rate. The key question is the size of the cross-polarization rate, which in turn is connected with the magnitude of the muon dipolar coupling to the adjacent quadrupolar nucleus. There is already evidence that this is large enough in the osmium cluster in $Cs_2\{Os_{10}C(CO)_{10}\}$ in which the (Gaussian) line width of 0.07 μs^{-1} at 100 K has been ascribed to dipolar coupling to ^{189}Os ($I = 3/2$, 16.1%) [21]. Another cluster surely worthy of study is the tetrahedral As_4 species in non-metallic arsenic, offering the intriguing possibility of trapping a muon at the centre of the tetrahedron (^{75}As, $I = 3/2$). Although there may still be uncertainties in the precise identification of the muon trapping site, assignments should be considerably assisted by *ab initio* theoretical calculations of the electric field gradient at the quadrupolar nucleus for various plausible locations of the implanted muon [22]. Techniques of dynamical averaging of one-electron molecular properties, already under development for the interpretation of hyperfine isotope effects [11], should apply equally to quadrupole isotope effects in diamagnetic species.

References

[1] A. Abragam, CR Acad. Sci. Paris 229 (1984) 95.
[2] S.R. Kreitzman, J.H. Brewer, D.R. Harshman, R. Keitel, D.-Ll. Williams, K.M. Crowe and E.J. Ansaldo, Phys. Rev. Lett. 56 (1986) 181.
[3] S.F.J. Cox, J.A.S. Smith and M.C.R. Symons, Hyp. Int., 65 (1990) 987 (companion paper).
[4] G.M. Muha, J. Mag. Res. 49 (1982) 431.

[5] G. Leppelmeier and E.L. Hahn, Phys. Rev. 141 (1966) 724.
[6] D. Buttar and S.F.J. Cox, Experiments at ISIS and PSI (unpublished).
[7] M.W. Schmidt, J.A. Boatz, K.K. Baldridge, S. Kaseki, M.S. Gordon, S.T. Elbert and B. Lam, QCPE Bulletin, Vol. 7 (1987) 115.
[8] T.H. Dunning, Jr. J. Chem. Phys. 55 (1971) 716.
[9] P.G. Mezey, R.E. Kari and I.G. Csizmadia, J. Chem. Phys. 66 (1977) 964.
[10] S.F.J. Cox, T.A. Claxton and M.C.R. Symons, Rad. Phys. Chem. 28 (1986) 107.
[11] T.A. Claxton, S.F.J. Cox, A.M. Graham, Dj. Maric, P.F. Meier and S. Vogel, Hyp. Int, 65 (1990) 913.
[12] E. Roduner and I.D. Reid, Israel J. Chem. 29 (1989) 3.
[13] S.F.J. Cox, G.M. Eaton, J.E. Magraw and C.A. Scott, Chem. Phys. Lett. 160 (1989) 85.
[14] J.H. Brewer, J.F. Carolan, P. Dosanjh, W.N. Hardy, P. Sch, R.F. Kiefl, S.R. Kreitzman, Q. Li, T.M. Riseman, H. Zhou, E.J. Ansaldo, L.P. Le, G.M. Luke, Y.J. Uemura, K. Hepburn-Wiley and C.E. Stronach, Hyp. Int., 63 (1990) 177.
[15] H.T. Stokes and D.C. Ailion, J. Chem. Phys. 70 (1979) 3572.
[16] G.M. Luke, S.R. Kreitzman, J.H. Brewer, D.R. Noakes, M. Celio, R. Kadono and E.J. Ansaldo, Hyp. Int., 64 (1990) 721.
[17] T.L. Estle, Hyp. Int., 64 (1990) 525.
[18] S.F.J. Cox, P.R. Briddon and R. Jones, 64 (1990) 603 (plus references therein).
[19] B.F. Kirillov, B.A. Nikol'sky, A.V. Pirigov, V.G. Storchak, V. Grebinnik, V.H. Dodokhov, V.N. Duginor, S. Kapusta, A.B. Lazarev, S.N. Shilov and V.A. Zhukov, Hyp. Int., 65 (1990) 819.
[20] F.H. Field and F.W. Lampe, J. Amer. Chem. Soc. 80 (1958) 5583.
[21] P.H. Dallin, U.A. Jayasooriya, B.F. Johnson, J. Lewis, S.F.J. Cox, C.A. Scott and E. Marseglia, Hyp. Int., 64 (1990) 715.
[22] T.P. Das and P.C. Schmidt, Z. f. Naturforsch. 41a (1986) 47.

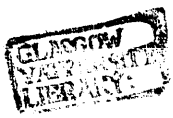

Vibrationally Averaged β-Hyperfine Coupling Constants for the Muonium-substituted Ethyl Radical

David Buttar and Brian C. Webster*
Chemistry Department, The University, Glasgow G12 8QQ, UK

A variation-perturbation approach is applied to compute isotope-dependent zero-point vibrational corrections to the β-hyperfine coupling constant of the ethyl radical. The corrections increase the coupling by *ca.* 5, 7 and 23% for the deuterium-, protium- and muonium-substituted radicals, respectively. The large vibrational correction to the muon β-hyperfine coupling constant could explain the 'residual' isotope effect observed experimentally.

Experimental studies of the muonium (Mu)-substituted ethyl radical using the methods of transverse-field muon spin rotation (μSR) spectroscopy and level-crossing resonance spectroscopy have shown that the β-hyperfine coupling is strongly isotope dependent.[1,2] Muonium is a one-electron atom having *ca.* one-ninth the mass of hydrogen and is formed by the combination of a positive muon (μ^+) and an electron. A direct comparison of the muon–electron β-hyperfine coupling constants (A_μ) and the analogous proton coupling constants (A_p) can be made by considering the reduced hyperfine coupling constant (A'_μ). A'_μ is defined as the observed muonic coupling constant scaled by the ratio of the muon and proton magnetic moments, $\mu_p/\mu_\mu = 0.3141$. For all β-substituted muonium radicals A'_μ is larger than A_p. This isotope effect has been interpreted to some extent by considering the conformational preference of isotopomers arising from the isotope dependent barriers to internal rotation.[3] Vibrational corrections to the hyperfine coupling constants should assist in the elucidation of the observed isotope effect on the coupling constants and the barrier to internal rotation of the radical.

A comparison of *ab initio* and experimental hyperfine coupling constants is restricted by the averaging over the populated vibrational states of the experimental results. However, recent calculations have shown that a good comparison can be achieved if the *ab initio* results are corrected for vibrational and correlation effects.[4] The introduction of vibrational effects also enables the effects of isotopic substitution on the hyperfine coupling constants to be studied. A comprehensive investigation by Raynes *et al.* on methane and its isotopomers has already shown the importance of including vibrational effects in the calculation of magnetic susceptibilities and NMR coupling constants.[5,6] Here we employ a vibrational averaging technique to calculate the vibrationally corrected β-hyperfine coupling constants of the ethyl radical and its isotopomers.

The isotopically substituted ethyl radical, as shown in Fig. 1, has the C—X bond eclipsing the singly occupied notional $2p_z$ orbital centred on the methylenic carbon. The vibrational motion of nucleus X can be described in terms of the variation of the internal coordinates R, θ_1 and θ_2 illustrated in Fig. 1; where R is the C—X bond length, θ_1 is the XCC bond angle and θ_2 is the $XCCH_\alpha$ torsion angle. The equilibrium geometry of the protium and muonium substituted radicals is that of Fig. 1; however, the equilibrium conformation of the deuterium substituted radical has D in the nodal plane of the $2p_z$ orbital. Here we are principally concerned with computing the β-hyperfine coupling constant of the muonium-substituted radical, the deuterated and protonated radicals (X = D, H) have also been considered to show the isotope effect on computed hyperfine couplings. For X = Mu or D the mass difference between the isotope and the remaining protons effectively decouples the vibrational motion of the C—X group from the rest of the radical as reported previously. Vibrational averaging[7–9] for X = Mu or D can therefore be achieved using only three of the normal modes of vibration of the radical. The three normal modes can be described as the C—X bond stretching mode (ν_1), the XCC angle bending mode (ν_2) and the $XCCH_\alpha$ torsional rotation mode (ν_3). These normal modes can be expressed in terms of the internal coordinates R, θ_1 and θ_2. Although the protonated (X = H) form of the radical can not be treated by simply considering these modes, the results obtained for $C_2H_5^\bullet$ are given for comparison with the muonium and deuterium calculations. When X = H, coupling with the remaining normal modes must be considered, unlike the situation where the C—X normal modes are decoupled from the rest of the radical by muonium or deuterium substitution.

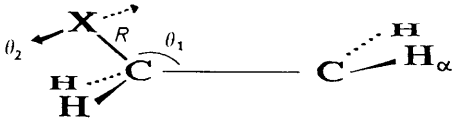

Fig. 1 Internal coordinates R, θ_1 and θ_2 of the isotopically substituted ethyl radical

A study of the vibrational corrections to the β-hyperfine couplings of the ethyl radical by Claxton *et al.*[8] limited its approach to averaging over each of the three normal modes describing the vibrational motion of the C—X group separately. Chipman[10] has also calculated vibrational corrections to the hyperfine couplings by a systematic examination of the dependence of the couplings on the out-of-plane bending at the methylenic carbon, on the torsional motion around the C—C bond and the coupling between them. The vibrational corrections reported here are computed using complete vibrational averaging over the three normal modes ν_1, ν_2 and ν_3 and therefore include the effects of coupling between the normal modes.

Computational Details

A successful study of the vibrational corrections to the dipole moment and the quadrupole coupling constant of isotopomers of water has already been completed.[11] The same approach is applied to the ethyl radical; however, it is limited to the consideration of only three normal modes as described previously. A surface scan of 252 points around the stationary point geometry has been performed at the SCF level using the GAMESS molecular orbital package.[12] All calculations were carried out at the 6-31G* level.[13] Correlation effects have been neglected in the energy and property surfaces computed as a recent study has shown that the correlation corrections are effectively constant over the region of

the surface spanned by the vibrational motion.[4] The neglect of correlation effects will therefore not affect the trends observed in the computed isotope vibrational corrections but will considerably reduce the time required to compute the necessary property and energy surfaces.

The energy and property surfaces of the radical were built up by varying the three internal coordinates R, θ_1 and θ_2 from their equilibrium values R_e, θ_1^e and θ_2^e over the ranges ± 8 pm, $\pm 10°$ and $\pm 10°$, respectively. The points obtained from the variation of R, θ_1 and θ_2 will therefore provide a surface describing the vibrational motion of the C—X group of the radical. The computer program SURVIB developed by Harding and Ermler[14] has been used to perform a least-squares fit to the surfaces and to compute the vibrational corrections to the energy and the β-hyperfine coupling constant. The internal-coordinate functions obtained from the fitting procedure consists of a Simons–Parr–Finlan[15] expansion in terms of the bond length and a Taylor series expansion in terms of the bond angle and dihedral angle. The computed property function can be expressed in the form

$$P = P_0 + \sum_{i=1}^{3} K_i S_i + \frac{1}{2} \sum_{i,j=1}^{3} K_{ij} S_i S_j + \sum_{i,j,k=1}^{3} K_{ijk} S_i S_j S_k \quad (1)$$

where S_1, S_2 and S_3 are to be identified with the bond displacement $\Delta R = R - R_e$, and angle displacements $\Delta\theta_1 = \theta_1 - \theta_1^e$ and $\Delta\theta_2 = \theta_2 - \theta_2^e$, respectively. The term P_0 is the value of the property at the equilibrium geometry of the radical and K_i, K_{ij} and K_{ijk} are the expansion constants derived from the fitting procedure. The computed energy function reproduces the calculated energies with a maximum error of 7.9×10^{-6} a.u. and a root-mean-square error of 2.7×10^{-6} a.u. The analytic energy function is used in a standard normal mode analysis which enables the transformation matrix to normal coordinates to be computed. The property and energy expansions are re-expanded as Taylor series functions of the normal coordinates. These expressions are then used in a standard perturbation theory analysis of the vibrational corrections.

The perturbation approach has been fully described previously by Kern and Matcha[16] and Ermler and coworkers,[17–19] therefore only a brief description is outlined here. The cubic expansion coefficients obtained from the analytic normal coordinate energy function,

$$P = P_0 + \sum_{i=1}^{3} \alpha_i q_i + \sum_{i,j=1}^{3} \beta_{ij} q_i q_j + \sum_{i,j,k=1}^{3} \gamma_{ijk} q_i q_j q_k \quad (2)$$

where $P_0 = E_0$ is the value of the energy at the minimum-energy conformation and α, β and γ are expansion coefficients, enable first-order corrections to the harmonic vibrational wavefunctions to be calculated. The vibrational wavefunction x used in this analysis is defined as

$$x = x^0 + x^1 \quad (3)$$

Here x^0 is the zero-order solution which is a product of harmonic oscillator wavefunctions and x^1 is the first-order correction expanded in terms of the zero-order solutions. Vibrationally averaged properties can therefore be computed by substitution of the normal-coordinate expansions of the form of eqn. (2) into eqn. (4).

$$\langle P \rangle_v = \langle x | P | x \rangle \quad (4)$$

This procedure leads to a final expression for the vibrationally averaged property $\langle P \rangle_v$,

$$\langle P \rangle_v = C + \sum_{i=1}^{3} A_i(v_i + 1/2) + \sum_{i<j}^{3} B_{ij}(v_i + 1/2)(v_j + 1/2) \quad (5)$$

where C, A and B are expansion coefficients derived from the quadratic and cubic coefficients of eqn. (2). Explicit expressions for the expansion coefficients are given by Krohn *et al.*[18] The vibrational corrections to the computed properties can therefore be defined as the difference between the vibrationally averaged property $\langle P \rangle_v$ and the value of the property at the stationary point of the property function P_0. The vibrational corrections obtained from this method will reflect both the harmonic and anharmonic nature of the vibrational motion.

Results and Discussion

For $C_2H_5^*$ the energy and property surfaces were fitted to a fourth-order internal-coordinate expansion. Although the fourth order terms are not required for the calculation of the vibrational corrections, they are included as we find that they result in reduced errors in the third order terms. The stationary point energy of the radical was $-78.597\,15\ E_h$ with the internal coordinates having the values $R_e = 109.068$ pm, $\theta_1^e = 111.751°$ and $\theta_2^e = 81.828°$. Table 1 lists the internal-coordinate displacement expansion parameters for the energy function of the form of eqn. (1). The harmonic frequencies, obtained by a normal-mode analysis using this energy function are listed in Table 2 for some isotopomers. The expectation values of the root-mean-square amplitudes and the bond angle displacements over the vibrational wavefunctions are given in Table 3. The size of the quantities in Table 3 gives an estimate of the magnitude of the harmonic and anharmonic motion of the three isotopes when substituted at position X in Fig. 1.

As expected, the zero-point energy is significantly higher for the muonic species. We could therefore predict that the vibrational corrections to the muonic isotopomers will be

Table 1 Calculated quadratic and cubic expansion constants (au) of the analytic internal displacement coordinate energy function

quadratic expansion constants		cubic expansion constants	
K_{11}	0.7577	K_{111}	−0.01043
K_{22}	0.1247	K_{222}	−0.00675
K_{33}	0.0978	K_{333}	0.00072
K_{12}	−0.01316	K_{112}	−0.00139
K_{13}	0.000029	K_{122}	−0.04011
K_{23}	−0.000051	K_{113}	−0.00003
		K_{223}	−0.00130
		K_{133}	−0.03900
		K_{233}	−0.02720
		K_{123}	−0.00026

Table 2 Calculated harmonic frequencies (ν)/cm^{-1} and zero-point energies (E_{zp})/cm^{-1}

	C—H	C—Mu	C—D
ν_1	3187.32	9136.32	2344.08
ν_2	1895.18	3819.56	1699.35
ν_3	1359.22	3725.59	1036.83
E_{zp}	3220.86	8340.73	2540.13

The subscripts 1, 2 and 3 refer to the bond stretch (ν_1), angle bend (ν_2) and dihedral motion (ν_3).

Table 3 Expectation values of internal displacement coordinates $\langle \Delta R \rangle$ (pm) and $\langle \theta \rangle$ (degrees)

bond	$\langle \Delta R \rangle$	$\langle \Delta\theta_1 \rangle$	$\langle \Delta\theta_2 \rangle$	$\langle \Delta R^2 \rangle^{1/2}$	$\langle \Delta\theta_1^2 \rangle^{1/2}$	$\langle \Delta\theta_2^2 \rangle^{1/2}$
C—H	1.45	0.077	−0.072	7.54	6.40	8.50
C—Mu	4.70	0.251	−0.030	12.78	10.58	12.08
C—D	0.73	0.056	−0.092	6.46	5.60	8.05

larger than the corresponding proton or deuterium corrections. This is found to be the case for the average bond length, C—X, which is 109.80, 110.52 and 113.77 pm for X = D, H and Mu, respectively. Similarly the results in Table 3 show that muonium substitution increases the XCC bond angle and the $XCCH_\alpha$ dihedral angle of the ethyl radical. These results follow the same trends as those found for muonium-substituted water.

Table 4 lists the expansion coefficients of the analytic expression obtained from fitting the computed spin density surface about nucleus X. The vibrational corrections to the energy and to the spin density (ρ^s) at nucleus X are given in Table 5. The corrections to the β-hyperfine coupling constant of each isotopomer are calculated from the spin density using the relationship,

$$A_x = \frac{8\pi}{3h} g_e \mu_B g_N \mu_N |\rho^s| \quad (6)$$

where g_e and g_N are the elctron and nuclear g factors, respectively, μ_B is the Bohr magneton and μ_N is the nuclear magneton. Since spin density is often calculated in atomic units we can write A_x expressed in atomic units by,

$$A_x = \frac{\alpha^2}{3m_x} g_e g_N |\rho^s| \quad (7)$$

where α is the fine structure constant and m_x is the nuclear mass. The velocity of light in atomic units is specified as α^{-1} and has a value of 137 a.u. Note that if the spin density alone is reported in a.u. then A_μ/MHz = 14 229.0 $|\rho^s|$, similarly the conversion factors for deuterium and protium are 1372.26 and 4469.879, respectively. The corrections to the β-hyperfine coupling constants of each isotopomer have been calculated from the spin densities and are given in Table 6. These vibrational corrections are decomposed into harmonic and anharmonic contributions and the coupling constants of Mu and D are reported in their reduced form to facilitate comparisons.

In Table 6 the quantity C is a constant, independent of the vibrational state, which arises from the inclusion of anharmonicity in the vibrational analysis. For all cases the anharmonic corrections reinforce the dominant harmonic corrections and result in an increased value of the coupling. The coupling increases from 142.172 MHz for the C—D species to 166.097 MHz for the C—Mu species. Table 6 shows that the harmonic and anharmonic terms are isotope dependent. In the Born–Oppenheimer approximation all the isotopomers have the same equilibrium bond length and bond angles. The calculated isotope effects must therefore arise from the different nuclei sampling different regions of the spin density surface. Table 7 lists the normal-coordinate expansion coefficients for the spin density functions of the isotopomers C—D, C—H and C—Mu. As a consequence of the normal coordinates being mass dependent the expansion coordinates are clearly isotope dependent. The values of the coefficients in Table 7 can therefore be seen to account for the difference in spin density of the three isotopomers considered.

Table 4 Computed expansion coefficients (au) of the internal displacement coordinate analytic function describing the spin density at nucleus X

K_1	0.05686	K_{111}	0.06602
K_2	0.00995	K_{222}	0.04090
K_3	−0.000004	K_{333}	0.00093
K_{11}	0.20910	K_{112}	0.03183
K_{22}	−0.00762	K_{122}	0.01377
K_{33}	0.01038	K_{113}	−0.01350
K_{12}	0.02472	K_{223}	0.00002
K_{13}	0.00128	K_{133}	0.0585
K_{23}	0.00008	K_{233}	−0.0107
		K_{123}	−0.0007

Table 5 Zero-point vibrational corrections to the energy (E) and spin density (ρ^s)

		vibrational correction/au		
property	P_0[a]	C—H	C—Mu	C—D
E	−78.59715	−0.0145	−0.0368	−0.0116
ρ^s	0.03022	0.002 (5)	0.007 (5)	0.0015 (4)

[a] P_0 denotes the value of the property at the stationary point of the potential analytic function. The error limits given in parentheses are three times the standard deviations.[14]

Table 6 Harmonic and anharmonic corrections to the β-hyperfine coupling constant (A/MHz)

	A_p	A'_μ	A'_D
P_0	135.079	135.079	135.079
C	0.0616	−0.0073	0.0039
harmonic	8.743	24.504	6.539
anharmonic	0.831	6.521	0.550
total	144.715	166.097	142.172

Table 7 Normal-coordinate expansion coefficients ($\times 10^4$) for the spin density function of the isotopomers C—X(X = D, H, Mu) (au)

	coefficient ($\times 10^4$)		
isotopomer	C—D	C—H	C—Mu
α_1	4.79269	6.60684	19.1578
α_2	−0.34385	−0.27199	−0.99184
α_3	−1.09422	−1.37124	3.47644
β_{11}	0.11122	0.20876	1.73556
β_{12}	−0.00924	−0.01033	−0.07494
β_{13}	−0.02090	−0.03170	−0.19523
β_{22}	0.03737	0.05477	0.40598
β_{23}	−0.00396	−0.00694	−0.09805
β_{33}	0.01301	0.02617	0.24970
γ_{111}	0.00194	0.00490	0.11551
γ_{112}	0.00015	0.00033	0.00590
γ_{113}	−0.00009	−0.00011	−0.00135
γ_{122}	0.00162	0.00310	0.06170
γ_{123}	−0.00010	−0.00017	−0.00294
γ_{133}	0.00078	0.00221	0.05816
γ_{222}	−0.00012	−0.00012	−0.00177
γ_{223}	0.00012	0.00011	−0.00553
γ_{233}	−0.00023	−0.00044	−0.01458
γ_{333}	−0.00043	−0.00096	−0.01825

The results also show that the dominant terms in describing the spin density at nucleus X are the coefficients of the normal coordinate describing the C—X bond-stretching motion. For example the value for the expansion constant α_1 is 0.000 479, 0.000 661 and 0.001 916 for C—D, C—H and C—Mu, respectively.

Fig. 2 and 3 show the variation of the energy and the spin density of the ethyl radical with internal coordinates R and θ_1. The figures clearly show that for displacements equivalent to those reported in Table 3 the region of the surface sampled by each isotope will be markedly different. Fig. 2 shows that due to the muon's large root-mean-square displacement it is averaged over a region of the surface where there is a large variation in the spin density. The large harmonic correction to the coupling constant of the muon can be attributed to this variation of the spin density within the limits of the muon's zero-point motion. The other isotopes experience less of an effect due to their smaller zero-point energies. Table 6 indicates that the anharmonic contribution to the vibrational correction is only significant for the light isotope muonium. For the protium- and deuterium-substituted species the anharmonic correction is almost negligible. In contrast the vibrational corrections to the β-hyperfine coupling constant leads to a residual isotope effect of *ca.* 15% for the muon over the proton.

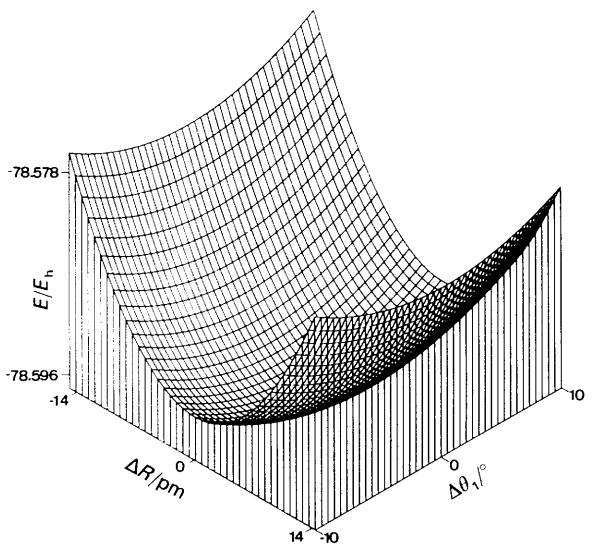

Fig. 2 Variation of the energy with internal displacement coordinates ΔR and $\Delta\theta_1$

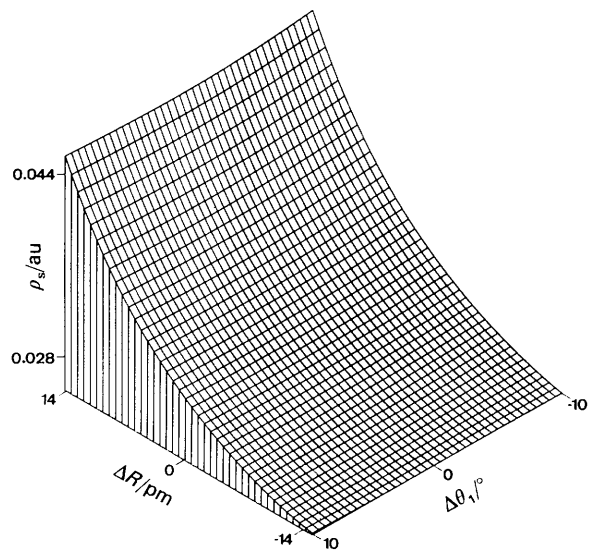

Fig. 3 Variation of the spin density with internal displacement coordinates ΔR and $\Delta\theta_1$

The computed theoretical results enable an estimate of the high-temperature limit ($\bar{A}$) of the β-hyperfine couplings of the ethyl radical to be calculated. At the high-temperature limit there is essentially free rotation about the central C—C bond of the radical. The β-hyperfine coupling constant is normally reported as the average of the β-couplings, $\bar{A}_\beta = 1/3(A_x + 2A_p)$, since free rotation is assumed. Where A_p is the hyperfine proton coupling constant of the β-protons not contained in the plane of the notional $2p_z$ orbital centred on the methylenic carbon. If it is assumed that the value of A_p is that obtained at the SCF level, $A_p = 37.87$ MHz. Then the high-temperature limits are $\bar{A}(CH_2Mu) = 80.65$ MHz and $\bar{A}(CH_3) = 73.48$ MHz. These results are in surprisingly good agreement with the experimentally measured high-temperature limits of $\bar{A}(CH_2Mu) = 79$ MHz[2] and $\bar{A}(CH_3) = 75.3$ MHz.[20] The computed proton high-temperature limit is probably less accurate because of the neglect of the vibrational coupling between the C—X group and the rest of the radical. These estimates could of course be improved by a more complete treatment of the vibrational averaging. The good agreement of the muon result, however, confirms that the major contributions to the vibrational corrections of the muon arise from the three normal modes considered and their coupling.

Conclusion

The present studies, and those of Claxton *et al.*,[8] show that the residual isotope effect observed for the muon β-hyperfine couplings can be explained through the consideration of vibrational averaging. The vibrational corrections are found to be composed of a dominant harmonic term and a small anharmonic term. The harmonic term arises from the fact that for each isotopomer the spin density is averaged over a different region of the surface about the stationary point. The large root-mean-square amplitude of the muon results in the muonic species having the largest anharmonic correction. The corresponding anharmonic corrections for the protium and deuterium species are negligible in comparison. These effects can also be used to explain the difference in the barriers to internal rotation of different isotopically substituted ethyl radicals.

It should be remembered that all the computed results have neglected vibrational–rotational coupling and assumed the radical to be in its ground vibrational state. Corrections over excited vibrational and rotational states would have to be included for a complete study, but this would greatly increase the complexity of the problem and the computational time required.

This work was supported by the Carnegie Trust for the Universities of Scotland. The award of a research studentship to D.B. by the SERC is gratefully acknowledged.

References

1 M. J. Ramos, D. McKenna, B. C. Webster and E. Roduner, *J. Chem. Soc., Faraday Trans. 1*, 1984, **80**, 255.
2 P. W. Percival, J-C. Brodovitch, S-K. Leung, D. Yu, R. F. Kiefl, D. M. Garner, D. J. Arseneau, D. G. Fleming, A. Gonzalez, J. R. Kempton, M. Senba, K. Venkateswaran and S. F. J. Cox, *Chem. Phys. Lett.*, 1989, **163**, 241.
3 M. J. Ramos, D. McKenna, B. C. Webster and E. Roduner, *J. Chem. Soc., Faraday Trans. 1*, 1984, **80**, 267.
4 I. Carmichael, to be published.

5 W. T. Raynes, *Mol. Phys.*, 1988, **63**, 719.
6 W. T. Raynes, P. W. Fowler, P. Lazzeretti, R. Zanasi and M. Grayson, *Mol. Phys.*, 1988, **64**, 143.
7 B. C. Webster and R. Macrae, *Chem. Phys. Lett.*, 1988, **150**, 18.
8 T. A. Claxton, A. M. Graham, S. F. G. Cox, D. M. Maric, P. F. Meier and S. Vogel, *Hyperfine Interactions*, 1990, **65**, 913.
9 J. Pacansky and M. Dupuis, *J. Am. Chem. Soc.*, 1982, **104**, 415.
10 D. Chipman, *J. Chem. Phys.*, 1991, **94**, 6632.
11 B. C. Webster and D. Buttar, in preparation.
12 M. W. Schmidt, J. A. Boatz, K. K. Baldridge, S. Koseki, M. S. Gordon, S. T. Elbert and B. Lam, *QCPE Bull.*, 1987, **7**, 115.
13 P. C. Hariharan and J. A. Pople, *Theor. Chim. Acta*, 1973, **28**, 213.
14 L. B. Harding and W. C. Ermler, *J. Comput. Chem.*, 1985, **6**, 13.
15 G. Simons, R. G. Parr and J. M. Finlan, *J. Chem. Phys.*, 1973, **59**, 3229.
16 C. W. Kern and R. L. Matcha, *J. Chem. Phys.*, 1968, **49**, 2081.
17 W. C. Ermler and C. W. Kern, *J. Chem. Phys.*, 1971, **55**, 4851.
18 B. J. Krohn, W. C. Ermler and C. W. Kern, *J. Chem. Phys.*, 1974, **60**, 22.
19 W. C. Ermler and B. J. Krohn, *J. Chem. Phys.*, 1977, **67**, 1360.
20 R. W. Fessenden and R. H. Schuler, *J. Chem. Phys.*, 1963, **39**, 2147.

Paper 1/02305E; *Received* 16*th May*, 1991

ROYAL SOCIETY
OF
CHEMISTRY

Reprinted From

J. Chem. Soc., Faraday Communications.

Issue 1 1990

Competitive Muonium Addition to 3-Methyl-2-butenal

David Buttar, Roderick M. Macrae and Brian C. Webster
Chemistry Department, The University, Glasgow G12 8QQ, Scotland
Emil Roduner
Physikalisch-Chemisches Institut der Universität, CH-8057 Zürich, Switzerland

Competitive Muonium Addition to 3-Methyl-2-butenal

David Buttar, Roderick M. Macrae and Brian C. Webster
Chemistry Department, The University, Glasgow G12 8QQ, Scotland
Emil Roduner
Physikalisch-Chemisches Institut der Universität, CH-8057 Zürich, Switzerland

We report the observation of muonium-substituted radicals formed in 3-methyl-2-butenal. The reduced hyperfine coupling constants (A'_μ) at 273 K are 59.96 MHz for addition to the C=C bond and 2.89 MHz for muonium attachment to C=O.

Recently we have reported the μSR spectrum for the 2-muoxyprop-2-yl radical over the temperature range 180–319 K.[1] Here we wish to report the first clear observation of competitive muonium addition to an α,β-unsaturated carbonyl compound,3-methyl-2-butenal, $(CH_3)_2C{=}CHCHO$. With two functional groups in the molecule there is the possibility of Mu addition to C=C and C=O bonds.

The implantation of positive muons (μ^+) in unsaturated liquid hydrocarbons can lead to the formation of muonium-substituted free radicals. The resulting radicals are thought to be formed by the formal addition of a neutral muonium atom, Mu, to the unsaturated compound, where muonium consists of a bound state of the positive muon with an electron. Such radicals are observed using the technique of muon spin rotation (μSR) spectroscopy. This technique has been successfully applied to the study of conformational analysis, kinetic isotope effects, and the regioselectivity of muonium addition for a wide range of organic free radicals.[2,3]

Data were collected at the Paul Scherrer Institute (PSI), Villigen, Switzerland, using the μE4 beamline. Samples were degassed using the normal freeze–pump–thaw procedure before being sealed and placed in the cryostat of the μSR spectrometer. Using an applied field of 0.2 T transverse to the muon spin direction in the polarised beam, each muonium-substituted radical gives rise to two precession frequencies. The absolute value of the isotropic muon-electron hyperfine coupling constant $|A_\mu|$ can be deduced directly from the frequencies of the two signals observed in the Fourier-transformed spectrum. The theory for the analysis of μSR spectra is well documented.[4]

Fig. 1 shows the Fourier-transform μSR spectra for the radicals formed from 3-methyl-2-butenal and the effect of temperature upon the position and linewidth of the signals. The diamagnetic signal at *ca.* 27 MHz has been excised from the spectrum using a procedure based upon the minimisation package MINUIT.[5] The signal at Cy derives from the cyclotron frequency.

The spectrum consists of a pair of doublets R_1 and R_2, and each doublet can be attributed to a muonium-substituted free radical. In 3-methyl-2-butenal there are four inequivalent positions for muonium addition. The radicals formed by muonium addition to C_3 and muonium attachment to C=O are shown in fig. 2. The two other possible radicals are the result of muonium addition at C_1 and C_2. The strong signals, R_1 correspond to a radical with a reduced muon–electron hyperfine coupling constant, $A'_\mu = |A_\mu|\mu_p/\mu_\mu$, of 1.3 MHz at 197 K, increasing slightly to 4.7 MHz at 347 K. These low coupling constants and the associated temperature dependence are characteristic of muonium addition to a C=O group; R_1 is therefore assigned to the delocalised muoxyalkyl radical (**II**).

Table 1 presents a comparison of reduced muon–electron

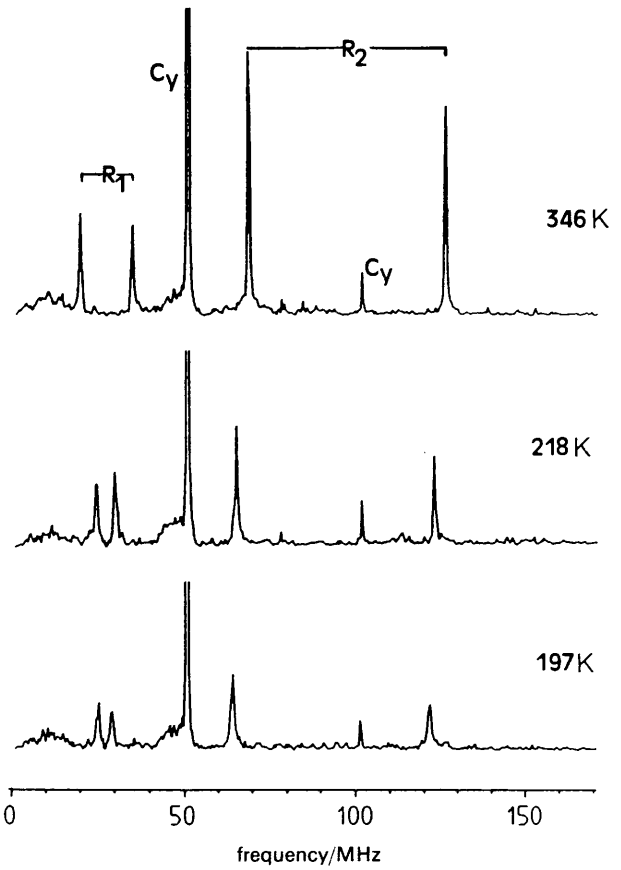

Fig. 1. Fourier-transform μSR spectra for 3-methyl-2-butenal at three temperatures and with an applied transverse field of 0.2 T.

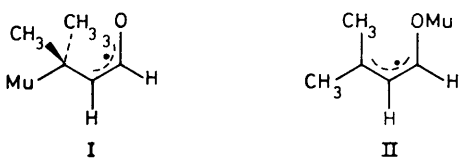

Fig. 2. Radical products from muonium addition to inequivalent sites of 3-methyl-2-butenal.

hyperfine coupling constants for a series of muoxyalkyl radicals at around 295 K. It can be observed from the table that the coupling constants of muoxyalkyl radicals formed from α,β-unsaturated carbonyl compounds are significantly lower than those of radicals such as 2-muoxyprop-2-yl. The lower coupling constants are the result of delocalisation of the unpaired electron.

The major doublet denoted R_2 is due to the presence of a second muonium-substituted radical with a reduced coupling constant of 58.2 MHz at 197 K up to 60.9 MHz at 347 K. By comparison with muonium-substituted dienes,[2] in particular 2,5-dimethyl-hexa-2,4-diene, we think that R_2 arises from muonium addition at the C=C bond, yielding the thermodynamically more stable allyl type radical (**I**).

This assignment is in accordance with values measured for the α,β-unsaturated carbonyl compound, *trans*-2-butenal, $CH_3CH{=}CHCHO$. In this case only a single radical signal is clearly observed corresponding to reduced hyperfine coupling constants decreasing from 94.8 MHz at 209 K to 82.8 MHz at 353 K. By comparison with the coupling constants of the terminal alkene, vinylacetate,[6] the radical corresponding to these signals was identified as an allyl-type radical formed from muonium addition to the C=C bond. As with 3-methyl-2-butenal the product is the delocalised allyl type radical. In the case of *trans*-2-butenal the radical signals due to muonium addition to the carbonyl group were observed to be very weak and accurate data were difficult to obtain.

The opposite temperature dependence of the hyperfine coupling constants for the two α,β-unsaturated carbonyl compounds could arise from different equilibrium conformations. The difference can probably be attributed to Mu attachment in the nodal plane of the $2p_z$ orbital centred at C_2. Consequently the observed coupling constant increases in value with rising temperature in radical (**I**).

The polarisations, corrected for experimental time resolution,[7] corresponding to muons in the muonic radicals formed from 3-methyl-2-butenal are found to be 0.109 for radical (**I**) and 0.064 for radical (**II**), at 298 K. If we assume that each radical has undergone proportionally the same depolarisation, we can convert the fractional muon polarisations into fractional rate constants for radical formation.[2] The fractional rate constant for muonium addition to the C=C bond is 0.63 for 3-methyl-2-butenal at 298 K, which is substantially lower than the corresponding fractional rate constant for *trans*-2-butenal, which we think to be close to unity. We are surprised to find that the fractional rate constant for Mu attachment to the C=O group in 3-methyl-2-butenal is as high as 0.37. Methyl substitution of *trans*-2-butenal clearly has a strong effect on the regioselectivity of muonium addition. Further experimental and theoretical studies of α,β-unsaturated carbonyl compounds are in progress.

Table 1. Hyperfine coupling constants (A'_μ/MHz) of selected muoxy radicals at ambient temperatures[a]

substrate	radical	A'_μ
1,1,1-trifluoropropan-2-one	$CF_3\dot{C}(OMu)CH_3$	9.78
hexane-2,5-dione	$CH_3\dot{C}(OMu)CH_2CH_2COCH_3$	8.57
propan-2-one	$CH_3\dot{C}(OMu)CH_3$	8.56
ethanal	$CH_3\dot{C}H(OMu)$	6.82[b]
trans-2-butenal	$CH_3CH{=}CH\dot{C}(OMu)H$	2.9[c,d]
3-methyl-2-butenal	$(CH_3)_2C{=}CH\dot{C}(OMu)H$	2.89[c]

[a] 295 ± 5 K unless noted otherwise. [b] 288 ± 5 K. [c] 273 ± 5 K. [d] Approximate value estimated from weakly observed signals.

The work is supported by the Carnegie Trust for the Universities of Scotland, the Swiss National Foundation for Scientific Research and the Paul Scherrer Institute. The award of a research studentship by the S.E.R.C. to D.B. and R.M.M. is gratefully acknowledged.

References

1 R. M. Macrae, B. C. Webster and E. Roduner, *Muon Studies in Solid State Physics*, IOP Short Meetings no. 22, 1988, 95.
2 E. Roduner and B. C. Webster, *J. Chem. Soc., Faraday Trans. 1*, 1983, **79**, 1939.
3 B. C. Webster, *Annual Report C* (Royal Society of Chemistry, London, 1984).
4 E. Roduner, in *Muons and Pions in Materials Research*, ed. J. Chappert and R. I. Grynszpan (North Holland, Amsterdam, 1984), chap. 12.
5 F. James and M. Roos, *Comput. Phys. Commun.*, 1975, **10**, 343.
6 E. Roduner, W. Strub, P. Burkhard, J. Hochmann, P. W. Percival, H. Fischer, M. Ramos and B. C. Webster, *Chem. Phys.*, 1982, **67**, 275.
7 E. Roduner, G. A. Brinkman and P. W. F. Louwrier, *Chem. Phys.*, 1982, **73**, 117.

Communication 9/04395K; *Received* 11*th October*, 1989